Laboratory for Solid State Physics
Department of Physics

Annual Report 2007

ETH
Eidgenössische Technische Hochschule Zürich
Swiss Federal Institute of Technology Zurich

Cover page:

Coaxial cabling carrying microwave frequency photons to millikelvin temperatures in a dilution refrigerator, for probing the quantum states of superconducting circuits.
From the Quantum Device Lab of Prof. Andreas Wallraff.

This annual report was edited by: Dr. S. Gustavsson

PREFACE

In this Annual Report the Laboratory for Solid State Physics at ETH Zurich is pleased to present an overview of its productive and successful work in 2007. Members of the research groups pursue their broad scientific interest in solid state physics and several results have been well recognized by the community. It is a challenging, exciting and gratifying endeavor to push the frontiers of solid state physics and to enter uncharted territory.

In addition to research, members of the Laboratory for Solid State Physics continue to devote significant time and energy to teaching. All levels of teaching are covered, from introductory courses and laboratory courses for physics students and for students of other departments at ETH, to advanced courses for students at the MSc and doctoral level. The introduction of the BSc/MSc studies and the associated modifications of the curriculum have required an even higher level of commitment to teaching.

The excellent infrastructure and support on all levels provided by the Physics Department of ETH Zurich is a most valuable and solid basis for our work. With appreciation we thank all people in the Laboratory, in the Department and at ETH in general for their expertise and continued support in all technical and administrative matters.

We very gratefully acknowledge the unwavering substantial support first and foremost by the Schulleitung of ETH, but also by the Swiss National Science Foundation, KTI, industrial partners and all other sources.

Many thanks to Dr. S. Gustavsson, Prof. L. Degiorgi and Mrs. H. Hediger for their help in preparing this Annual Report.

Zürich, May 2007

Der Vorsteher

Prof. Dr. B. Batlogg

Contents

Chapter 1

Physics of new materials

(http://www.pnm.ethz.ch/)

Head
Prof. Dr. Bertram Batlogg

Academic Staff

Dr. Simon Haas	Dr. Petra Häfliger	Wolfgang Kalb
Lisa Kreuzer	Thomas Mathis	Kurt Pernstich
Dr. Blandine Alloing	Dr. Peter Cristea	PD Dr. Hans von Känel

Technical Staff
Kurt Mattenberger

Academic Guest
Prof. Dr. Yoshihiro Kubozono, Research Laboratory for Surface Science, Okayama University, Okayama (Japan)

Administrative Staff
Gabriela Strahm

Doctoral theses
Kurt Pernstich
The influence of trap states on charge transport in organic transistors
May 2007

Diploma theses

Thomas Brenner	HS 2007
Roger Häusermann	SS 2007
Pierre Joris	SS 2007
Jakob Kanter	SS 2007 - FS 2008
Tobias Morf	HS 2007
Tim Schulze	SS 2007
Valentin Wittwer	HS 2007

Semester students

Stephanie Bubenhofer	Martina Lechner	Miriam Gantert
Andreas Fognini	Matthias Walser	Valentin Wittwer
Fabian Meng	Ralph Chati	Simon Gerber
Lukas Morf		

High pressure materials synthesis group

Head
Dr. Janusz Karpinski

Academic Staff
Andrey Belousov
Dr. Zbigniew Bukowski
Dr. Sergiy Katrych
Dr. Nikolai Zhigadlo

Academic Guests
Dr. Roman Puzniak, Polish Academy of Sciences, Warsaw (Poland)
Dr. Krzysztof Rogacki, Polish Academy of Sciences, Wroclaw (Poland)
Mauro Tortello, Politecnico di Torino, Torino (Italy)
Jan Jun, Institute of High Pressure Physics, Warsaw (Poland)

Students
Wojciech Makowiecki

Optical and Magneto-optical Spectroscopy

Head
Prof. Dr. L. Degiorgi

Academic Staff
M. Lavagnini
F. Pfuner

Technical Staff
J. Müller (until March 2007)

Administrative Staff
I. Mettler

1.1 High performance C_{60} thin-film field-effect transistors with parylene gate insulator

S. Haas, W. L. Kalb, P. Joris, F. Meng, B. Batlogg in collaboration with Y. Kubozono (Research Laboratory for Surface Science, Okayama University, Japan) and A. Fujiwara (Japan Advanced Institute for Science and Technology, Ishikawa, Japan)

Organic semiconductors are promising for the future's low-cost, flexible electronics such as rollable displays. In order to implement complementary logic, however, transistors with both n- and p-type semiconductors are needed. We have fabricated high performance n-type organic thin-film transistors with vacuum evaporated C_{60} as the active material. The devices employ the organic gate dielectric parylene. The C_{60} thin-film transistors were made on Si/SiO_2 substrates and on flexible poly(ethylene terephthalate) [PET] substrates or on commercially available transparent sheets. The field-effect mobility is a key figure of merit and mobilities up to 0.41 cm^2/Vs were achieved which is comparable to the mobilities in hydrogenated amorphous silicon.

C_{60}-baased thin-film transistors generally need to be annealed even after a short exposure to ambient air. It is most remarkable that the annealing step is not necessary when a parylene gate dielectric is used. This may be due to the high water repellency of the parylene gate dielectric on a microscopic level. Water is known to be detrimental for the charge transport in organic semiconductors, even more so in the case of certain n-type materials.

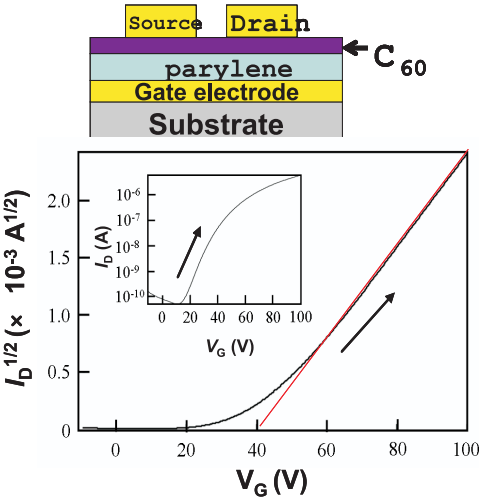

Figure 1.1: Structure of the C_{60} field-effect transistor with parylene dielectric and transfer characteristic from a device made on a PET substrate.

In the case when flexible substrates were employed, the effect of bending the substrates on the performance of the field-effect transistors was investigated. These results are of importance since organic field-effect transistors are envisioned to play a key role in flexible electronic devices. The field-effect mobility of the C_{60} transistors decreases only slightly down to a bending radius of 6 mm. If the samples are bent further, however, the mobility drops significantly and the mobility degradation is irreversible.

1.2 Modulating the Seebeck coefficient in organic transistors

K. P. Pernstich, B. Rössner, B. Batlogg

As a basic transport property of solids, the Seebeck coefficient S provides deep insight as it is given by the entropy transported by thermally excited charge carriers and involves in the simplest case only electronic contributions where the transported entropy is determined by details of the band structure and scattering events. We have succeeded for the first time to measure the temperature- and carrier density dependent thermopower in Rubrene single crystal transistors and in pentacene thin film transistors [1]. Fig. 1.2 shows the gate voltage dependent Seebeck coefficient in a Rubrene transistor measured at various gate voltages and temperatures. Also shown in Fig. 1.2 is the calculated Seebeck coefficient that has been obtained from a numerical model and the separately measured transistor characteristics. By using the transistor model, we were able to predict the gate voltage and the temperature dependence of the Seebeck coefficient, which allowed us to determine the parameter $\mathcal{A}$ in the general equation of S in a semiconductor

$$S = \frac{k_B}{e}\left(\frac{E_F - E_v}{k_B T} + \mathcal{A}\right) \tag{1.1}$$

The value of the parameter $\mathcal{A}$ falls in the narrow range of $2...4$ which is well within the range of the electronic contribution in conventional inorganic semiconductors. This close agreement highlights the similarity of transport mechanisms in organic and inorganic semiconductors. Charge and entropy transport in these devices is best described as band-like transport of quasiparticles that are subjected to scattering, with exponentially distributed in-gap trap states, and without further contributions to S.

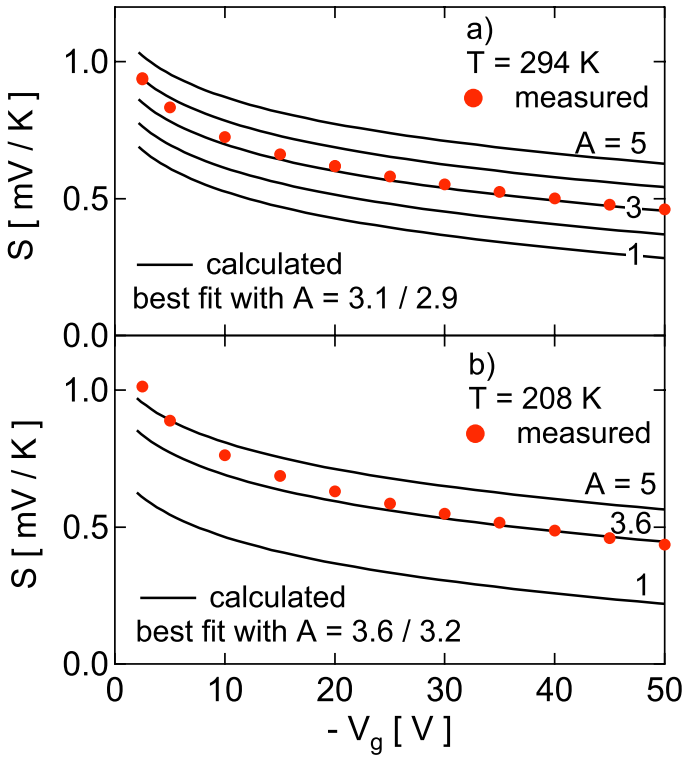

Figure 1.2: Measured and calculated Seebeck coefficient in a Rubrene single-crystal field-effect transistor at various gate voltages and temperatures. The value of the parameter $\mathcal{A}$ is consistent with values found in conventional inorganic semiconductors.

[1] K. P. Pernstich, B. Rössner, and B. Batlogg, Nature Materials 7, 321-325 (2008).

1.3 Defect healing at room temperature in pentacene thin films and improved transistor performance

W. L. Kalb, F. Meier, K. Mattenberger, and B. Batlogg

Charge transport in organic semiconductors takes place in extended states above a mobility edge. The charge carriers, however, are multiply trapped by and thermally released from trap states below the mobility edge. Consequently, trap states are of crucial importance to the performance of organic field-effect transistors. We observed a healing of structural defects at room temperature in the prototypical organic semiconductor pentacene.

Pentacene thin-film transistors were fabricated by thermal evaporation and were characterized *in situ* by gated four-terminal measurements. Under high vacuum conditions (base pressure of order 10^{-8} mbar), the device performance improves with time. The effective field-effect mobility increases by as much as a factor of two and the contact resistance decreases by more than an order of magnitude. Oxygen/nitrogen exposure and annealing experiments reveal, that the improvement of the electronic parameters is driven by a healing of structural defects at room temperature and not by chemical doping. This peculiar effect is a direct consequence of the weak van der Waals type intermolecular interaction which is characteristic of organic semiconductors.

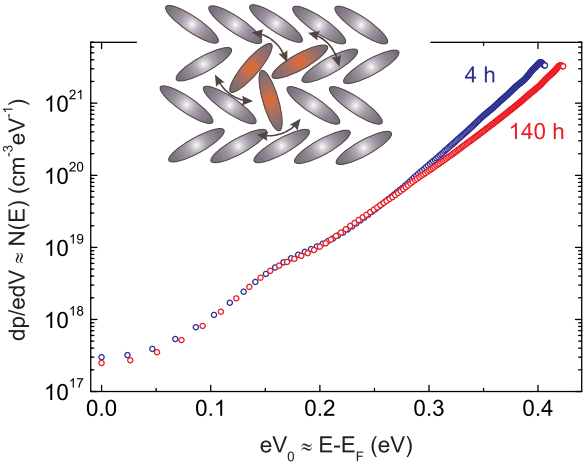

Figure 1.3: Due to the weak van der Waals type interaction between the pentacene molecules, some structural defects within the crystals "anneal" even at room temperature. This leads to a reduction in density of shallow traps close to the valence band edge.

To gain information about the energies and densities of the charge carrier traps caused by the structural defects, the spectral density of states was extracted from the transistor characteristics with a straightforward scheme. The scheme allows for a calculation of the trap densities with high accuracy. The performance improvement could thus be related to a reduction in the density of shallow traps $\leq 0.15\,\mathrm{eV}$ from the valence band edge, while the energetically deeper traps are essentially unaffected.

1.4 X-ray induced trap states in organic semiconductors

T. Morf, S. Haas, B. Batlogg

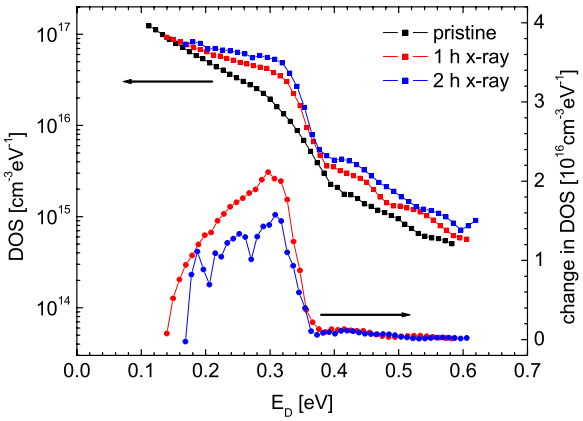

Figure 1.4: Density of states in the band gap of a rubrene single crystal. When exposed to x-ray radiation ($8\,keV$) for one hour, the DOS increases significantly in the range of 0.18 – $0.35\,eV$.

Localised states in the band gap of organic semiconductors are an important limitation to intrinsic conductivities as they are able to trap a large part of the injected space charge. The understanding of processes introducing such states is therefore of great significance for the development of industrial products based on organic semiconductor technology.

Temperature-dependent space-charge limited current spectroscopy probes the density of states (DOS) by shifting the quasi-Fermi level towards the conducting band edge. In a controlled degradation experiment, we here studied the formation of trap states in response to x-ray irradiation. High quality rubrene crystals with an inital trap state density of $10^{15} - 10^{17}\,cm^{-3}eV^{-1}$ are exposed to x-rays for one and two hours. Due to radiation exposure the trap DOS increases by up to one order of magnitude in the range of 0.18 – $0.35\,eV$ from the conducting band edge. The newly formed states are partially attributed to chemical defects while the structural ones are annealed at elevated temperature.

1.5 Direct link between high temperature Na-vacancy ordering and low temperature magnetism in Na_xCoO_2

J. Kanter, V. Wittwer, T. F. Schulze, P. Häfliger, K. Mattenberger and B. Batlogg

The sodium cobaltates (Na_xCoO_2), built of CoO_2 layers intercalated with Na ions, constitute an interesting model system for studying the interplay between localized spins and itinerant charge carriers on a triangular lattice. The rich phenomenology as a function of sodium concentration (Na_xCoO_2 displays an enhanced thermopower, various magnetic orderings and even superconductivity when hydrated) has lead to many studies about the doping dependence of physical properties and the underlying phenomena. One main reason for the rich phase diagram is that the Co-d bands, origin of the electronic properties, are strongly influenced by the Na sheets, both through valence tuning (the sodium atoms are each donating an electron) and through the Coulomb potential landscape of the Na ions. In addition to the well know dependence on sodium concentration, we found that for x $\approx$ 0.80 - 0.85 the magnetic ground states at low temperatures (i.e. below 22 K) are controlled by the cooling speed through a temperature range of 200-240 K, below 200 K Na loses its mobility, i.e. the ability to change sites within a sodium layer. A slow cooling process ($<$ 10 K/min) leads to newly found phase transition at 8 K which is suppressed by fast cooling ($>$ 40 K/min) but results in turn in a phase transition at 15 K. This proves that not only the sheer Na concentration but as well the Na patterning are responsible for influencing the CoO_2-layers. The fast cooling process affects the sodium ordering by suppressing either reordering or healing processes of the sodium superstructures. Using this dependence might lead to a better understanding of the magnetic ground states of this compound.

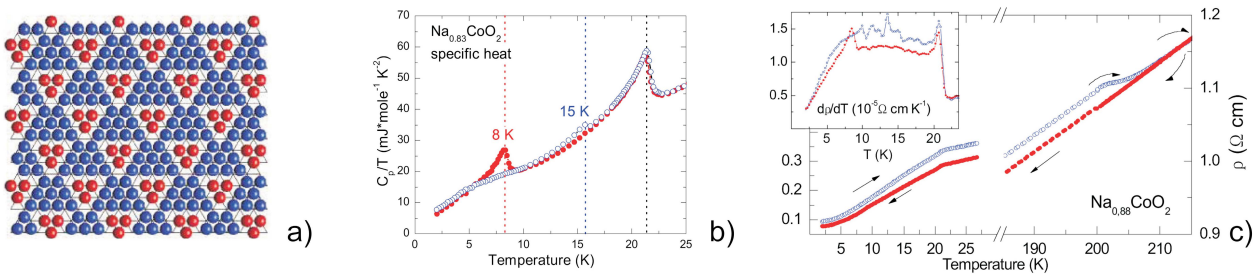

Figure 1.5: **a)** is showing a possible sodium superstructure, red dots represent occupied Na1 positions, i.e. Na ions sitting directly above a Co ion, blue dots are Na2 positions, Na2 are energetically more favourable than Na1 positions but Coulomb repulsion between Na ions leads to the occupation of Na2 sites, figure from Roger et al Nature **445**, 631 (2007) **b)** specific heat data in the slow cooled (red) and fast cooled (blue) state showing the 8 K, respectively 15 K transition **c)** resistivity measurements reveal the transition process from the fast to the slow cooled state around 200 K, the inset shows the temperature derivative of ρ, the 8 and 15 K transitions can be seen

1.6 High pressure crystal growth, thermodynamics and physical properties of $Al_xGa_{1-x}N$

A. A. Belousov, S. Katrych, P. Wägli, J. Karpinski and B. Batlogg

$Al_xGa_{1-x}N$ bulk single crystals with x=0.85 at % were synthesized from the solution in Ga melt under high pressure (up to 10 kbar) and high temperature using the high nitrogen gas pressure system. Typically, a growth run lasted for 5-6 days at about 7 kbar and at 1800°C, using a constant thermal gradient of about 20K/cm. The synthesized crystals are colorless, up to 0.8x0.8x0.8 mm^3 in size and have a hexagonal shape (Figure 1.6).

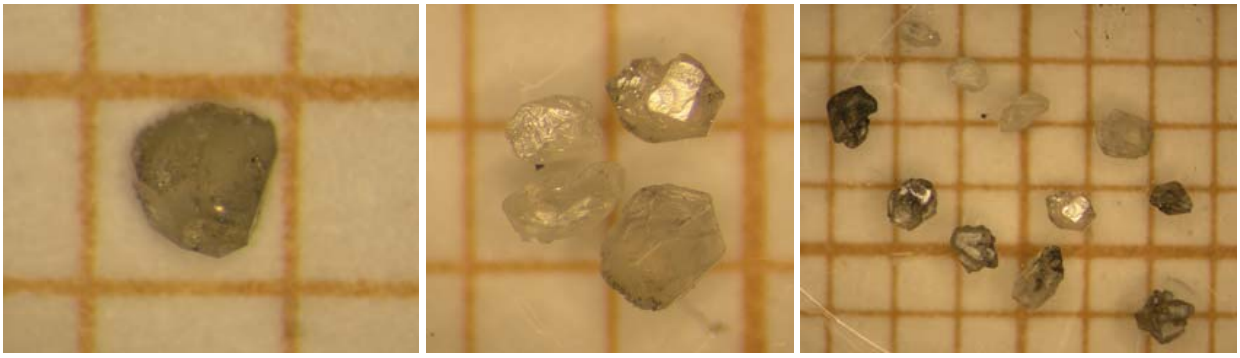

Figure 1.6: $Al_xGa_{1-x}N$ (x=0.8 - 0.85) crystals grown at 7 kbar and 1780°C.

As precursor for the crystal growth, polycrystalline $Al_yGa_{1-y}N$ pellets have been synthesized in an anvil apparatus. The pellet was placed in the Ga melt in the upper part of graphite crucible that has an internal diameter of 7.8 mm and 70 mm length. The amount of $Al_yGa_{1-y}N$ was chosen so that the total concentration of aluminium in the Ga melt should not exceed 1 at % (typically 0.4 - 0.55 at %). The applied pressure and temperature during the synthesis, especially during the cooling, have been optimized in order to prevent the growth of GaN crystals.

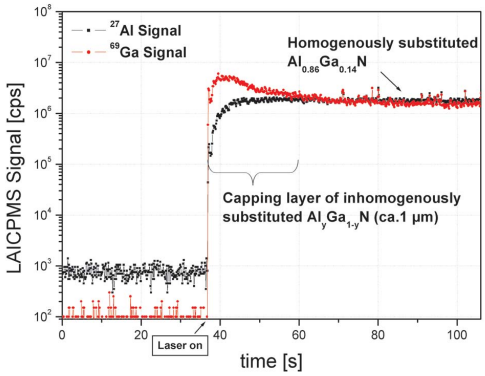

Figure 1.7: Depth profile of Al/Ga composition using LAICP Mass Spectrometry.

The EDX measurements confirmed the growth of the Al-GaN phase. No evidence of any additional phases such as oxides were found. The structure refinement of various crystals, determined by 2 four-circle Oxford x-ray diffractometer using Mo radiation equipped with a CCD showed the hexagonal $Al_xGa_{1-x}N$ phase and the structure refinement gave an aluminium content of 80-85 at %. The typical c-axis lattice constant of $Al_xGa_{1-x}N$ (x=0.85) was 5.015(1) Å, smaller than that of pure GaN (5.185 Å). This is assumed to be due to the smaller Al atomic radius (1.18 Å) than Ga (1.26 Å). The preferred crystal growth on the wall and bottom of crucible is along the c-axis. LAICP Mass Spectrometry was performed using an ArF excimer laser (193nm) for ablation the $Al_xGa_{1-x}N$ crystals in a He flow and it showed the constant distribution of Al content of about 86 at % in the bulk, in agreement with X-ray diffraction measurements (Figure 1.7). A thin, inhomogenously substituted $Al_yGa_{1-y}N$ capping layer with lower Al content forms on the crystal surface during the final cool-down of during the growth phase. The layer thickness is estimated to be in range of ca. 1 μm. Oxygen, carbon (as dopants), or nitrogen can not be detected due to a high analytical background.

1.7 Exploring InN crystal growth: phase stability studies.

A. A. Belousov, J. Jun, J. Karpinski and B. Batlogg

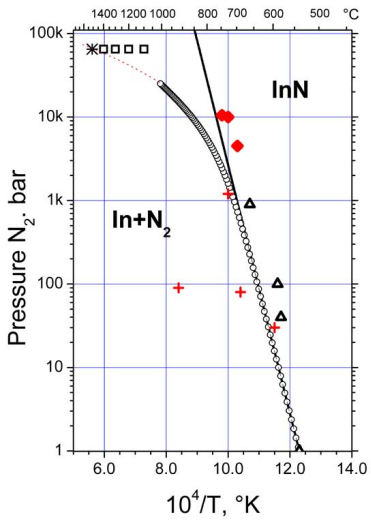

Figure 1.8: p-T equilibrium diagram of InN

A hemispherical anvil high pressure cell, capable of reaching 70 kbar, was used to investigate thermodynamic properties and synthesis of InN crystals. InN is characterized by the highest nitrogen equilibrium pressure among III-V nitrides. Available experimental data are not enough to evaluate the InN/In phase diagram at high pressure and at high temperature above 920°C. The p-T equilibrium curve was studied by decomposition of InN under high pressure of about 65 kbar (Figure 1.8). Metallic Indium was placed in a BN crucible together with InN powder, serving as a nitrogen source. The setup is completed by a graphite heater and a ceramic cell was used as a solid pressure transmitting medium. Under pressure of 65 kbar the decomposition of InN starts at 1510°C. After 1 hour dwell time at 1510°C the InN powder is completely decomposed. Thereby the kinetics of the process plays a major role and at this temperature the decomposition is rather fast. The figure 3 summarizes the data obtained from InN decomposition experiments (symbols: o - calculated curve described in text, square - and * - high pressure annealing: InN undecomposed and InN decomposed respectively, straight line - extrapolation of ideal gas approximation according to MacChesney's data [1] and some data points from the literature [1,2].) Assuming that at 1 bar, InN is in equilibrium with its constituents at 813°C, we evaluated the equilibrium p-T curve of the reaction InN$\longleftrightarrow$ In+1/2 N_2 (circled line) by using the van't Hoff equation. At higher pressure the chemical potential (free energy) cannot longer be described by the logarithm of pressure but the pressure for real gases has to be replaced by the fugacity **f**. The fugacity coefficient as function of pressure and temperature was calculated up to 25 kbar pressure according to the numerically estimated equation of J. Unland et. al [3]. As it can be seen in the figure 3, our experimental points are comparable with the calculated data extrapolated to the high pressure. As at high temperature (up to ca. 1400°C) InN seems to be stable it might be possible to synthesize InN crystals from the solution in In melt.

References:

[1]- T. Detchprohm, K. Hiramatsu, K. Itoh and I. Akasaki, Relaxation process of the internal strain in the GaN/a-Al_2O_3 heterostructure and determination of the intrinsic lattice constants of GaN free from the strain, Jap. J. Appl. Phys., Part 2 Letters, 31 (10B), 1992, pp. 1454-1456.

[2] - J.B.MacChesney, P.M. Bridenbaugh and P.B. O'Connor, Mater. Res. Bull. 5. (1970), 783-792.

[3] - J. Unland et al., J. Crystal Growth, 256 (2003), 33-51.

1.8 New high pressure polymorphic modification of KOs_2O_6

S. Katrych, Z. Bukowski, N.D. Zhigadlo, J. Karpinski

A new compound, the representative of a new structural type was synthesized employing high pressure technique (Pearson symbol a*P*18, *a*=5.5664(2) Å, *b*=6.4554(3) Å, *c*=7.2363(3) Å, α=65.398(4) °, β=70.546(3) °, γ=75.679(3) °, space group P-1, no. 2). Its structure was determined by single-crystal X-ray diffraction.

This structure is a polymorphic modification of the cubic KOs_2O_6 pyrochlore and reveals close structural relation to this compound, which is superconductor at 9.6 K [1]. The high pressure triclinic KOs_2O_6 modification is about 17 % more dense than the cubic prototype. It is very interesting that, as in the cubic KOs_2O_6 - pyrochlore structure [2], the structure of triclinic KOs_2O_6 involves a network with the same OsO_6 octahedra as the building blocks, and K atoms are located in the big voids (Figure 1.9).

The calculated enthalpies of formation show that both phases are stable at normal pressure and have almost the same enthalpy, but at high pressure the formation of the triclinic modification is energetically more favourable than formation of cubic prototype. Formation of triclinic KOs_2O_6 could explain the vanishing of superconductivity in the cubic KOs_2O_6 at high pressure [3]. We found that a first order phase transition between both structures occurs at high pressure (3 GPa) and high temperature (900 °C).

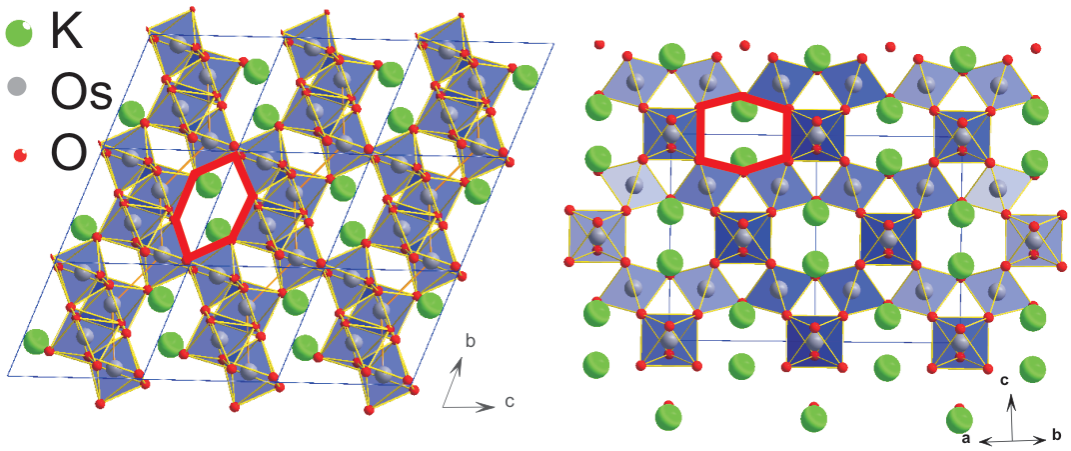

Figure 1.9: Schematic representation of KOs_2O_6 crystal structures. Left side: 3x3x3 unit cells projection of a triclinic KOs_2O_6 along the a direction. Right side: unit cell projection of a cubic pyrochlore KOs_2O_6. Red polygons indicate the big voids where K atoms are located.

References:

[1] S. Yonezawa; Y. Muraoka; Y. Matsushita; Z. Hiroi, Journal of Physics-Condensed Matter 2004, 16, (3), L9-L12.

[2] J. Yamaura; S. Yonezawa; Y. Muraoka; Z. Hiroi, Journal of Solid State Chemistry 2006, 179, (1), 336-340.

[3] T. Muramatsu; N. Takeshita; C. Terakura; H. Takagi; Y. Tokura; S. Yonezawa; Y. Muraoka; Z. Hiroi, Physica B-Condensed Matter 2006, 378-80, 882-883.

1.9 Studies of intermetallic compounds with the Ir_3Ge_7-type structure. Mo_3Sb_7 - superconductor exhibiting a spin-gap in the normal state.

Z. Bukowski, J. Karpinski and B. Batlogg, in collaboration with V. H. Tran (Inst. Low Temp. Wroclaw, Poland)

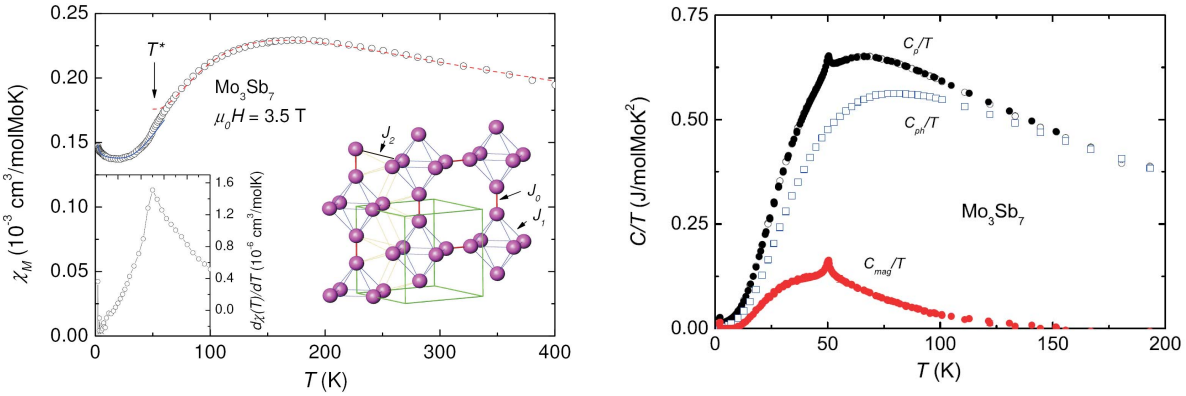

Figure 1.10: Left: Magnetic susceptibility of Mo_3Sb_7 measured at 3.5 T. The susceptibility below T^* follows $\chi_M(T) =\sim exp(-2\Delta_c/k_BT)$, as predicted for a spin-gap systems. The insets show the temperature derivative of the magnetic susceptibility and the schematic crystal structure of Mo_3Sb_7 with Mo ions only (solid spheres). The intradimer J_0 and interdimer exchange interactions J_1 and J_2 are indicated. Right: The specific heat of Mo_3Sb_7 divided by temperature as a function of temperature. The phonon specific heat was calculated from the phonon part of specific heat of $Ir_3Ga_3Ge_4$ after correction of the mass effect. The magnetic specific heat is the difference C_{mag} = $C_p(Mo_3Sb_7)$ - γT - C_{ph}.

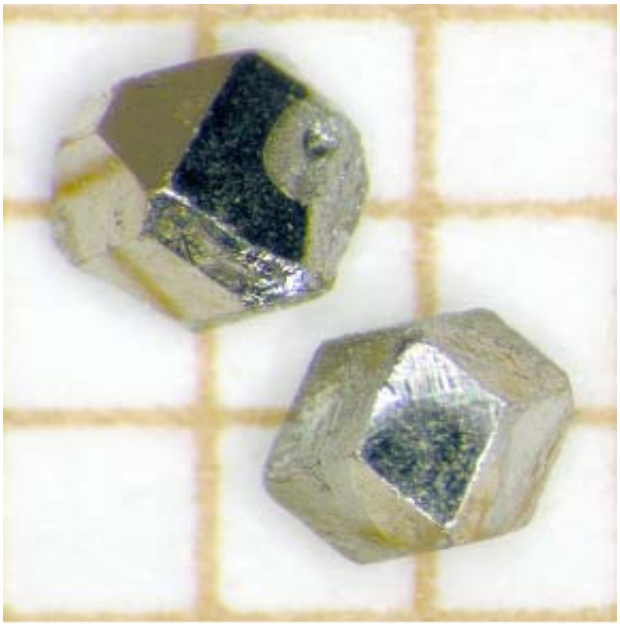

Figure 1.11: Single crystals of Pt_3In_7 grown from In flux.

The intermetallic compounds T_3X_7 (T=transition metal; X=As, Sb, Ge, Sn, Ga, In) crystallize with the D8*f*-type structure (cubic Im3m space group). Superconductivity has been observed for Ir_3Ge_7 (T_c=0.87 K) and Mo_3Sb_7 (T_c=2.2 K). Our magnetization, specific heat and electrical resistivity measurements on polycrystalline Mo_3Sb_7 revealed another anomalous feature at 50 K which has been attributed to the opening of a spin-gap [1].

We have successfully grown single crystals of Pt_3In_7 - another member of the family of Ir_3Ge_7-type compounds. It shows diamagnetic properties down to 2 K. Further studies are in progress.

[1] V. H. Tran, W. Miiller, Z. Bukowski, Phys. Rev. Lett., (2008)

1.10 Influence of Mg deficiency in MgB_2 single crystals on crystal structure and superconducting properties

N.D. Zhigadlo, S. Katrych and J. Karpinski

The influence of Mg deficiency in MgB_2 single crystals on crystal structure and superconducting properties has been investigated. To this end MgB_2 single crystals were annealed in vacuum ($4x10^{-6}$ mbar) at various temperatures between 800 and 1000 °C for 2 hr followed by cooling at 300 °C/h to room temperature. After each step of annealing, single crystals were characterized by SQUID magnetometry and single crystal X-ray diffraction. The results show that MgB_2 is a stable phase up to 975 °C. Increasing the annealing temperature results in a slight broadening of the superconducting transition from 0.55 K at 800 °C to 1.3 K at 975 °C (Fig. 1.12b). The critical temperature T_c=38.7 K has not been changed with annealing, but the magnetic moment decreases at annealing temperatures above 850 °C, which indicate lowering of the superconducting volume fraction (Fig. 1.12a). The Mg deficiency was determined by X-ray structural refinement. The Mg deficiency slightly increased with the annealing temperature until complete decomposition of MgB_2 at 1000 °C (Fig. 1.12a). Crystal annealed at 975 °C has composition $Mg_{0.92}B_2$. X-ray diffraction analysis shows that the final product of decomposition is polycrystalline MgB_4. MgB_4 is the product expected for decomposition of MgB_2 due to Mg volatility at elevated temperatures. The decomposition of MgB_2 can thus be described as follows: $2MgB_2(s)=MgB_4(s)+Mg(g)$.

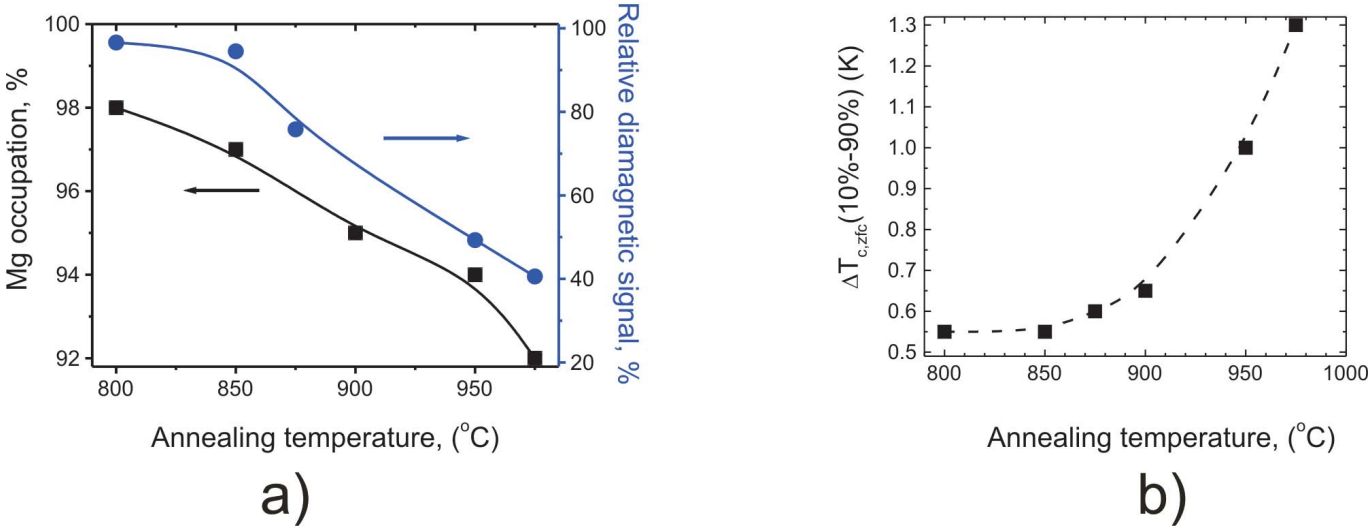

Figure 1.12: a) Mg occupation in MgB_2 single crystals and relative diamagnetic signal measured on annealed crystals as a function of annealing temperature in vacuum. b) Broadening of the superconducting transition width as a function of annealing temperature.

1.11 GaN/Si(111) heteroepitaxy

B. Alloing, P. Cristea, H. von Känel
in collaboration with E. Choumas, M. Kummer (EpiSpeed AG)

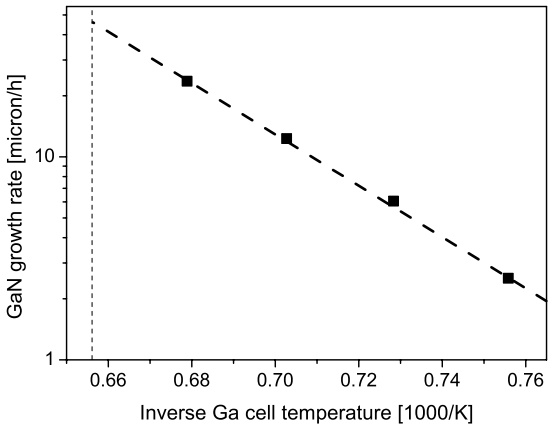

Figure 1.13: GaN growth rate on Si(111) as a function of inverse temperature of the Ga effusion cell. The dashed vertical line corresponds to an effusion cell temperature of 1250^{o} C.

The development of a new process for the economical deposition of group III nitride layers was continued. This process, called low-energy plasma-enhanced vapor phase epitaxy (LEPEVPE), is based on elemental metal and nitrogen sources rather than toxic gases as are used in metal-organic chemical vapor deposition (MOCVD). The experiments were carried out on a custom-built tool suitable for 2-inch substrates designed by the industrial partner. Epitaxial GaN layers were grown at exceptional rates onto AlN/Si(111) substrates in magnetically confined high-density DC plasmas (Fig. 1). X-ray diffraction experiments did not reveal any indications of diminished crystal quality or even epitaxy break down at growth rates above 20 μm/h. Layer morphology, thickness uniformity, process stability and scalability turned out to be incompatible with magnetically confined DC plasmas. A second generation 4-inch tool is therefore based on an inductively coupled RF plasma source. The tool was again developed by the industrial partner, and is currently undergoing the initial hardware tests.

1.12 Pressure dependence of the optical properties of the charge-density-wave compound $LaTe_2$

M. Lavagnini, A. Sacchetti and L. Degiorgi

work in collaboration with E. Arcangeletti, L. Baldassarre, P. Postorino, S. Lupi and A. Perucchi, Università "La Sapienza" Rome, Italy, and K.Y. Shin and I.R. Fisher, Stanford University, California, U.S.A.

Peierls was the first, in the early sixties, to predict the formation of a charge-density-wave (CDW) ground state for one-dimensional (1D) metals, when turning on the electron-phonon interaction. The CDW phase transition relates to a balance between electronic energy and lattice structural stability. For 1D metals it is energetically favorable to introduce a lattice distortion which, combined with a so-called Fermi-surface (FS) nesting, leads to a novel collective charge ordering. The formation of the CDW condensate implies the opening of a gap on FS and therefore the lowering of the overall electronic energy.

The discovery of superconductivity at high temperature in the low-dimensional layered-like cuprates also induces a revival of interest in the prototype CDW systems, because they provide excellent opportunities for theoretical investigation towards how strongly-correlated electron-phonon systems behave and how electron-phonon interaction affects the band structure. In this context the rare-earth polychalcogenide $R\mathrm{Te}_n$ (R stays for rare earth, and n= 2, 2.5 and 3) systems have attracted a great deal of interest, due to their intrinsic low dimensionality. Their crystal structure shares some similar features with that of the cuprates, both in terms of the symmetry and also in terms of having two-dimensional layers which are responsible for the electronic properties and which are doped by interleaving block layers. The interest on these systems principally resides in the onset at high temperature of a CDW broken symmetry ground state, driven by a suitable FS nesting.

Recently, we have intensively investigated the $R\mathrm{Te}_3$ and $R\mathrm{Te}_2$ series by optical means. Our first optical reflectivity data on $R\mathrm{Te}_3$ (R=La, Ce, Nd, Sm, Gd, Tb and Dy), collected over an extremely broad spectral range, allowed us to observe both the Drude component and the single-particle peak, ascribed to the contributions due to the free charge carriers and to the excitation across the CDW gap, respectively. We have then measured the pressure dependence of the optical reflectivity on CeTe_3 at 300 K (i.e., in the CDW state). Upon increasing the externally applied pressure the excitation due to the CDW gap decreases, in a quite equivalent manner when compressing the lattice by substituting large with small ionic radius rare-earth elements (i.e., by reducing the lattice constant a). Furthermore, the metallic (Drude) weight was found to be moderately enhanced with chemical pressure (i.e., along the rare earth series). These results demonstrate that chemical and applied pressure similarly affect the electronic properties and equivalently govern the onset of the CDW state in $R\mathrm{Te}_3$.

The latest optical investigation of the related rare-earth di-tellurides $R\mathrm{Te}_2$ (R= La and Ce) confirms our previous findings on $R\mathrm{Te}_3$. We have extracted the energy for the CDW gap and found that the CDW collective state gaps a large portion of the Fermi surface. Analogous to CeTe_3 pressure dependent optical investigations may be of great relevance, since applied pressure might affect to some extent the electronic structure and the CDW condensate in $R\mathrm{Te}_2$, as well. It is then instructive to establish a comparison between the physical properties of the two classes of rare-earth telluride compounds upon lattice compression.

We have then studied the pressure dependence of the optical response of LaTe_2, which is deep in the charge-density-wave (CDW) ground state even at 300 K. The reflectivity spectrum $R(\omega)$ (Fig. 1.14) is collected in the rather large mid-infrared spectral range at room temperature and at pressures between 0 and 7 GPa. These are important prerequisites in order to expand and precisely interpolate our measured spectra within the phenomenological Lorentz-Drude approach and consequently in oder to extract the energy scale due to the single particle excitation (ω_{SP}) across the CDW gap and the Drude weight (i.e., the plasma frequency ω_p). The low pressure $R(\omega)$ reproduces the depletion around 5000 cm^{-1}, already observed at ambient pressure and ascribed to the onset of the CDW gap excitation. The striking feature in Fig. 1.14 is the progressive increase with increasing pressure of the reflectivity signal, accompanied by the filling-in of the deep minimum in $R(\omega)$ at about 5000 cm^{-1}. We established that the gap decreases upon compressing the lattice, which shares common features with the behavior seen previously in the $R\mathrm{Te}_3$ series and in our recent data on CeTe_3 under pressure (Fig. 1.15). This signals a reduction in the quality of nesting upon applying pressure, therefore

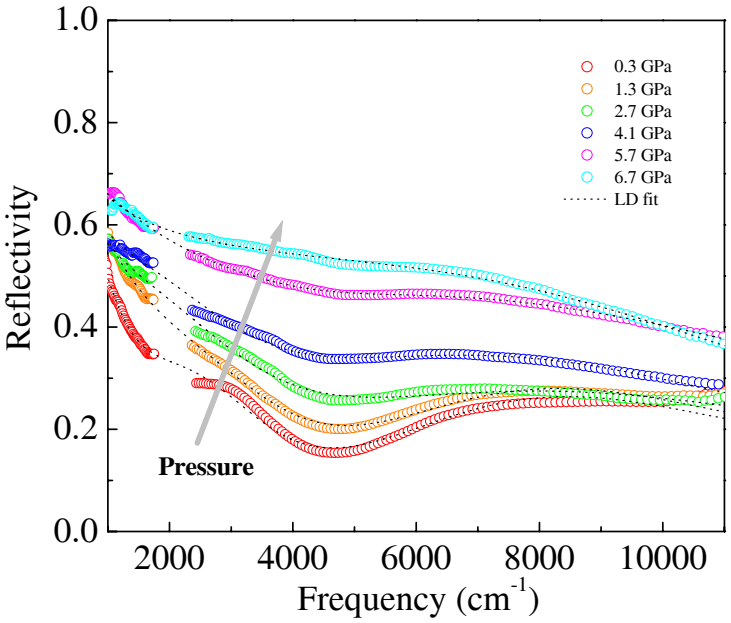

Figure 1.14: Pressure dependence of the reflectivity spectra $R(\omega)$ in the mid-infrared spectral range of $LaTe_2$ at 300 K. The arrow indicates the trend of the reflectivity data upon increasing pressure. The $R(\omega)$ points in the energy interval of the diamond absorption (i.e., 1700-2300 cm^{-1}) have been omitted. The thin dotted lines are fits to the data within the Lorentz-Drude (LD) approach.

inducing a lesser impact of the CDW condensate on the electronic properties of $LaTe_2$. The consequent suppression of the CDW gap leads to a release of additional charge carriers, manifested by the shift of weight from the gap feature into the metallic component of the optical response and indicated by the enhancement of ω_p (inset of Fig. 1.15).

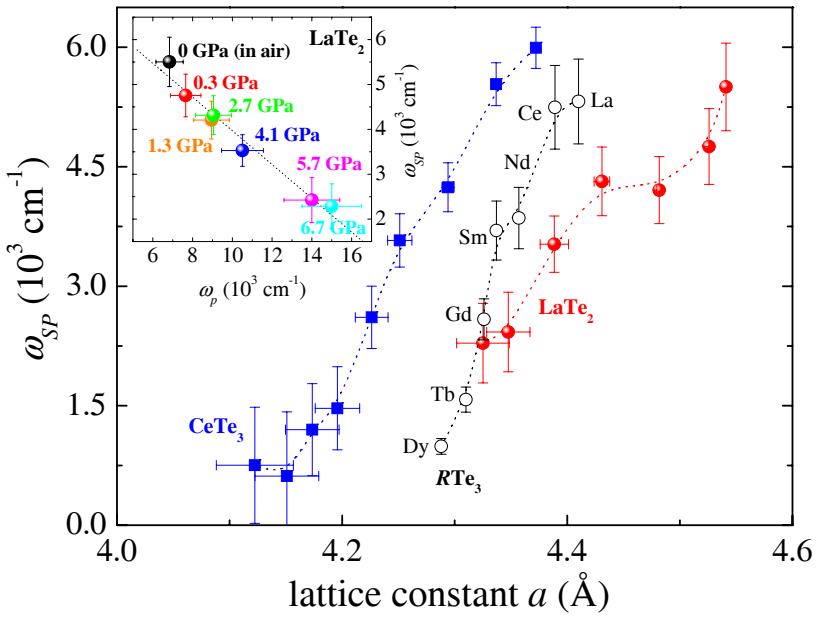

Figure 1.15: Single particle peak energy ω_{SP} (i.e., the CDW gap) as a function of the lattice constant a for $LaTe_2$, $CeTe_3$ and the RTe_3 series. Inset: single particle peak energy ω_{SP} versus plasma frequency ω_p for $LaTe_2$, as a function of pressure. Pressure is here an implicit variable.

Finally, it is worth mentioning that the investigated spectral range as a function of pressure is broad enough to allow furthermore educated guesses on the issue to which extent the applied pressure may influence the effect of electron-electron interactions. The power-law behavior, seen in the optical conductivity at energies above the gap excitation and indicating a weakly interacting limit within the Tomonaga-Luttinger liquid scenario (not shown here), seems to be only moderately dependent on pressure. Therefore, the lattice compression weakly affects the electronic correlations in $LaTe_2$.

1.13 Magneto-optical behavior of $EuIn_2P_2$

F. Pfuner and L. Degiorgi

work in collaboration with H.R. Ott, ETH Zurich, and A. Bianchi and Z. Fisk, Department of Physics, University of California at Irvine, U.S.A.

$EuIn_2P_2$ belongs to the broad class of materials known as Zintl compounds. The Zintl concept for the formation of compensated-valence intermetallic compounds is based on a complete charge transfer from an alkali or alkaline-earth element to a post-transition element of the groups 13 (IIIA) or 15 (VA) in the periodic table. The concept was later extended to synthesize more complicated intermetallic compounds with new types of structures and a variety of physical properties, such as magnetic order and superconductivity. Concerning magnetism, Zintl-phase compounds with rare-earth elements as one of the regular constituents were investigated. For $EuIn_2P_2$, the magnetic order involves the local moments of the partially occupied Eu 4f-electron orbitals and is thought to be induced by common exchange interactions. In the latter case, the onset of magnetic order is accompanied by a considerable reduction of the electrical resistance in the ordered state and related magnetoresistance effects upon the application of external magnetic fields. In view of similar observations in previous studies of materials, such as the perovskites LVO_3 (L=La, Lu and Y), EuO and EuB_6, and the discovery of giant magneto-optical effects, at least in EuB_6, it seemed of interest to probe the optical properties of $EuIn_2P_2$ in a wide spectral range and, in addition, their variation with temperature and external magnetic field.

Figure 1.16 displays the measured optical reflectivity $R(\omega)$ as a function of temperature (panel (a)), and as a function of magnetic field at 10 and 30 K (panels (b) and (c)), respectively. The main panels of Fig. 1.16 emphasize the far-infrared (FIR) range, where the temperature and magnetic field dependences are significant. Above 50 K the magnetic field dependence is negligible. The inset of Fig. 1.16(a) displays $R(\omega)$ across the entire measured spectral range at room temperature. It exhibits a metallic component with a plasma edge at very low frequencies ($\omega \leq$250 cm^{-1}), a strong infrared active phonon mode, peaking at 270 cm^{-1} with a shoulder on its high frequency tail, a broad excitation centered at 600 cm^{-1} and several absorptions above 1000 cm^{-1}. The strong absorption centered at 600 cm^{-1} bears a striking similarity with what has been often observed in heavy-electron or Kondo materials and was ascribed to excitations across the hybridization gap (hg). For each combination of temperature and magnetic field the high-frequency parts of all spectra merge. Remarkable is the extremely low plasma edge which suggests that $EuIn_2P_2$ is a system with a low itinerant charge-carrier density. The reflectivity is significantly influenced by magnetic field [Fig. 1.16(b) and 1.16(c)], much less so, however, by temperature [Fig. 1.16(a)].

The decomposition of the optical properties into their characteristic components (i.e., metallic component, hg, phonon and interband transitions) also provides the basis for discussing the distribution of the spectral weight (S) in the absorption spectrum. To this end, the spectra were described within the phenomenological Lorentz-Drude approach, ascribing the Drude term to the metallic component and a selection of Lorentz harmonic oscillators (h.o.) to the finite frequency excitations. Figure 1.17 shows the spectral weight distribution for some of these components as a function of magnetic field at selected temperatures. Included are the effective metallic component, i.e., the Drude term plus its high frequency tail described by the h.o. at 150 cm^{-1}, the phonon signal at 270 cm^{-1} together with its high frequency shoulder at 310 cm^{-1} and the broad absorption peaking at 600 cm^{-1}. The most significant result of the spectral weight analysis presented in Fig. 1.17 is the remarkable gain of spectral weight of the effective metallic component (i.e., for frequencies $\omega \leq$ 200 cm^{-1}) and the hg feature centered at about 600 cm^{-1}. It is particularly pronounced at 30 K and even more so at 10 K [Fig. 1.17(a) and 1.17(b)]. The renormalized density of states is significantly enhanced both at low temperatures and in high magnetic fields and is due to the increasing hybridization between the localized 4f states and the itinerant states of the d bands. This immediately leads to an enhancement of the transition probability, across the hg, i.e., a gain of the mode strength. The enhancements of the metallic component and hg excitation tend to saturate in high magnetic fields at all temperatures. This saturation is actually expected because of the fully ordered magnetic state in high fields. The spectral weight for all components of $\sigma_1(\omega)$ remains almost constant at any fields above 50 K [Fig. 1.17(c)], confirming the direct experimental observation that at these temperatures, there is nearly no magnetic field dependence in the $R(\omega)$ spectra. In order to satisfy the optical sum rule, the gain of spectral weight of the low energy excitations of $EuIn_2P_2$ below 30 K is accounted for by an equivalent loss of signal at high energies, possibly above 1 eV. The transfer of weight from energies even higher than the experimentally covered spectral range

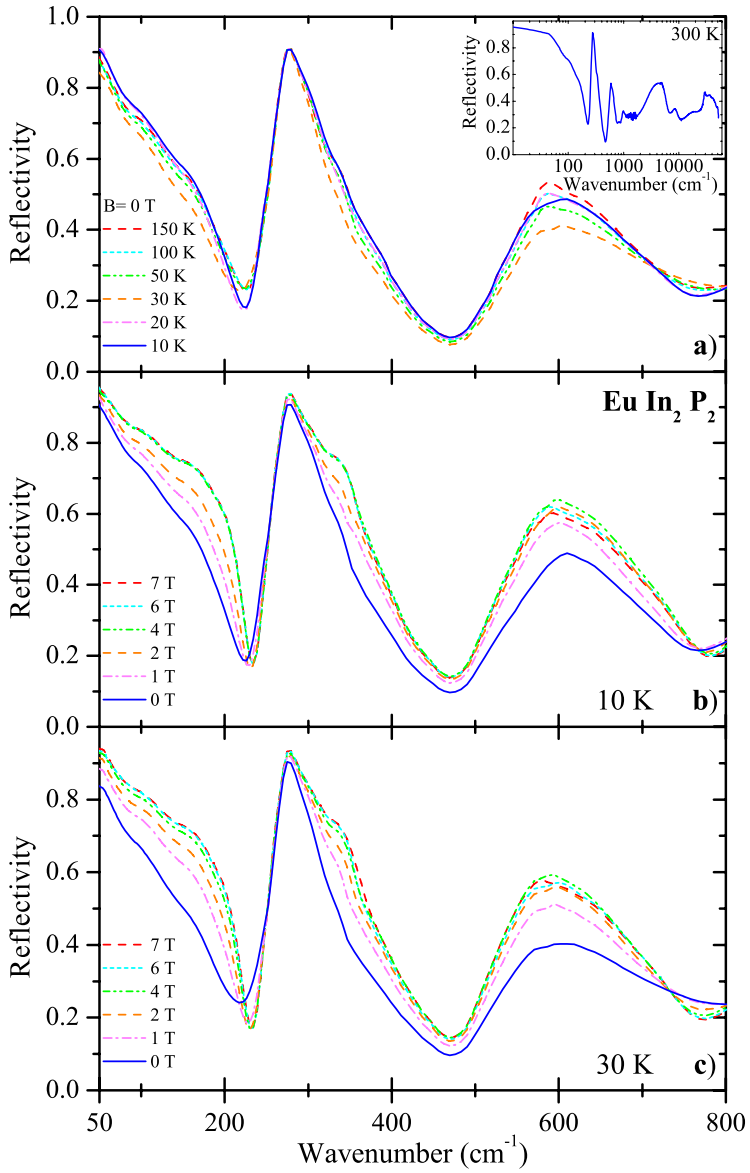

Figure 1.16: Reflectivity spectra $R(\omega)$ of $EuIn_2P_2$ in the infrared spectral range as a function of temperature at $B = 0$ T (a). Panels (b) and (c) show $R(\omega)$ at 10 and 30 K, and in magnetic fields between 0 T and 7 T, respectively. The inset in panel (a) displays $R(\omega)$ at 300 K in the whole measured spectral range (logarithmic energy scale).

seems to be a common feature of highly correlated systems.

The non-negligible enhancement of spectral weight in $\sigma_1(\omega)$ into the low-energy metallic component with increasing magnetic field implies a release of additional charge carriers upon spin polarizing the material. Therefore, $EuIn_2P_2$ shares common features with other CMR compounds. An intimate relation between the magnetization and the electronic conductivity, leading to large or colossal magnetoresistive effects (CMR), has been indeed identified in a variety of compounds (e.g., $Eu_{1-x}Ca_xB_6$ and the well-known manganites), which were intensively studied both experimentally and theoretically. In interpreting our data on $EuIn_2P_2$ as well as on the $Eu_{1-x}Ca_xB_6$ series we favored the recently developed concepts based on the double-exchange scenario, which, although by no means unique, catches some of the experimental findings. The reduced itinerant carrier concentration in these systems places the Fermi level near a magnetization dependent mobility edge, which emerges in the spectral density because of the disordered spin background. Within this scenario it may then be argued that the increasing magnetization due to increasing magnetic fields shifts the mobility edge away from the Fermi energy towards the lower band edge, therefore inducing substantial changes in the concentration of itinerant charge carriers. An obvious consequence of this scenario is the expectation of a redistribution of spectral weight between excitations at higher energies in the optical absorption spectrum and the Drude component. Since additional charge carriers are indeed released, the Drude weight then grows upon magnetizing the system.

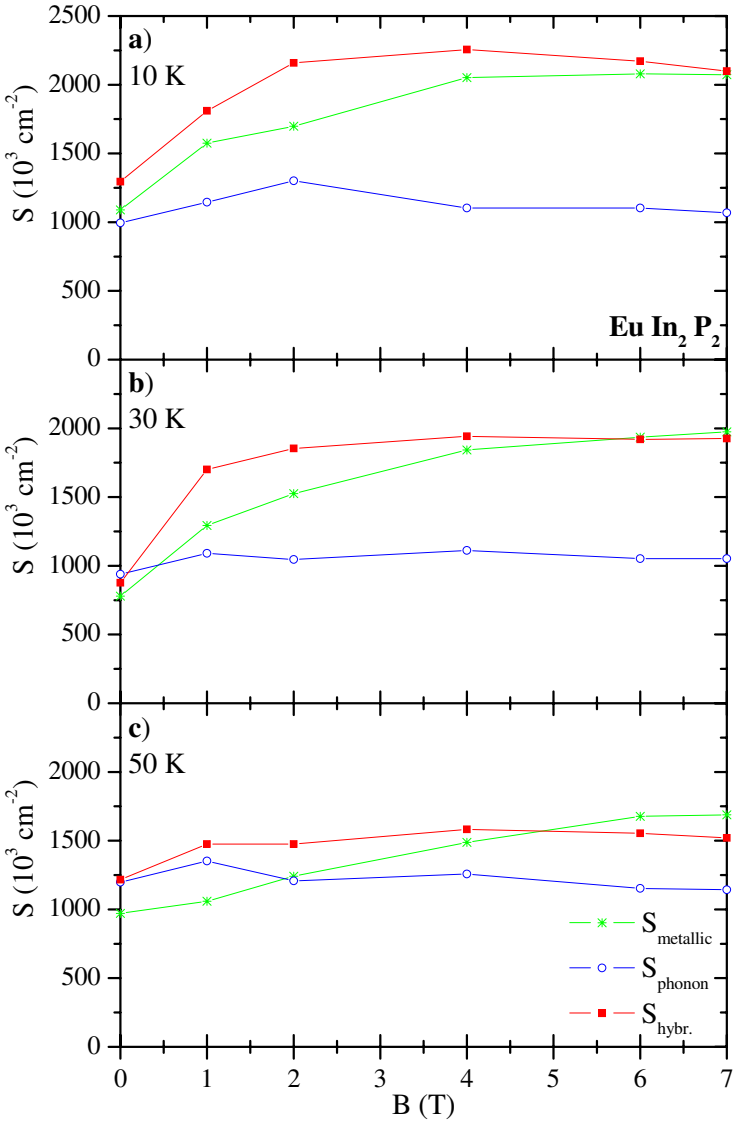

Figure 1.17: Magnetic field dependence of the spectral weight distribution at (a) 10, (b) 30 and (c) 50 K in the effective metallic component ($S_{metallic}$=ω_p^2(Drude)+ω_p^2(150 cm^{-1})), the lattice phonon mode (S_{phonon}=ω_p^2(270 cm^{-1})+ω_p^2(310 cm^{-1})) and the hybridization gap feature ($S_{hybr.}$=ω_p^2(600 cm^{-1})+ω_p^2(590 cm^{-1})). ω_p^2 is the squared plasma frequency and mode strength for the Drude term and h.o. at the resonance frequency given in the brackets, respectively.

Chapter 2

Physics of semiconductor nanostructures

(http://www.nanophys.ethz.ch)

Head
Prof. Dr. K. Ensslin
Prof. Dr. T. Ihn
Prof. Dr. R. Monnier

Academic Staff

Dr. Ilona Blatter	Simon Gustavsson	Thomas Müller
Dr. Milos Csontos	Magdalena Hüfner	Andreas Pfund
Susanne Dröscher	Dr. Slavo Kicin	Dr. Renaud Leturcq
Urszula Gasser	Yashar Komijani	Elisabeth Ruh
Arnd Gildemeister	Bruno Küng	Stephan Schnez
Davy Graf	Christian May	Dr. Ivan Shorubalko
Boris Grbic	Lorenz Meier	Dr. Christoph Stampfer
Johannes Güttinger	Francoise Molitor	Matthias Studer

Technical Staff

C. Barengo	P. Studerus

Administrative Staff
B. Abt

Academic Guests
Prof. Yigal Meir, Ben-Gurion University, Israel, 28.2. - 2.3.2007

Doctoral theses
Arnd Gildemeister
Scanning Gate Microscopy of Semiconductor Quantum Circuits
30.5.2007

Boris Grbic
Hole transport and spin-orbit coupling in p-type GaAs nanostructures
30.5.2007

Davy Graf
Electrons in reduced dimensions: from finite lateral superlattices in AlGaAs heterostructures to few-layer graphene
31.5.2007

Lorenz Meier
Manipulation of electron spins in quantum wells with magnetic and electric fields
1.6.2007

Diploma theses
Matthias Studer
Time-resolved transport of individual electrons through a double quantum dot
WS 06/07

Roland Krischek
Etched quantum dots in InAs nanowires with charge read-out
WS 06/07

Johannes Güttinger
Graphene Single Electron Transistor
SS 2007

Erich Schurtenberger
Graphene single electron transistor
HS 2007

Kevin Interbitzin
Transport in Carbon Nanotubes
HS 2007

2.1 Frequency-Selective Single-Photon Detection Using a Double Quantum Dot

S. Gustavsson, M. Studer, R. Leturcq, T. Ihn, and K. Ensslin, in collaboration with D. C. Driscoll and A. C. Gossard, University of California, Santa Barbara, USA

The interplay between quantum optics and mesoscopic physics opens up new horizons for investigating radiation produced in nanoscale conductors. Microwave photons emitted from quantum conductors are predicted to show nonclassical behavior such as antibunching and entanglement. Experimental investigations of such systems require sensitive, high-bandwidth detectors operating at microwave frequency. On-chip detection schemes, with the device and detector being strongly capacitively coupled, offer advantages in terms of sensitivity and large bandwidths.

The sample [see Fig. 2.1] was fabricated by local oxidation of a GaAs=AlGaAs heterostructure, containing a two-dimensional electron gas (2DEG) 34 nm below the surface. The structure consists of two quantum dots in series (marked by 1 and 2 in the figure) with a nearby quantum point contact used as a charge detector (lower-right corner of the figure). The dots are coupled via two separate tunneling barriers, formed in the upper and lower arms between the QDs

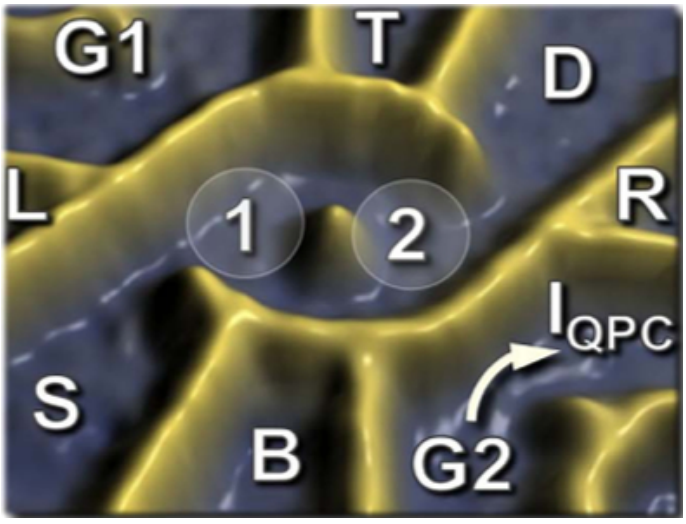

Figure 2.1: The sample fabricated by local oxidation of an AlGaAs heterostructure. The two quantum dots are marked by 1 and 2, a nearby quantum point contact by QPC.

The idea is sketched in Fig. 2.2, showing the energy levels of the double quantum dot (DQD) together with a quantum point contact (QPC) acting as a noise source. The DQD is operated with a fixed detuning δ between the electrochemical potentials of the left and right QD. If the system absorbs an energy $E = \delta$ from the environment, the electron in QD1 is excited to QD2. This electron may leave to the drain lead, a new electron enters from the source contact and the cycle can be repeated. The process induces a current flow through the system. Since the detuning may be varied continuously by applying appropriate gate voltages, the absorbtion energy is fully tunable.

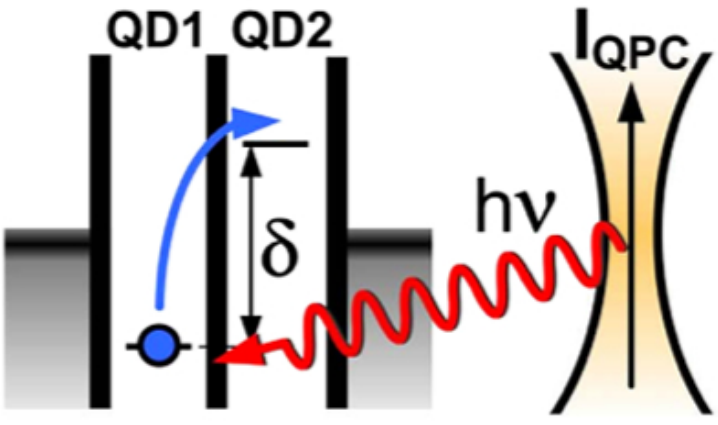

Figure 2.2: Schematic for operating a double quantum dot (DQD) as a high-frequency noise detector. The tunable level separation δ of the DQD allows frequency selective detection.

The scheme is experimentally challenging, due to low current levels and fast relaxation processes between the QDs. We have shown that these problems can be overcome by using time-resolved charge-detection techniques to detect single electrons tunneling into and out of the DQD. Apart from giving higher sensitivity than conventional current measurement techniques, the method also allows us to directly relate a single-electron tunneling event to the absorbtion of a single photon. The system can thus be viewed as a frequency-selective single-photon detector for microwave energies. This, together with the fact that the charge-detection methods allow precise determination of the device parameters, provide major advantages compared to other setups. To prove the principle of the device we have investigated the high-frequency spectrum of radiation emitted from a voltage-biased QPC. The emission rate was found to increase linearly with applied bias, with a spectrum having a sharp cutoff for frequencies higher than the QPC bias.

2.2 Suppression of Spin Relaxation in an InAs Nanowire Double Quantum Dot

A. Pfund, I. Shorubalko, K. Ensslin, and R. Leturcq, in collaboration with E. Gini, FIRST lab, ETH Zurich

Coherent spin manipulation has been demonstrated on quantum dots in GaAs heterostructures, benefiting from the high quality of these systems and the highly developed manufacturing technology. Alternative materials such as InAs may offer advantageous spin properties. The large electronic g-factor could allow for easier spin control with magnetic fields, while the enhanced spin-orbit interactions motivated recent proposals for purely electrical manipulation of individual spins.

Spin relaxation can be probed by the leakage current through a double quantum dot (DQD) in the Pauli spin blockade regime. We consider three different leakage processes: (i) cotunneling through the DQD, (ii) relaxation due to spin-orbit interaction, and (iii) relaxation as a result of hyperfine interaction with the nuclei of the host material. When studying the kinetics of different processes occurring in parallel, it is common to consider a global reaction rate as the sum of the individual rates. We show that the interplay between the different spin relaxation mechanisms can lead to more complex phenomena, and even to a pronounced reduction of the global relaxation rate.

The InAs nanowires (NWs) are catalytically grown using metal organic vapor phase epitaxy, and are subsequently transferred to an oxidized silicon substrate. Ohmic contacts and top gates are then created in a two-step lithographic process, yielding devices as shown in Fig. 2.3. We perform transport measurements in a dilution refrigerator at a base temperature of 30 mK. A magnetic field is applied perpendicular to the wire axis. Two quantum dots in series are formed along the NW by applying voltages to the top gates G1, G2, and GC. In the Coulomb blockade regime, the number of electrons (n, m) in dot 1 or 2 can be tuned with the gates G1/G2, while the gate GC is used to adjust the coupling between the dots. This way the double dot is tuned to the Pauli spin-blockade (SB) regime.

To investigate the relaxation processes, we measure the leakage current through the SB as a function of magnetic field and level detuning Δ_{12}. The observed relaxation changes drastically for different coupling between the two dots. We can tune the tunnel coupling energy over a wide range in our device and estimate values of $75 - 125\mu eV$ for the regimes considered here.

For weakly coupled dots, we observe a current peak around $B = 0$ mT with a width of ≈ 1.5 mT. In InAs dots, spin-orbit interaction is strong which results in an additional broadening of the peak compared to GaAs. The situation is reversed for strong interdot coupling. Spin blockade is observed around $B = 0$ mT and lifted for finite fields. After a monotonic increase for small fields, the leakage current saturates to a field independent value probably limited by the coupling to the leads.

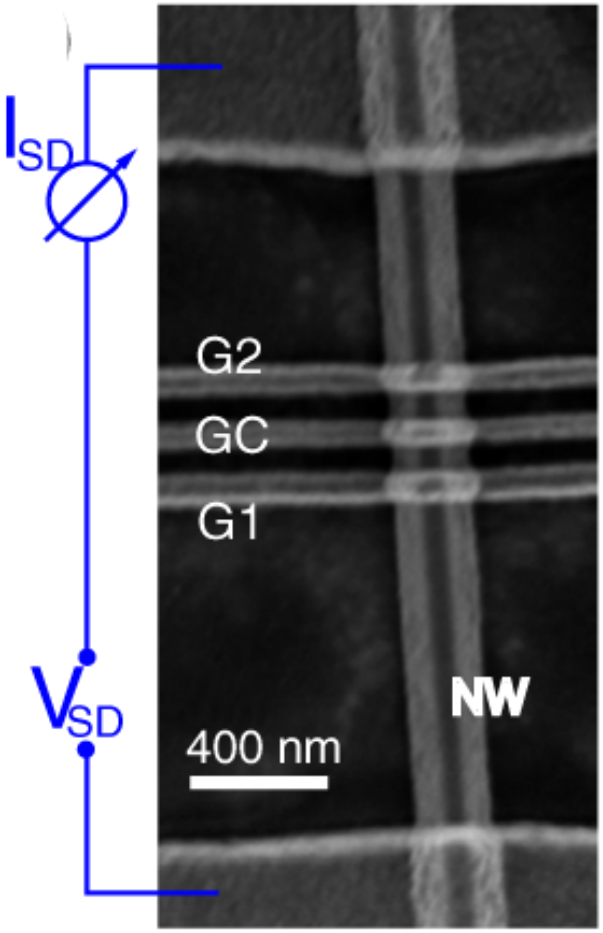

Figure 2.3: Scanning electron microscope image of a nanowire device. The current I_{SD} for an applied source-drain voltage V_{SD} is measured between the outer contacts to the nanowire. Voltages on the top gates G1, G2, GC create a double quantum dot.

Tuning to intermediate coupling, we observe a complex behavior. The leakage current is suppressed by an order of magnitude in a sharply defined region of magnetic field and detuning. The reduced leakage current exhibits a pronounced bistability. In Fig. 2.4(c), current traces for up (green) and down (black) sweeps of the magnetic field are

shown. The bistable suppression abruptly vanishes above a critical temperature of $T_{cr} = 600$ mK; see Fig. 2.4(d). At high temperatures, the current traces are similar to the ones for high coupling [dotted line in Fig. 2.4(c)].

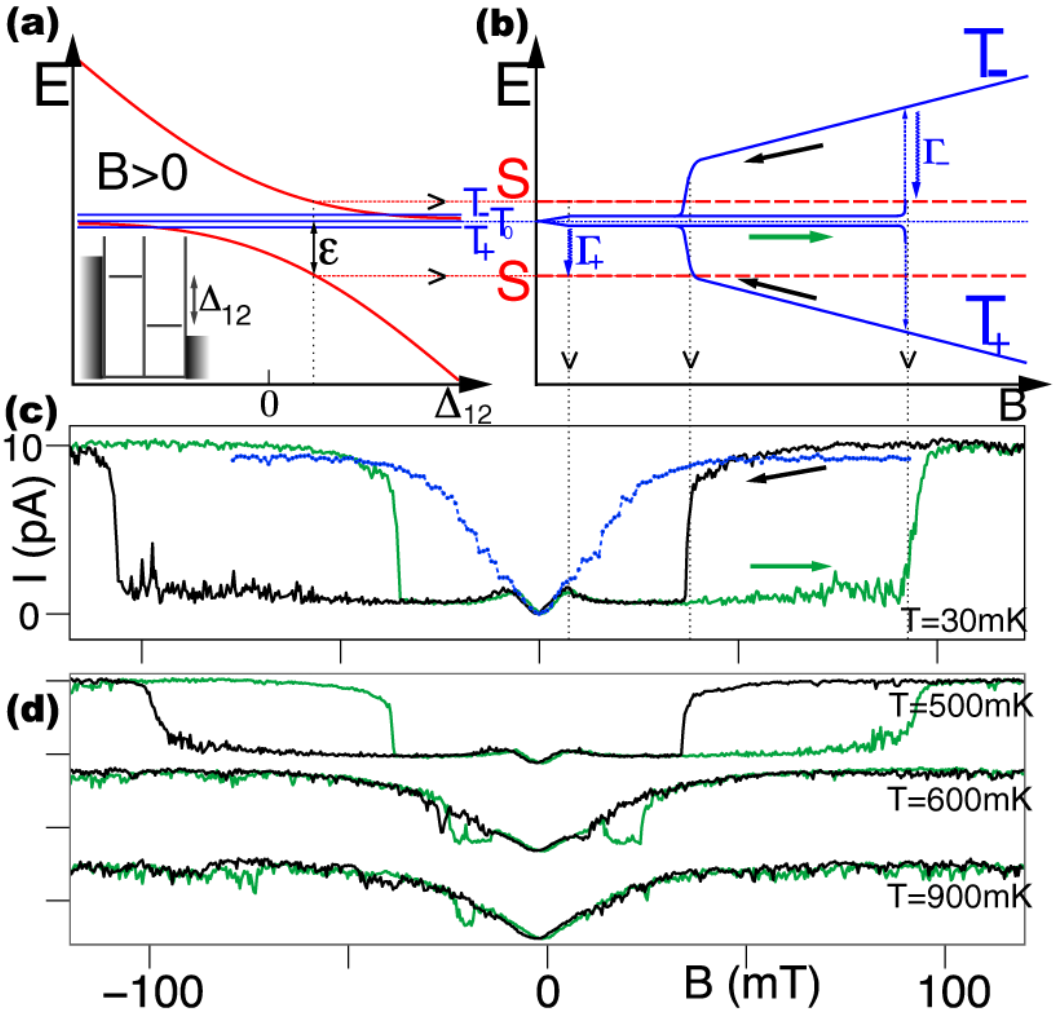

Figure 2.4: (a) Dependence of the singlet branches S and the three triplets $T_{0,\pm}(1,1)$ on the detuning Δ_{12} of the dot levels. (b) Evolution of the triplet energies at fixed Δ_{12} for up and down sweeps of the magnetic field, including the influence of dynamical nuclear polarization. Arrows indicate the sweep direction. (c) Current traces: up sweeps (green) and down sweeps (black). The dotted curve for strong coupling does not exhibit bistability. (d) Same for different temperatures.

To explain our results, we propose a model where a net nuclear polarization can be achieved only when hyperfine-induced processes occur in parallel with alternative relaxation paths, which we attribute to spin-orbit interaction. The polarized nuclei then create an effective magnetic field B_N opposite to the external field B, which suppresses the relaxation at larger fields.

The scenario we propose is depicted in Fig. 2.4(b). For small fields, T_+ approaches the lower singlet branch S, while T_- is shifted away in energy. The relaxation T_+ to S thus dominates. During this process, an electron is flipped from parallel to antiparallel alignment with the external field. Correspondingly, an increasing amount of nuclear spins are flipped parallel to the field. Due to the negative g factor in InAs, the nuclear field BN therefore counteracts the external field. Further Zeeman splitting is inhibited and the triplets evolve along the inner traces in Fig. 2.4(b) (green arrow). The leakage current is thus sustained at the low field value ≈ 1 pA [Fig. 2.4(c)]. For further increasing field, a saturation for the nuclear polarization is reached and the triplets split more. As soon as T_- crosses the upper singlet branch, the T_+ to S relaxation becomes energetically possible. This flip-flop process builds up a nuclear field that supports the external field, which leads to a sharp rise of the Zeeman splitting and to a step in current. Decreasing the B field, the high-current state is stable until T_+ crosses S again and the nuclei reduce the effective field for the

electrons. The small reproducible peak at $\approx \pm 7$ mT in Fig. 2.4(c) is not captured by this simple model. This feature could be explained by considering a dependence of the relaxation rates on the external magnetic field in a quantitative model. The bistable behavior vanishes above a critical value for the coupling.

2.3 Aharonov-Bohm Oscillations in the Presence of Strong Spin-Orbit Interactions

B. Grbic, R.Leturcq, Y. Komijani, M. Csontos, T. Ihn, and K. Ensslin, in collaboration with Dirk Reuter and Andreas D. Wieck, Univ. Bochum, Germany

Interference phenomena with particles have challenged physicists since the foundation of quantum mechanics. A charged particle traversing a ringlike mesoscopic structure in the presence of an external magnetic flux Φ acquires a quantum mechanical phase. The interference phenomenon based on this phase is known as the Aharonov-Bohm (AB) effect, and manifests itself in oscillations of the resistance of the mesoscopic ring with a period of $\Phi_0 = h/e$, where Φ_0 is the flux quantum. The Aharonov-Bohm phase was later recognized as a special case of the geometric phase acquired by the orbital wave function of a charged particle encircling a magnetic flux line. The particle's spin can acquire an additional geometric phase in systems with spin-orbit interactions (SOI).

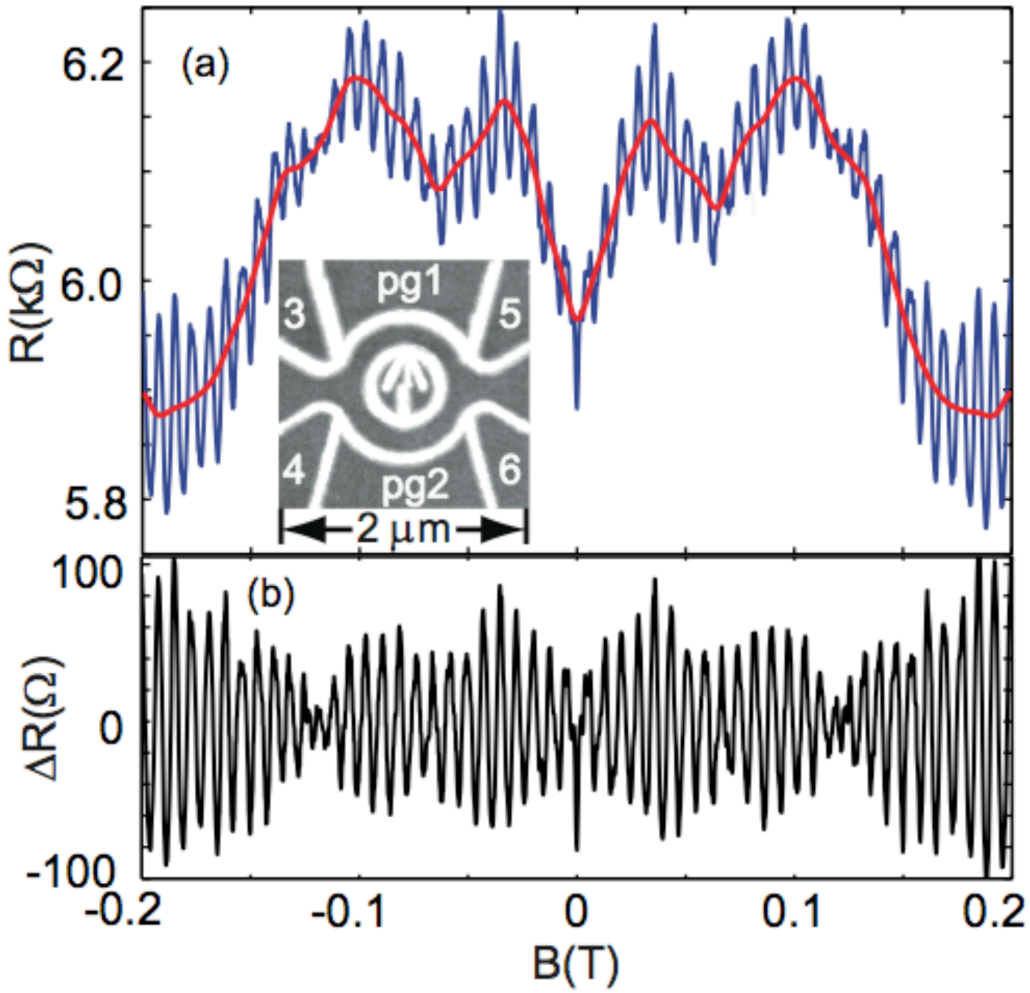

Figure 2.5: (a) Measured magnetoresistance of the ring (strongly oscillating curve, red online) together with the low-frequency background resistance (smooth blue curve); Left inset: AFM micrograph of the ring with designations of the in-plane gates. Bright oxide lines fabricated by AFM oxidation lithography lead to insulating barriers in the 2DHG. Right inset: Scheme of a carrier travelling around the ring in the presence of the external field Bext and SO induced intrinsic field Bint. (b) AB oscillations obtained after subtraction of the low frequency background from the raw data. A clear beating pattern is revealed in the AB oscillations.

In systems with strong SOI, an inhomogeneous, momentum dependent intrinsic magnetic field B_{int}, perpendicular to the particle's momentum, is present in the reference frame of the moving carrier. The total magnetic field seen by the carrier is therefore $B_{tot} = B_{ext} + B_{int}$, where B_{ext} is the external magnetic field perpendicular to the 2D system and B_{int} is the intrinsic magnetic field in the plane of the 2D system present in the moving reference frame [right inset Fig. 2.5(a)]. The particle's spin precesses around B_{tot} and accumulates an additional geometric phase upon cyclic evolution.

The sample was fabricated by atomic force microscope (AFM) oxidation lithography on a p-type carbon doped (100) GaAs heterostructure, with a shallow two-dimensional hole gas (2DHG) located 45 nm below the surface. An AFM micrograph of the ring structure is shown in the inset of Fig. 2.5(a). The average radius of the circular orbit is 420 nm, and the lithographic width of the arms is 190 nm, corresponding to an electronic width of 60-70 nm. The Fermi wavelength is about 40 nm, and the mean free path is 2 μm. Since the circumference of the ring is around 2.5 μm, the transport through the ring is quasiballistic.

The presence of strong spin-orbit interactions in the heterostructure is demonstrated by a simultaneous observation of the beating in Shubnikov-de Haas (SdH) oscillations and a weak anti-localization dip in the measured magnetoresistance of the Hall bar fabricated on the same wafer.

Figure 2.5(a) shows the magnetoresistance of the ring (fast oscillating red curve). The low-frequency background resistance is indicated by a smooth curve (blue curve). The observed AB oscillations with a period of 7.7 mT (frequency 130 T^{-1}) correspond to a radius of the holes' orbit of 415 nm, in excellent agreement with the lithographic size of the ring. After subtracting the low-frequency background from the raw data, a clear beating pattern is revealed in the AB oscillations with a well defined node at 115 mT [Fig. 2.5(b)].

We associate the beating in the measured resistance oscillations with an interplay between the orbital Aharonov-Bohm and a spin-orbit induced geometric phase. In addition we resolve h/2e oscillations in the ring resistance, and find that they also show a beating-like behavior, which produces a splitting of the h/2e peak in the Fourier spectrum. A resistance minimum at B=0, present in all in-plane gate configurations, demonstrates the destructive interference of the hole spins propagating along time-reversed paths.

2.4 Measurement of the tip-induced potential in scanning gate experiments

A. E. Gildemeister, M. Hüfner, S. Schnez, T. Ihn, M. Sigrist, and K. Ensslin, in collaboration with D. C. Driscoll and A. C. Gossard, University of California, Santa Barbara, USA

Common to most experimental studies on transport in quantum dots is that they investigate the various aspects based on macroscopic current and voltage measurements, not based on local measurements. An interesting goal for a local study of quantum dots would be, for example, to measure the spatial variation of the probability density of the electrons in the dot. A promising approach to this and other questions pertaining to local properties of quantum dots is the scanning gate technique, where the sharp conducting tip of a scanning force microscope (SFM) is employed as a movable gate that can be scanned over the surface of the sample. The technique has already been successfully used to manipulate single electrons in quantum dots in carbon nanotubes and GaAlAs, where a singly occupied quantum dot could be studied.

In spite of the high number of studies that employ the scanning gate technique, relatively few data are available about an important factor common to all of the experiments, namely, the potential that the tip induces in the sample, here called "tip potential" for brevity.

We have used a quantum dot in the Coulomb blockade regime as a sensitive potentiometer to quantitatively measure the potential of a metallic SFM tip with high resolution over an area of up to 2x2 μm^2. The tip was scanned at a constant height of about 200 nm over the sample surface and we used a feedback mechanism to apply a voltage to a plunger gate of the quantum dot such that one of the quantized energy levels of the dot would always stay in resonance with the chemical potential of the source and drain leads. The voltage on the plunger gate corresponds to

the tip potential. With this technique we could ensure that the dot was a sensitive detector for every tip position and that we used only one quantum state for detection.

Additionally, we measured the lever arm of the tip as a function of position by applying an ac voltage to the tip and measuring how strongly the feedback of the plunger gate reacted to this. The lever arm helps to understand the origin of the tip potential, its behavior as a function of the voltage applied to the tip, and the contact potential difference between tip and sample.

In Fig. 2.6 (b) we show the tip potential that was measured with the feedback turned on. We have multiplied the potential with -e to show the more intuitive potential energy. On the large scale we see a roughly circularly symmetric repulsive potential peak which is about 700 nm wide and about 1 meV high. Close to the center we see a smaller attractive potential dip superimposed on the large peak. The dip is also circularly symmetric, about 250 nm wide, and around 0.5 meV deep.

In Fig. 2.6 (a) we show a scanning gate measurement of the quantum dot where we simply recorded the current through the dot as a function of tip position. The feedback was turned off and the grounded tip was scanned over the sample surface at a height of about 200 nm.

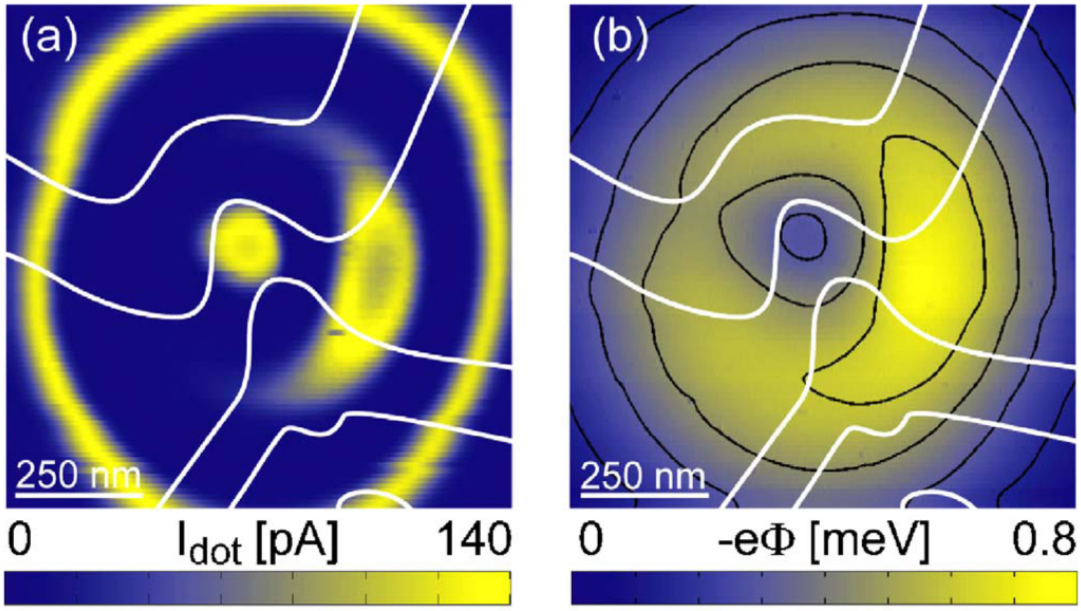

Figure 2.6: (a) Conventional scanning gate image of the current through a quantum dot. The grounded tip is moved over the dot at a constant height of about 200 nm above the sample surface. The oxide lines that define the quantum dot in the center are outlined in white. (b) The tip potential measured with the quantum dot. Equipotential contours are plotted as black lines.

When we compare the tip potential in Fig. 2.6 (b) with the current image of Fig. 2.6 (a) then it is evident that there is high current along equipotential lines of the tip potential. The interpretation of a current image becomes clearer when the tip potential is known. For example, it is now possible to associate the very small ring in the middle and the large ring with the same charge state of the quantum dot, whereas the crescent-shaped arc corresponds to a state with one electron less on the dot.

Clearly, this potential does not fulfill the requirements for probability density mapping. The potential is wider than the dot and, as we can see in the current image, it exceeds the charging energy of the dot. Also, it has both an attractive and a repulsive part which makes it complicated. In view of future experiments it is important to understand the origin of the tip potential and possibilities to improve it.

We have developed an experimental technique that can be used to measure quantitatively the spatial dependence of the potential induced in a quantum dot by the tip of a scanning force microscope. Furthermore, the technique allows one to quantitatively measure the spatial dependence of the lever arm of the tip. The feedback mechanism used for the measurements is able to minimize the tip potential and makes measurements in a least-invasive regime possible.

The tip potential generally can have two components, one that depends on the voltage applied to the tip and one that is independent of this voltage. In our measurements the tip voltage dependent part could be well described as the product of the tip's lever arm and the difference between the voltage applied to the tip and the contact potential difference between tip and sample. For a grounded tip it was a repulsive Lorentzian-shaped 700 nm wide and 1.6 meV high potential. The tip voltage independent potential was attractive, Lorentzian shaped, about 250 nm wide, and 0.8 meV deep. It could be caused by a charged particle on the tip. The measurements of the tip's lever arm revealed fine structure both in the lever arm and the dot current that was different for the three quantum states we measured. We speculate that this fine structure may be characteristic for a quantum state. Sharper and possibly cleaner tips are needed for future experiments. For the interpretation of results from any scanning gate experiment one should bear in mind that the tip potential could have an unexpected shape.

2.5 Local gating of a graphene Hall bar by graphene side gates

F. Molitor, J. Güttinger, C. Stampfer, D. Graf, T. Ihn, and K. Ensslin

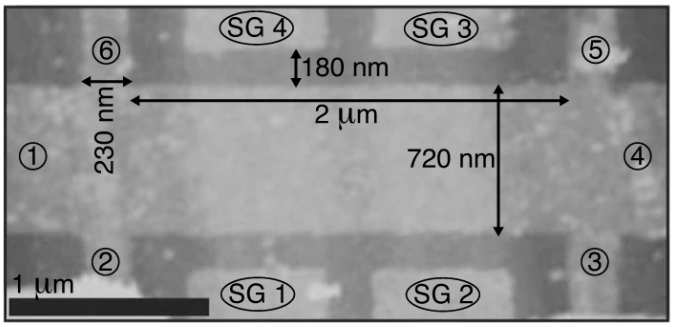

Figure 2.7: Scanning force micrograph of the Hall bar with graphene side gates. Numbers 1-6 indicate contact pads for transport measurement. Electrodes SG 1-SG 4 label the side gates.

The discovery of graphene flakes consisting of a single atomic layer facilitated measurements of the so-called half-integer quantum Hall effect. The electron and hole densities in planar structures were tuned using a backgate electrode. In order to achieve a lateral modulation of the charge density, additional laterally patterned gate electrodes are required. This has been achieved by covering the graphene flake with an isolating dielectric, and then depositing metallic top gates on the dielectric. The procedure includes additional processing steps, the dielectric material needs to be of very high quality in order to avoid charge traps, and for very small structures the alignment of the structure and top gates could be difficult. In order to fabricate nanostructures on graphene, such as quantum wires, ribbons, quantum point contacts, and quantum dots, more sophisticated gating schemes are required.

Side gates have become extremely useful for tunable electronic nanostructures realized for example in AlGaAs heterostructures. Here, we demonstrate the possibility to use graphene side gates as a tuning knob for the electron density in a neighboring narrow graphene Hall bar. Side gates and Hall bar are processed from the same graphene flake facilitating a single-step technological process. The scanning force micrograph in Fig. 2.7 shows the etched structure, a single layer Hall bar with four additional graphene side gates. The Hall bar has a width of 720 nm, a length between the voltage probes of 2 μm, and the gap to the side gates is 180 nm.

Conductivity traces as a function of backgate voltage are displayed in Fig. 2.8 as black curves. The different traces correspond to a varying voltage applied to all four side gates simultaneously. The curves are vertically offset for clarity by 4x4 e^2/h. The dashed lines indicate a conductivity value of $4e^2/h$. At both sides of the minimum in conductivity, where electron and hole densities compensate each other, the conductivity increases almost linearly with applied backgate voltage, since $n = \alpha \times V_{BG} - V_{BG,CN}$, where $\alpha = 7.2 \times 10^{10}$ cm^{-2}/V and $V_{BG,CN}$ is the position of the charge neutrality point in backgate voltage. Applying a voltage V_{BG} to all four side gates has mainly two effects: The position of the conductivity minimum in backgate voltage shifts according to the relative lever arm. The

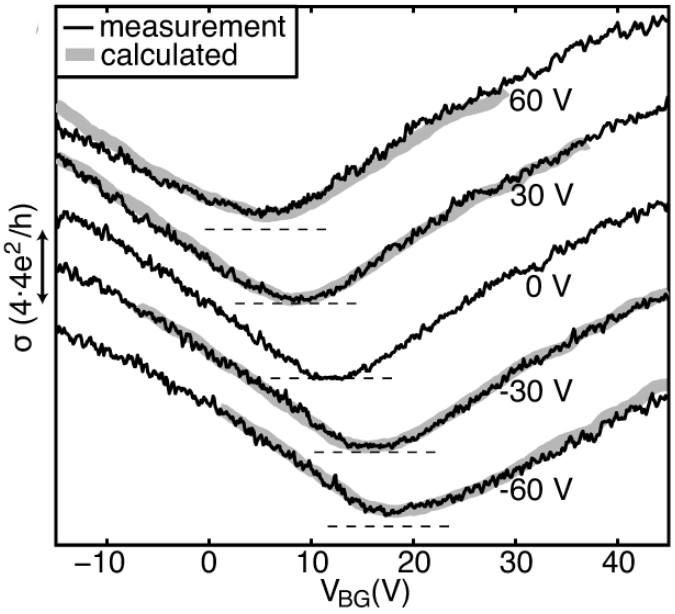

Figure 2.8: Conductivity versus backgate voltage V_{BG} for various settings of the side gate voltage V_{SG} as indicated. The same voltage is applied to all four side gates, and the measurement is performed with an ac of 20 nA rms. The black curves represent the measured traces, while the gray lines are calculated with a model taking into account two parallel conducting channels with different influences from the side gates.

minimum in conductivity, which has a value $\sigma_{min} \approx 4e^2/h$ for $V_{SG} = 0$ V, increases with both positive and negative side gate voltages.

2.6 Measurement of Rashba and Dresselhaus spin-orbit magnetic fields

L. Meier, I. Shorubalko, and K. Ensslin, in collaboration with G. Salis, IBM Rüschlikon, E. Gini and S. Schön, FIRST lab, ETH Zurich

Symmetry-breaking electric fields in semiconductors induce a spin splitting, because electric fields appear to a moving electron as magnetic fields, which interact with the electron spin and couple it with the electron momentum, or wavevector, k. In zinc-blende-type crystals, such as GaAs, the electric fields resulting from the lack of an inversion centre lead to bulk inversion asymmetry (BIA) and to the Dresselhaus term in the hamiltonian. In the conduction band, its coupling is linear or cubic in k with proportionality constants β and $gamma$, respectively. In heterostructures, further electric fields are introduced owing to structure inversion asymmetry (SIA), giving rise to the Rashba term, which for conduction band electrons is linear in k with coupling constant α.

Neglecting cubic terms, the Rashba and Dresselhaus spin-orbit couplings in a quantum well are linear in wave vector k and can be described by an effective magnetic field for a coordinate system with x and y as indicated in Fig. 2.9.

We have demonstrated that both fields can be measured by optically monitoring the angular dependence of the electrons' spin precession on their direction of motion with respect to the crystal lattice. To induce an oscillating spin-orbit field, we impose an oscillating drift momentum on the QW electrons by applying an in-plane a.c. electric field with a frequency of 160 MHz, at an angle with the x axis, see Fig. 3. We monitor the spin precession frequency, of optically polarized electron spins at different times using time-resolved Faraday rotation. By tuning the angles as indicated in Fig. 2.10 the strength of the Rashba and Dresselhaus magnetic fields are determined. Furthermore we demonstrate spin resonance induced by the spin-orbit fields. In electron spin resonance (ESR) experiments, spins that are initially polarized along the direction of a static magnetic field, perform Rabi oscillations between the states parallel and anti-parallel to B if an a.c. magnetic field (the tipping field) is applied in the plane perpendicular to B and at the Larmor frequency. Instead of an a.c. magnetic field, we use an a.c. electric field in the plane of the QW. It induces an oscil-

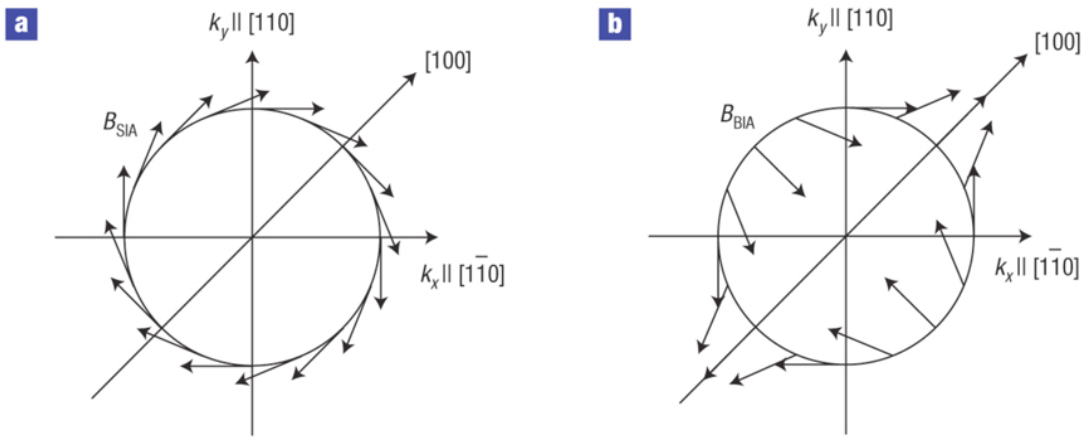

Figure 2.9: Rashba (a) and Dresselhaus (b) spin-orbit fields for different orientations of the k-vector on a unit circle.

lating spin-orbit field, which can serve as a tipping field for ESR, in this context referred to as electric-dipole-induced spin resonance (EDSR).

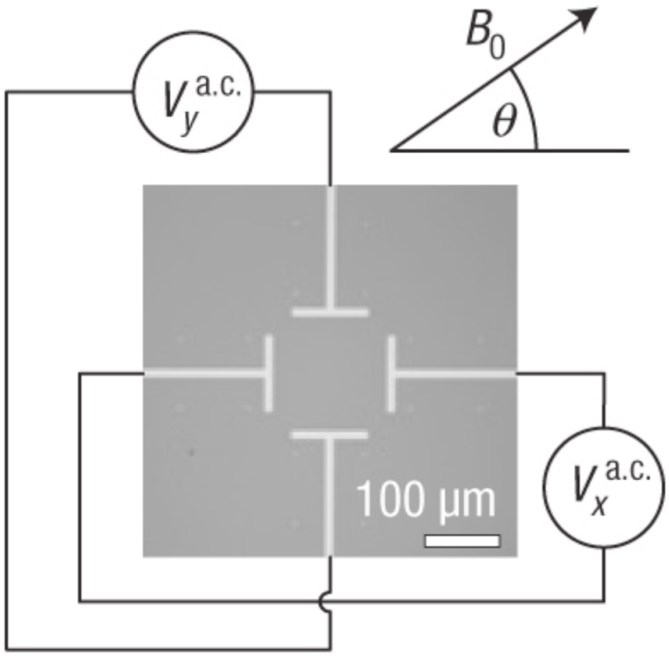

Figure 2.10: The bright lines indicate Schottky contacts to the electron gas below the wafer surface. By applying suitable voltages to the electrode pairs in x and y direction an electric field with arbitrary in-plane direction can be produced in the experiment.

2.7 Currents through quantum dots driven by a nearby quantum point contact

U. Gasser, B. Küng, S. Gustavsson, T. Ihn, and K. Ensslin, in collaboration with W. Wegscheider, Univ. Regensburg

We have set out to fabricate double dots containing only a small number of electrons. This has been achieved for split-gate defined quantum dots and is now also realized for AFM-defined quantum dots. It turns out that the combination of in-plane gates and patterned top gates is crucial to achieve few electron occupancy, see Fig. 2.11 .

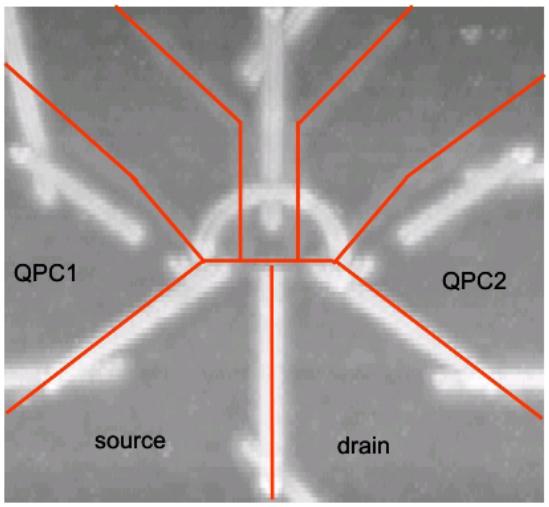

Figure 2.11: Scanning force microscope (SFM) micrograph of the sample. The 2DEG is depleted below the oxide lines written on the GaAs surface [bright lines] thus defining the ring interferometer. A Ti film evapo-rated on top is cut by local oxidation [orange lines] into mu-tually isolated top gates.

In this particular device it was possible to induce a significant current in the non-resonant double dot for a suitably biased quantum point contact. Similar experiments have been performed for a system containing two isolated QPCs as well as using a double dot coupled to a single QPC. The measurements (unpublished) in Fig. 2.12 show the current flow through the double dot system as a function of current flow through both QPCs. The question whether the energy transfer from QPC to dot is via phonons or photons needs to be resolved. The detuning between the levels in the two dots (x-axis in Fig. 2.12) is controlled by suitable gate voltages. The currents flowing through the two QPCs are changed in direction and also applied simultaneously to both QPCs. It turns out that the effects of two photon (phonon?) emitters in close vicinity to the double dot do not simply add up. A closer analysis reveals that saturation effects related to the excitation, relaxation and tunneling timescales of electrons in the quantum dot states may play a crucial role.

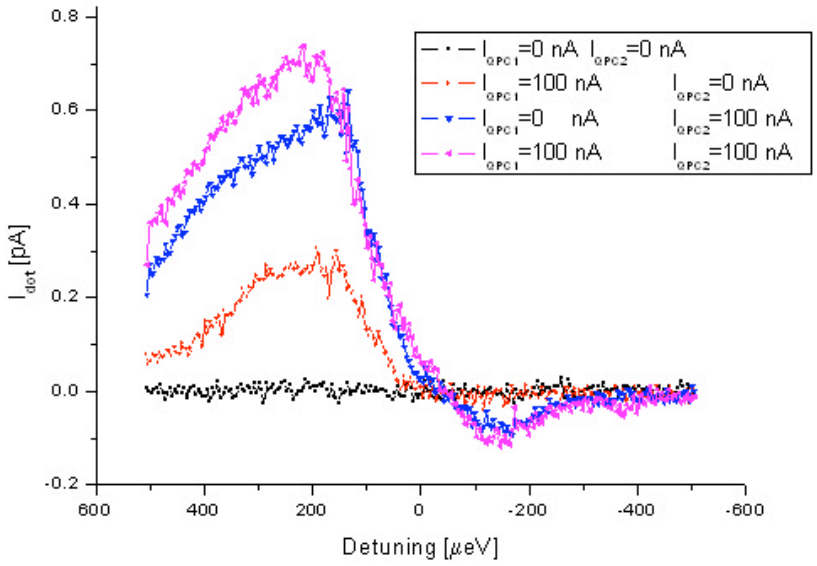

Figure 2.12: Current through the double dot as a function of detuning taken with zero bias across the DQD. No current is observed if both QPCs are grounded (black line). A driving current through neighbouring QPCs induces an inelastic tunneling current through the DQD (red and blue lines). The effect of the two QPCs is not additive (purple line).

2.8 Toward a radio-frequency charge read-out

T. Müller, T. Ihn, and K. Ensslin, in collaboration with W. Wegscheider, Univ. Regensburg

Time resolved charge detection was used to study the occupation probability of quantum dots. The full counting statistics of single electron transport through a quantum dot was experimentally established and super-Poissonian noise was detected. Fundamental experimental limitations such as finite measurement time and limited bandwidth were explicitly included in the data analysis.

Here we have focused on the realization of a fast measurement of the conductance of the quantum point contact. Present setups are limited by the time resolution of the cabling to the cryostat and typical bandwidth are about 30-40 kHz. In order to overcome these limitations we embed the quantum point contact (QPC) in a radio-frequency (RF) matching circuit and measure the reflection of an applied signal.

Alternatively, we also investigate a different way of embedding the QPC into a resonant circuit. Instead of using a lumped element circuit, a stub of transmission line (see Fig. 2.13) of a certain length can also transform the QPC's impedance. The underlying principle is that the admittance of the stub compensates for the load (QPC) impedance. This method allows for operation at higher frequencies which in turn can lead to a higher measurement bandwidth. Preliminary tests with an open stub made from a coaxial T-junction prove that the reflection coefficient of a stub-matched high frequency FET at room temperature does indeed strongly depend on the FET's impedance. Now, it remains to tune the stub in order to achieve good matching at low temperatures with a QPC incorporated.

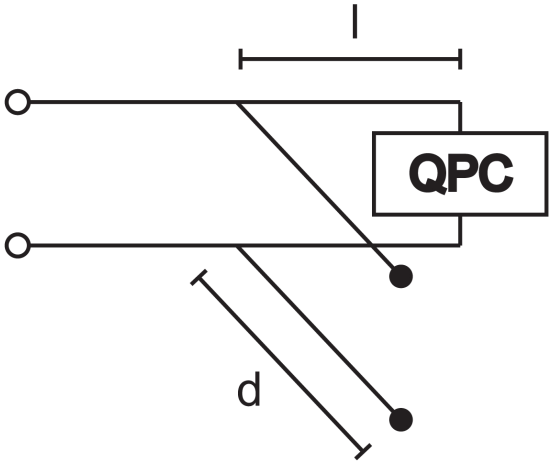

Figure 2.13: Schematic view of matching with an open stub. The admittance of the open stub is added to the admittance of the QPC, transformed by length l. Hence, by tuning l and d, any load can be matched to any admittance or impedance, respectively.

Chapter 3

Condensed matter at low temperatures

(http://www.solid.phys.ethz.ch/ott)

Head
Prof. Dr. H. R. Ott

Academic Staff
Dr. M. Weller Dr. A. Sacchetti

Technical Staff
H. R. Aeschbach

Academic Guests

Administrative Staff
C. Vinzens

Doctoral theses
Matthias Weller
NMR/NQR studies at very low temperatures and high pressures in strongly correlated electron systems
15.04.2003-15.06.2007

3.1 Cu NQR measurements on $PrCu_2$ at ambient and high pressure

A. Sacchetti, M. Weller, H. R. Ott, R. Monnier, B. Delley, and Y. Onuki

Results of μSR measurements [1] indicated an unexpected magnetic order in the Van Vleck paramagnet $PrCu_2$ [2 – 5] below 65 K. Our preliminary Cu-NQR signals probing this compound between 4 and 300 K were not consistent with the conclusion drawn from μSR. Additional NQR measurements collected in 2007, and the subsequent analysis clearly proved that no magnetic order develops in $PrCu_2$ at 65 K. Neither the NQR spectral properties (frequency and linewidth) nor the relaxation rates (spin-lattice T_1^{-1} and spin-spin T_2^{-1}) show the behavior expected in the presence of an ordering among the Pr^{3+} magnetic moments. We compare the experimental data with a simulation of the spectra by means of a dedicated package developed by us and considering the results of *ab initio* calculations of the electronic charge density in $PrCu_2$ [6]. The latter show that an implanted muon can enormously enhance a small and slowly-varying spin polarization in its environment. We therefore suggest a scenario in which the μSR results are explained by assuming the presence of intrinsic, small and slow spin fluctuations in the system which are strongly enhanced by the implanted muon and seen as a quasi static order by the fast μSR technique. Probing with the slower NQR spectroscopy these fluctuations are averaged to zero and they are only effective in the spin relaxation rates [6]. Our calculations show that the muon induces a compression of the Pr-Pr distances in the crystal (see Fig. 3.1). This is important in view of the fact that an order among the Pr^{3+} magnetic moments has recently been observed at around 9 K for pressures exceeding 10 kbar [7].

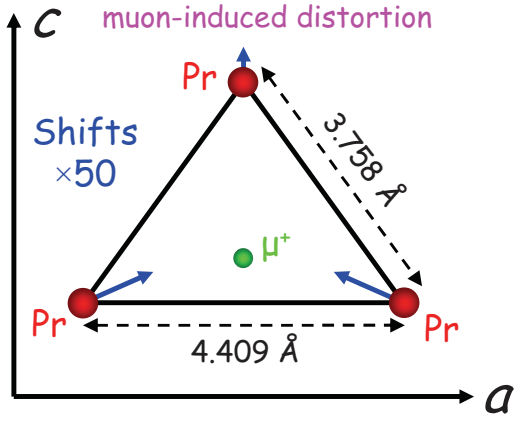

Figure 3.1: Muon-induced distortion of Pr atomic positions, as obtained from our *ab initio* calculations.

A second project concerning $PrCu_2$ aims at studying the magnetic order at high pressure by means of NQR measurements. A first set of pressure dependent spectra was collected at 50 K (see Fig. 3.2(a)). A strong broadening of the line profile is observed upon increasing the pressure up to 18.2 kbar. An abrupt increase of the linewidth (Fig. 3.2(b)) is observed around 10 kbar, which is the pressure where the new magnetic order is claimed to set in [7]. The NQR frequency (Fig. 3.2(c)) increases linearly with increasing pressure. The observation of this strong broadening already at 50 K suggests that the transition to the ordered phase at $\sim$ 9 K is preceded by strong fluctuations at higher temperatures. Additional experiments to clarify the situation are in progress.

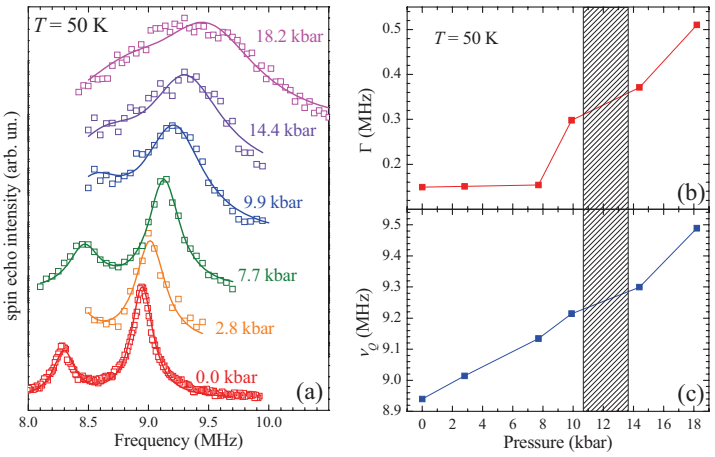

Figure 3.2: (a) Cu-NQR spectra of $PrCu_2$ as a function of pressure at 50 K and pressure dependence of the NQR (b) frequency and (c) linewidth.

References

[1] A. Schenck, F. N. Gygax, and Y. Ōnuki, Phys. Rev. B **68** 104422 (2003).

[2] K. Andres, E. Bucher, J. P. Maita, and A. S. Cooper, Phys. Rev. Lett. **28** 1652 (1972).

[3] M. Wun and N.E. Phillips, Phys. Lett. **50A**, 195 (1974).

[4] H. R. Ott, J.K. Kjems and K. Andres, Proc. of the Conf. on Rare Earth and Actinides, Durham 1977, IOP Conference Series **37**, 149.

[5] J.K. Kjems, H.R. Ott, S.M. Shapiro and K. Andres, J. Phys.(Paris), Colloq. **6**, 39 (1978).

[6] A. Sacchetti, M. Weller, J. L. Gavilano, R. Mudliar, B. Pedrini, K. Magishi, H. R. Ott, R. Monnier, B. Delley, and Y. Ōnuki, Phys. Rev. B **77** 144404 (2008).

[7] T. Naka, L. A. Ponomarenko, A. de Visser, A. Matsushita, R. Settai, and Y. Ōnuki, Phys. Rev. B **71**, 024408 (2005).

3.2 Pressure induced ground state variation in $CeAl_3$

M. Weller, J. L. Gavilano, A. Sacchetti, and H. R. Ott

^{27}Al NMR measurements probing the heavy electron compound $CeAl_3$ in very low magnetic fields (1.1 kG), at temperatures below 2 K and varying external pressures between ambient pressure and 9.15 kbar, were made. Prominent changes in the NMR response were observed upon increasing the pressure above 1.25 kbar. Inspection of the ^{27}Al NMR spectra reveals that previously reported magnetic and electronic inhomogeneities at ambient pressure and very low temperatures are removed. The spectral part which is thought to originate from the magnetically correlated phase is not present for $p = 1.25$ kbar and above. The remaining spectrum can be explained by assuming a single Al-site. Numerical simulations reproduce the ^{27}Al NMR spectra very well, thus providing evidence for a homogeneous ground state at pressures exceeding 1.25 kbar.

As shown in Fig 3.3, the spin lattice relaxation rate T_1^{-1} is reduced considerably upon increasing the pressure up to 9.15 kbar. In a Fermi liquid scenario, the Knight shift K and T_1 are connected by the Korringa relation

$$T_1 T K^2 R = \frac{\hbar}{4\pi k_B}\left(\frac{\gamma_e}{\gamma_N}\right)^2 \quad , \qquad (3.1)$$

with R as the only free parameter. $\sqrt{R}$ reflects the ratio between the interaction-induced enhancement of the electronic density of states $D(E_F)$ and the magnetic susceptibility, respectively. For a free electron gas $R = 1$, and for interacting electron systems $R < 1$. From the analysis of the ^{27}Al NMR spectra and $T_1^{-1}(T)$ data, values for R, valid for the paramagnetic phase, can be calculated for the selected pressures. We note a strong reduction of R by a factor of 18 if the pressure is increased from 1 bar to 9.15 kbar. Previously reported specific heat measurements under pressure indicated a reduction of the density of states by the application of pressure. A combination of these results with the pressure induced reduction in R implies a small increase of the enhancement factor of the spin susceptibility by a factor 1.5. This somewhat counterintuitive conclusion may indicate that a single interpretation of the results, based on a Fermi-liquid type approach, is inadequate.

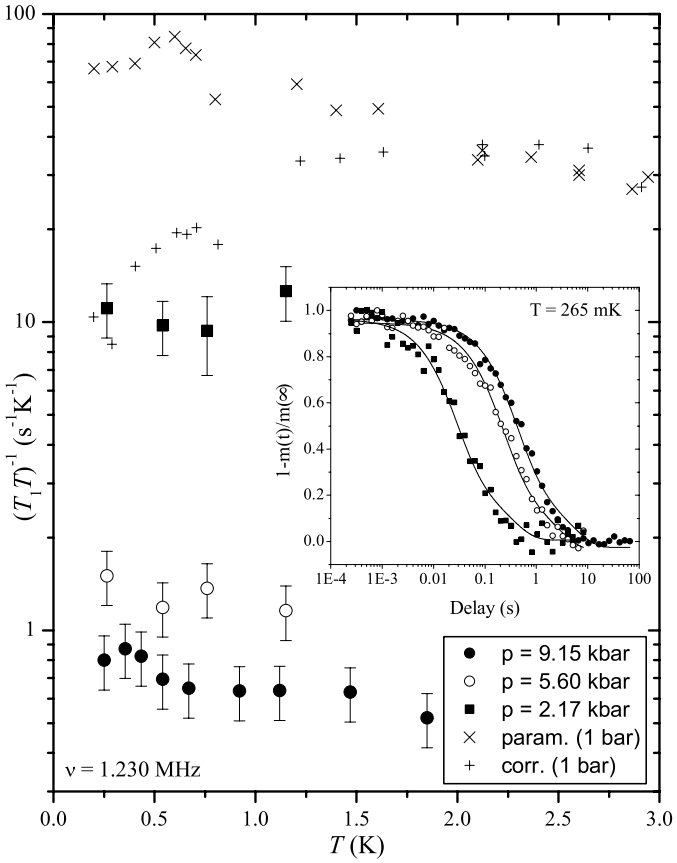

Figure 3.3: ^{27}Al NMR spin lattice relaxation rate of $CeAl_3$ for various external pressures, plotted as $(T_1T)^{-1}(T)$.

Nevertheless the low temperature physical properties of $CeAl_3$ are governed by strongly pressure dependent features of the electronic subsystem. At 9.15 kbar and above

0.25 K, $CeAl_3$ is a Pauli type paramagnet with a moderately enhanced mass of the itinerant charge carriers. Lowering the pressure to ambient pressure results in a strong variation of the renormalization effects that affect the electronic subsystem, in agreement with other pressure studies probing the effective electron mass in this material. Below 1.25 kbar, a phase separation in the electronic structure occurs, with similar fractions of the two phases close to $T = 0$ K. One phase still exhibits Pauli type paramagnetic features, while a second phase, of growing weight with decreasing pressure, is characterized by quasi static magnetic correlations.

References

[1] M. Weller, J. L. Gavilano, A. Sacchetti, and H. R. Ott, Phys Rev. B **77**, 132402 (2008) and references therein.

Chapter 4

Microstructure research

(http://www.microstructure.ethz.ch)

Head
Prof. Dr. D. Pescia
Prof. Dr. M. Erbudak

Academic Staff

S. Burkard (Ph.D. Student)	T. Michlmayr (Ph.D., 01.01-30.06)	J.-N. Longchamp (Ph.D., 01.01-30.09)
O. Portmann (Postdoc)	N. Saratz (Ph.D. Student)	T. Kirk (Ph.D. Student)
Dr. U. Ramsperger (Postdoc)	Dr. M. Hochstrasser (Postdoc)	Dr. A. Vindigni (Postdoc)
Dr. Y. Weisskopf	Dr. A. Vaterlaus (40%, Didactical teaching)	

Technical Staff
Th. Bähler (80%)

Academic Guests
Prof. D. Stariolo (21.06.-28.06)
Dr. Y. Acremann, Stanford, (29.05-31.05)
Prof. M. Mungan, Bogazici University, TR Istanbul, (23.01-28.01, 25.08-16.09)
Prof. H. Üstünel, METU, Ankara, (01.05-06.05)
M. Gündoğan, Bilkent University, Ankara, (29.07-01.09)
Dr. A. Bittner, MPI Stuttgart, (08.03-09.03)
S. Jeon, H. Baek, S.J. Lin, Seoul National University, (03.10)

Doctoral theses
Jean-Nicolas Longchamp
Thin films on icosahedral AlPdMn quasicrystal

S. Czekaj
Ferromagnetic and antiferromagnetic domain configurations in thin films and multilayer - toward a patterned exchange bias system

T. Michlmayr
Local magnetic field generation

Diploma theses

D. Efetov	Coherent charge transport in graphene nanostructures

Thin Film Physics Group

Head
PD. Dr. Hans Zogg

Academic Staff
Tiwari Ayodhya Nath Prof. Dr. (head PV)

Arnold Martin	Brémaud David	Bücheler Stephan
Chirila Adrian	Corica Dario	Felder Ferdinand
Moreira Osvaldo Dr.	Rahim Mohamed	Seyrling Sieghard
Verma Rajneesh		

Technical Staff

Däscher Jachen	Meier Oliver

Academic Guests
Dr. Maxim Ganchev, May - Nov 2007
Prof. Gennadiy Khrypunov, Jun - Aug 2007
Christopher Hibberd, Jul & Oct 2007
Sonya Calnan
Dr. Alessandro Romeo

Doctoral theses
Martin Arnold
Mid-Infrared Semiconductor Devices with Vertical Cavities, Diss. ETH 17507

Diploma theses

Ebneter, Christian	WS 06/07
Bücheler, Stephan	WS 06/07
Meyer, Stefan	SS 07
Corica, Dario	SS 07
Kambiz, Behfar	WS 06/07
Perrenoud, Julian	SS 07
Inderbitzin, Lukas	SS 07

Semester students

Boye, Dirk	29.01 - 09.03.07
Uehlinger, Thomas	12.02 - 02.03.07
Inderbitzin, Lukas	12.02 - 02.03.07
Heer, Pascal	26.02 - 16.03.07
Streuli, Daniel	26.02 - 26.03.07
Klenert, David	05.10 - 09.11.07
Wojtas, Nina	24.09 - 21.12.07
Blösch, Patrick	12.11.07 - 11.02.08

4.1 Nanoscale Magnetism

Stripe-domain nucleation and creep in ultrathin Fe films on Cu(100)

N. Saratz, T. Michlmayr, O. Portmann, U. Ramperger, A. Vaterlaus, D. Pescia, J. Phys. D **40**, 1268 (2007)

We provide images of the formation of the stripe phase in a system consisting of ultrathin Fe films grown with epitaxial accuracy on top of a Cu(100) single crystal surface. In the atomic-layer thickness limit, Fe films deposisted by Molecular Beam Epitaxy (MBE) onto a Cu(100) surface are magnetized over a sizeable temperature range perpendicularly to the film plane. In this situation, two interactions appear. The exchange interaction – of quantum mechanical origin – which favours parallel alignment of neighbouring spins, is frustrated by the much weaker dipolar interaction – of classical origin – which favours antiparallel spin alignment. The dipolar interaction decays "only" as the third power of the distance between two spins and is long-ranged. Thus, perpendicularly magnetized Fe films realize precisely the kind of competition needed to produce *mesocale phase separation*. Indeed, the Fe films are observed to self-organize into stripes of opposite perpendicular magnetization that modulate the order parameter (the local perpendicular component of the magnetization vector in the present case) in one direction and establish one-dimensional order. The most remarkable features of the stripe phase are stripe meandering, stripe corrugation and four types of topological defects – dislocations. Here we focus on imaging stripe nucleation and stripe creep at the micrometer scale, with particular attention to the role of quenched defects, film edges and self-induced defects. We show that quenched and self-generated defects inevitably lead to the appearance of a sizeable amount of disorder in the stripe pattern, which is bound to loose long-range translational order. The magnetic domain structure of the Fe films is imaged using Scanning Electron Microscopy with Polarisation Analysis (SEMPA). An electron beam with typically 2 keV primary energy is focused onto the Fe film and the secondary electrons excited out of the top few surface layers are analyzed according to their intensity and their spin polarization. By scanning the beam over selected regions of the surface we can obtain an image of the topographical contrast and, simultaneously, an image of the perpendicular component of the local magnetization vector. The value of the spin polarization is converted into a gray scale so that the black-white contrast visible in the images corresponds to domains with opposite perpendicular magnetization. The Fe-films are grown by slow (typically few minutes per ML) ultra-high vacuum (UHV, base pressure: $8 \cdot 10^{-11}$ mbar) deposition using MBE on a Cu(100)-surface. The strategy adopted to image stripe nucleation and creep consists in applying a perpendicular magnetic field in one direction – which we define, in order to simplify the description – as "negative", sufficiently strong to produce an (almost) uniform magnetic state – the "dark" state in the following images. A field in the opposite – positive – direction with variable strength is then used to launch nucleation and development of the "white"- state with opposite magnetization. The stripe creep is often slow enough so that it can be captured by the present SEMPA set-up, where imaging can be performed with minutes temporal resolution. In the following figure, which summarizes all essential elements of stripe formation, we observe how stripes penetrate a uniformly magnetized state (dark), achieved by applying an external "negative" magnetic field of 24 Oe. The end of the field pulse is set to t_0. The image recorded immediately after t_0 (A) shows an almost uniformly magnetized film (dark). A small (≈ 1 G) "positive" field launches the penetration of the "white" state into the dark background. Progressively, stripes (mainly nucleating at defects and at the edge of the film, not shown here) penetrate the film (white in (A). Stripes form side branches (marked by arrows in (B)-(D)) that ultimately will appear as dislocations in the stationary pattern (Q) by avoiding topographic defects (marked with arrows in the topographic image (R) acquired simultaneously to the magnetic micrograph (Q)). In (D)-(F) two stripes run into each other frontally but avoid themselves (arrow in (F)) and glide away (G), leaving behind a self-generated defect. Images (H)-(L) were recorded at a higher magnification between images (G) and (N). They again show two finger-like white domains headed for frontal collision. As they approach each other, the lateral space left is not enough to allow their gliding away so that their growth stops, again leaving behind a self-generated dislocation. Images (N)-(P) show a finger-like domain which gets stuck at a constriction (marked in (P) with an arrow) (self-generated dislocation). Notice that topographic defects such as those in (Q) are quite rare and that self-generated defects dominate the pattern formation process. Acquisition times: images (A), (M)-(R): 4.5 minutes, images (B)-(L): 1.16 minutes. The excess of "white" in the final image is due to the small 'positive' field applied. (R) and (M) give the topographic contrast recorded simultaneouly with (Q) and (L), respectively.

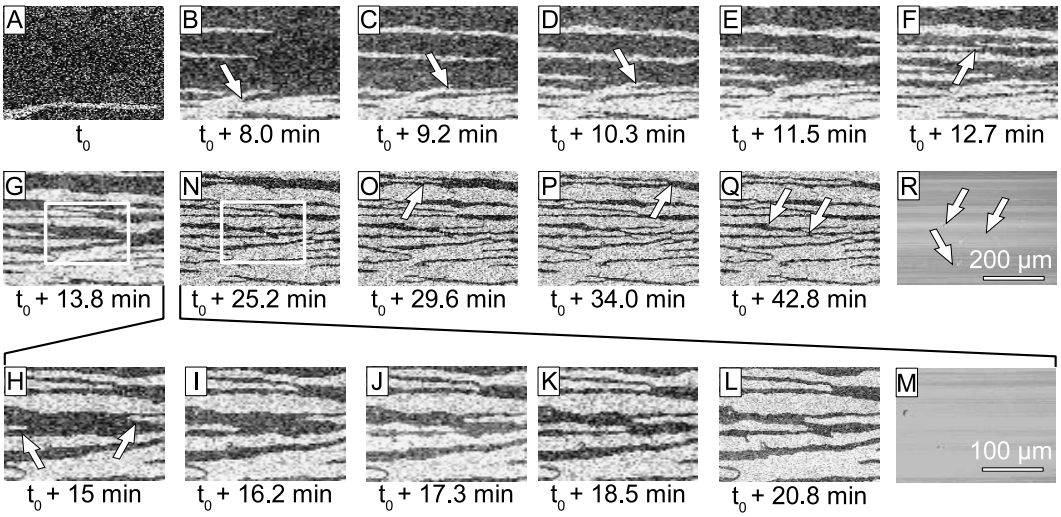

Figure 4.1:

We conclude that, besides structural disorder provided by the substrate, we detect an important amount of self-induced disorder intrinsic to the stripe formation process where many interacting domains are involved. Both type of sources of disorder produce strong deviations from the perfect stripe order which one would suspect to be the lowest free energy state. Thus, in line with a theorem by Imry and Ma, which foresees the loss of long range translational order in systems with quenched disorder in dimensions less than 4, we expect a strong perturbation of long range order as a consequence of the appearance of such deviations from stripe order. We are in the process of analyzing the images to extract the relevant correlation functions and to study the role of the various elements of disorder, with the aim of clarifying what type of order is actually realized in this system of two dimensional striped matter. As a preliminary result we can state that translational order is not long-ranged as expected e.g. in common three-dimensional crystalline matter, while orientational order is long-ranged. This behaviour points to the realization of an anomalous state of matter which we are in the process of characterizing.

4.2 Quasicrystal surface phenomena

Crystals possess a periodic arrangement of atoms, while quasicrystals lack periodicity, yet exhibit long-range orientational and quasiperiodic translational order. Owing to this fundamental difference, a crystal-quasicrystal interface gives rise to interesting phenomena. In particular, the epitaxial growth of matter on a quasicrystalline substrate leads to well-ordered and self-size-selected clusters with a diameter of typically $3 - 4\,\mathrm{nm}$. We have studied crystalline growth processes experimentally as well as in computational simulations.

4.3 Co deposition onto the icosahedral Al-Pd-Mn

Y. Weisskopf, S. Burkardt, M. Erbudak

We have evaporated Co onto the pentagonal surface of an icosahedral Al-Pd-Mn quasicrystal, kept at room temperature. For submonolayer Co deposits, the growth of five AlCo domains is observed exposing their (110) faces parallel to the surface and rotated by 72° with respect to each other. The orientational relationship betweeen these domains and the substrate is determined by the optimum matching of the average quasicrystal structure and the CsCl structure with a lattice constant of about 0.29 nm [B. Bolliger et al., Phys. Rev. Lett. **80**, 5369 (1998)]. During further deposition, Co grows epitaxially on the AlCo domains in a novel body-centered cubic structure. The growth mode of Co on Al-Pd-Mn is similar to the growth of Fe and Ni on the same substrate [Y. Weisskopf et al., Surf. Sci. **578**, 35 (2005); *ibid.* **600**, 2594 (2006)] except for the thickness of the alloy formed at the interface. In the case of Co, it is practically one single monolayer, while for Fe it is about $4 - 6$ monolayers.

4.4 Well-ordered alumina layers on the icosahedral Al-Pd-Mn

J.-N. Longchamp, S. Burkardt, M. Erbudak, Y. Weisskopf

We have observed the formation of a well-ordered aluminum oxide film when the pentagonal surface of icosahedral Al-Pd-Mn, kept at 700 K, is exposed to several hundred Langmuirs of O_2. The film is about 0.5-nm thick having a local structure which resembles that of the oxide layers formed on ordered binary alloys of Al [A. Stierle et al., Science **303**, 61 (2004); G. Kresse et al., Science **308**, 1440 (2005)] except that the quasicrystalline substrate makes the film consist of five pairs of nanometer-size aluminum oxide domains exposing their nominal (111) faces parallel to the substrate surface and rotated by 72° with respect to each other. Domain parameters of $a_1 = 1.06\,\mathrm{nm}$, $a_2 = 1.79\,\mathrm{nm}$, and $\alpha = 88.7°$ reproduce the experimental electron-diffraction results satisfactorily. The orientational relationship between these domains and the substrate is a consequence of the affinity of the icosahedral and the CsCl structure.

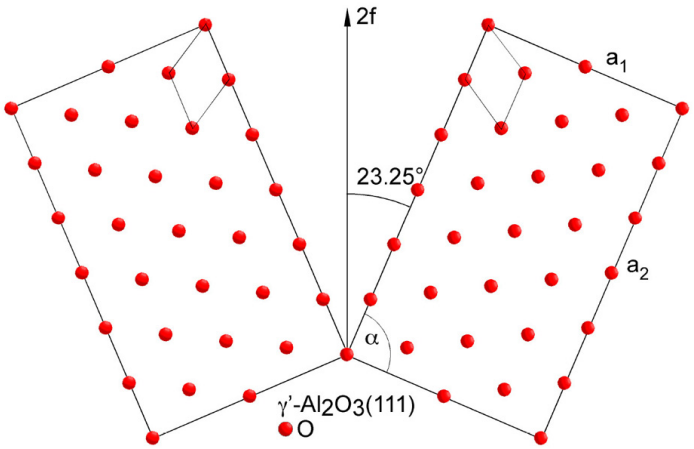

Figure 4.2: The orientation of one pair of oxygen domains along one twofold-symmetry axis of the pentagonal surface.

4.5 Nanometer-size alumina substrates on quasicrystal surfaces

J.-N. Longchamp, S. Burkardt, M. Erbudak

By virtue of the relative ease of preparation of ordered, nanometer-size aluminum-oxide domains, quasicrystals bare the potential use of catalyst carriers of active metals without resorting to self-size-selecting processes of growing films. The natural limit of the lateral size in the order of few a nm promotes such alumina domains to attractive substrates for nanometer-scale epitaxy. This possibility has been examined by depositing CdTe and PbTe onto the oxidized pentagonal surface of an icosahedral AlPdMn quasicrystal. As expected, crystalline domains are formed with well-defined polar orientations and exposing their low-index faces, which are parallel to the pentagonal surface of the quasicrystal. The azimuthal orientation of the crystallites are found to be random. The chemically inert oxide layer also acts as an efficient capping on the quasicrystal surface preventing it from contamination.

4.6 Molecular dynamics study of structure formation on quasicrystals

M. Mungan, M. Erbudak, Y. Weisskopf

We have studied the three-dimensional structure formation when atoms are deposited onto a substrate with a decagonal quasicrystalline order. Already at a monolayer coverage the adsorbed atoms assemble in ordered domains whose orientation is given by the underlying substrate symmetry. The domain size is found to mainly depend on the relative strength η of the adsorbate interactions with each other and the substrate. For thicker layers, different morphologies are observed ranging from layer-by-layer growth to cluster formation, depending on η. We also find that the fim thickness also affects the overall structure of the growing film: Depending on the relative strength of the interaction η, a structural transition of the configutation of the adsorbate layers closest to the substrate can occur as the number of deposited layers increases. For the simulations, we have used a scale sufficiently large to capture in three-dimensions the formation of multiple domains. The results are consistent with earlier investigations of Al grown on the decagonal surface of an Al-Co-Ni quasicrystal [T. Flückiger et al., Nano Lett. **3**, 1717 (2003)].

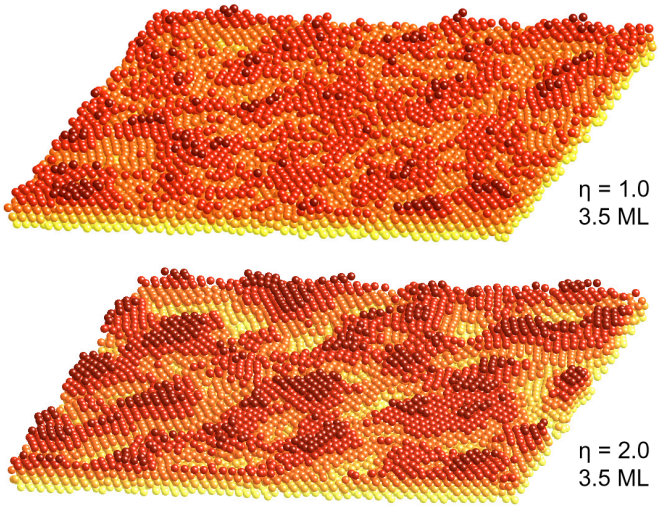

Figure 4.3: Configuration of adsorbates at 3.5 monolayers coverage with two different relative interaction strengths η (see text).

4.7 Epitaxial IV-VI narrow-gap semiconductor layers

M. Arnold, F. Felder, M. Rahim, A.N. Tiwari, and H. Zogg; www.tfp.ethz.ch

Epitaxial narrow gap lead chalcogenide (IV-VI) layers like PbX, $Pb_{1-x}Sn_xX$, $Pb_{1-y}Eu_yX$ and $Pb_{1-y}Sr_yX$ (X=Te, Se) are investigated for applications and basic research. The band gaps of the active infrared layers are between 0.1 and 0.25 eV (corresponding to wavelengths in the mid-IR range). Larger band gaps are realized with larger y values for the cladding $Pb_{1-y}Eu_yX$ and $Pb_{1-y}Sr_yX$ layers. All layers are grown by solid source molecular beam epitaxy (MBE) onto Si(111)-substrates by employing a CaF_2 buffer layer, or onto BaF_2(111) substrates. The layers are heavily lattice- and (for Si-substrates) thermal-expansion mismatched. However, lead-chalcogenides are fault tolerant, and allow to realize high quality mid-infrared optoelectronic devices. In addition, Bragg mirrors with very high reflectivity over a broad spectral range are easily obtained with a few quarter wavelength layers with alternating high and low refractive indices. With such mirrors Fabry-Perot cavities are formed.

Resonant cavity enhanced detector (RCED)

By placing the active detector layer inside the cavity, a *resonant cavity enhanced detector (RCED)* is obtained. It is sensitive at the resonance wavelengths only where it exhibits a high quantum efficiency. The positions of the resonances are determined by the length of the cavity. In order to change the cavity length, the top mirror can be moved by micromechanical means. Such an arrangement forms a micro infrared spectrometer (Fig. 4.4). With a cavity length of $\sim 15\ \mu\mathrm{m}$ this yields a spectral tuning range of $0.6\ \mu\mathrm{m}$ at wavelengths around $5\ \mu\mathrm{m}$. Spectral width of the line is $< 1\%$.

A convenient way to describe the sensitivities (determined by the noise current densities) of photovoltaic infrared sensors are the $\mathrm{R_0A}$ products where $\mathrm{R_0}$ is the differential resistance of the current-voltage curve at zero bias and A is the diode area. Fig. 4.5 shows the the absolute diffusion limits for bulk and thin absorbers, as well as the Shockley-Read generation/recombination for different lifetimes τ. For $T > 200$ K, the measured $\mathrm{R_0A}$-products are above the theoretical limit for an ideal bulk photodiode. This is due to the limited thickness (volume) of the active device part where S-R generation/recombination noise of charge carriers is possible. With RCED, it is therefore possible to obtain higher sensitivities compared to conventional (thick) photodiodes.

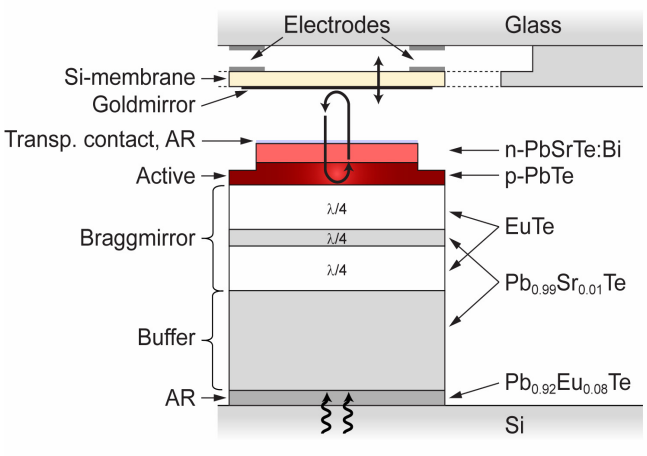

Figure 4.4: Micromid-infrared spectrometer.

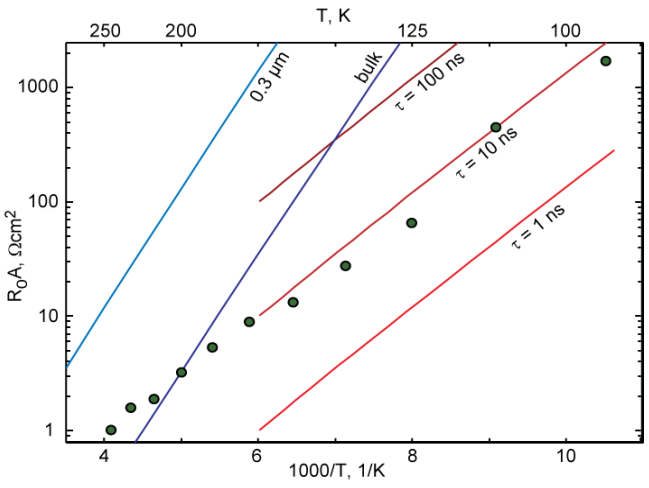

Figure 4.5: Sensitivity ($\mathrm{R_0A}$ product) vs temperature.

Vertical *external* cavity surface emitting laser (V*E*CSEL)

VECSELs for the visible and near-infrared range are becoming popular due to their easy fabrication, scalability, and good beam quality. We realized the first VECSEL in the mid-infrared. The active layer is PbTe with emission wavelength around 5 μm. It is optically pumped with a commercial laser diode with 1.55 μm wavelength (Fig. 4.6). Light in/light out characteristics are shown in Fig. 4.7. Multimode excitation is observed at higher pump powers, while at low power cw (continuous wave) emission is monomode. Maximum operation temperatures are presently 175 K. Similar VECSELs on Si(111) substrates are realized, too. Here, somewhat higher threshold powers are needed.

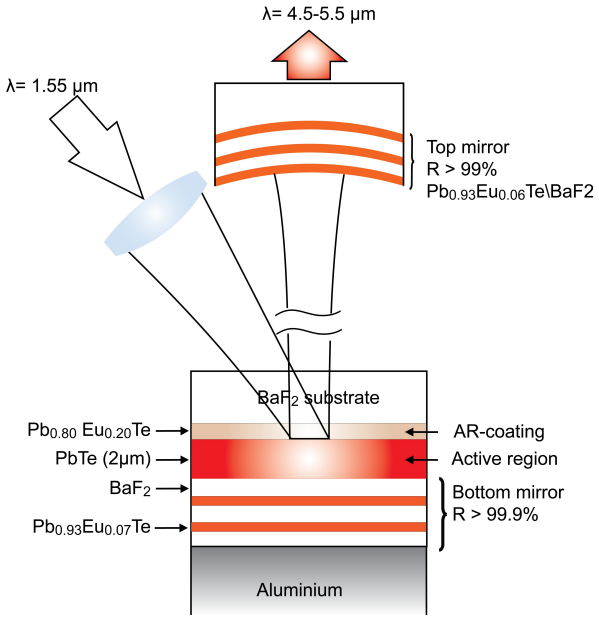

Figure 4.6: Schematic representation of the IV-VI VECSEL. The curved DBR is used as output coupler.

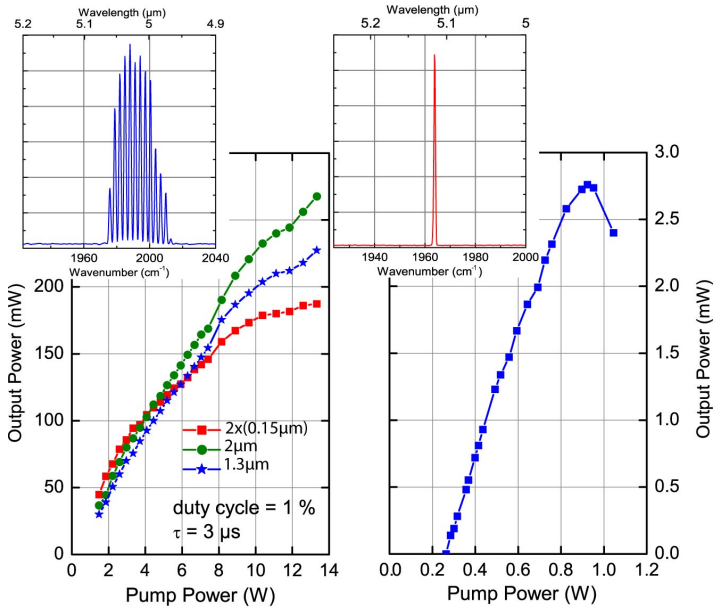

Figure 4.7: Light-in/light-out characteristics at 100 K for pulsed (left) and CW excitation (right).

4.8 Thin-film solar cells based on Cu(In,Ga)Se_2 compound semiconductors

D. Brémaud, S. Bücheler, A. Chirila, S. Seyrling, R. Verma, H. Zogg and A.N. Tiwari; www.tfp.ethz.ch

Safe, cheap, abundant, renewable, and environment-friendly generation of electricity is of considerable interest for our society. Thin-film solar cell technology based on the polycrystalline compound semiconductor Cu(In,Ga)Se_2 (usually abbreviated as ”CIGS”) is a very promising solution for this task. New cell concepts to improve the stability and efficiency are among further projects.

High Growth Rate CIGS layers

Deposition of the CIGS absorber layer in the solar cell by elemental co-evaporation is the currently slowest and one of the most expensive processing steps. Optimizing and simplifying this processing step in terms of increasing the growth rate will provide guidelines for cost-effective industrial production. Development of a suitable growth process requires investigation of the influence of process parameters on structural, compositional, electronic properties of layers and solar cells. We have scaled down our 45 min long state-of-the-art process which yielded a best efficiency of 15.3% to a 20 min long process that yielded 13.2%.

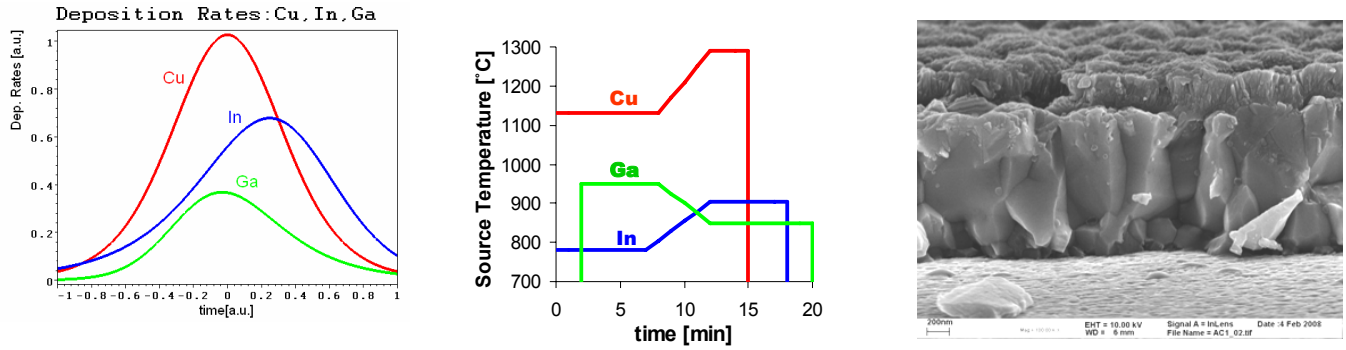

Figure 4.8: Left: Simulated in-line deposition process. Middle: Applied first-order approximation of the simulation. Right: SEM cross section of finished solar cells with CIGS grown in 20 min.

In_2S_3 Buffer layers deposited by physical vapor deposition

Physical vapor deposition was employed to deposit In_2S_3 buffer layers on CIGS absorber. The buffer layers were grown by evaporation of In_2S_3 powder as a source material. The microstructural behavior and chemical composition of the source materials as a function of the time of evaporation have been studied. A significant amount of sulfur loss was detected in coarse powder, while the finer powder was found to be chemically stable. Solar cells made of a buffer layer deposited from fine powder resulted in lower efficiency (8.6%) than that made from coarse powder (11.6%). A highly efficient solar cell of 14.1% efficiency was developed with a ~ 60 nm thin In_2S_3 buffer layer.

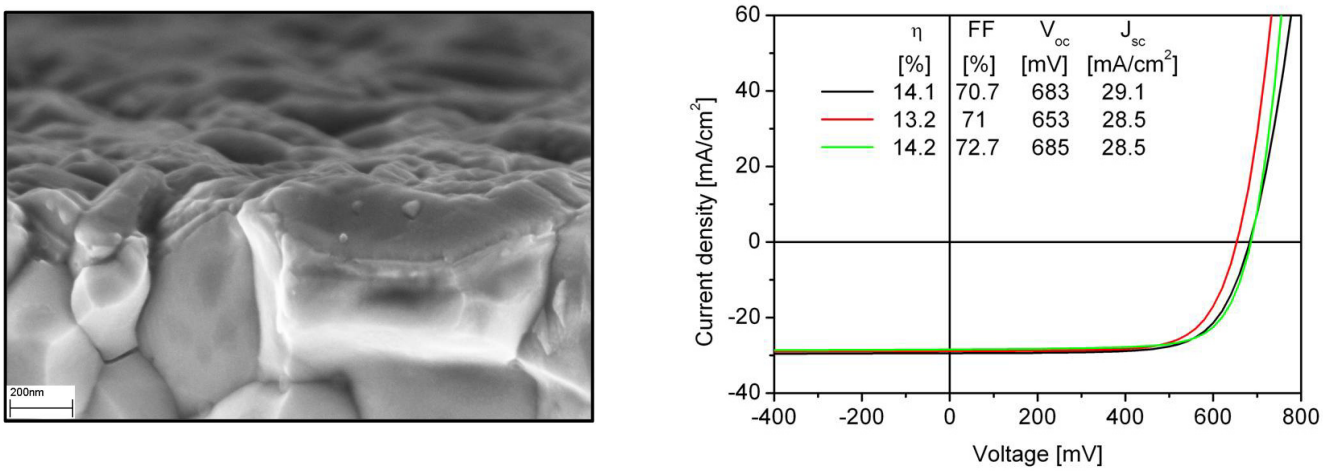

Figure 4.9: Left: a uniform coverage of a ~ 30 nm thick evaporated InxSy layer on CIGS was clearly distinguishable in the SEM cross-section image. Right: J-V characteristic of solar cell with 60 nm thin InxSy buffer layer: (black) as-grown; (red) cell air annealed for 5 min at 200 °C and, (green) CBD-CdS reference cell.

Nanocrystalline dye-sensitized / Cu(In,Ga)Se_2 tandem solar cells

The opto-electronic properties of Cu(In,Ga)Se_2 (CIGS) absorbers, especially the high photon absorption even at longer wavelengths (> 900 nm) and the possibility to adapt the band gap of the semiconductor from 1.04 eV to 1.67 eV, makes them highly attractive candidates for the bottom cell in a tandem configuration. In collaboration with EPFL we used a novel concept of nanocrystalline dye sensitized solar cells as a top cell for the conversion of the high energy photons (wavelengths of 350 - 700 nm) and applied a CIGS solar cell as the bottom cell for the remaining

unabsorbed photons of wavelengths $> 700\ \mathrm{nm}$. The resulting tandem solar cell shows a conversion of 15.1% under AM1.5 illumination and further potential for efficiency improvement.

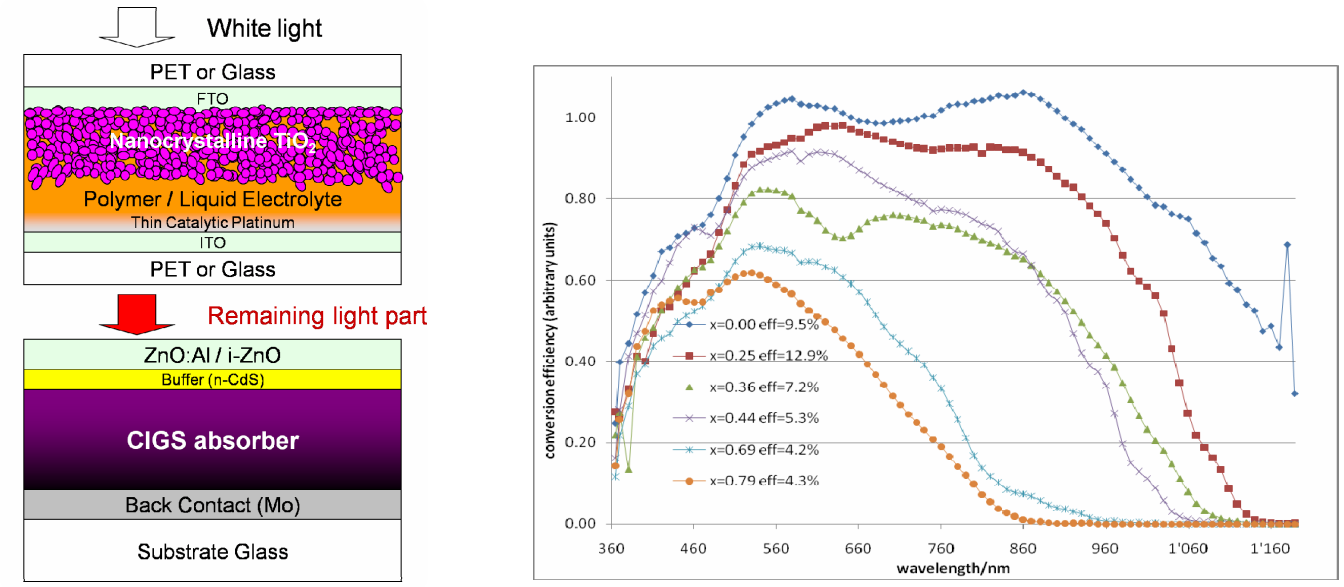

Figure 4.10: Left: Schematic configuration of the mechanical stack of top nanocrystalline dye and bottom CIGS tandem solar cell showing various device layers. Right: Quantum efficiency of CIGS cells with different Ga contents to adapt the band gap.

Chapter 5

Quantum device lab

(http://qudev.ethz.ch/)

Head
Prof. Dr. Andreas Wallraff

Academic Staff
Matthias Baur
Romeo Bianchetti
Deniz Bozyiqit
Dr. Stephan Filipp
Johannes Fink
Andreas Fragner
Tobias Frey
Martin Göppl
Dr. Peter Leek
Peter Maurer
Gabriel Puebla
Lars Steffen
Prisca Studer
Wolf Wüster

Technical Staff
Hansrudolf Aeschbach

Administrative Staff
Gaby Strahm

Diploma theses
Matthias Baur
Quantum Electrodynamics with Superconducting Circuits:
Measurement of the Cavity Photon Number using Ramsey Interference
August 2007

Johannes Fink
Single Qubit Control and Observation of Berry's Phase in a Superconducting Quantum Circuit
August 2007

5.1 Geometric Phases in Superconducting Qubits

P. J. Leek, J. M. Fink, R. Bianchetti, M. Göppl, A. Wallraff

in collaboration with A. Blais, Université de Sherbrooke, Canada, J. M. Gambetta, University of Waterloo, Canada, and D. I. Schuster, L. Frunzio, and R. J. Schoelkopf, Yale University, New Haven, USA.

In quantum information science, the phase of a wavefunction plays an important role in encoding information. A promising new approach to manipulating quantum phases is to use an effect known as geometric phase. This approach has come to the fore in recent years, since it has been argued to have potential for fault tolerance, an important requirement for practical scaling of a quantum information processor. Geometric phases have been used to carry out basic quantum operations using both nuclear magnetic resonance [1] and ion trap based systems [2], and there has been considerable interest in the quantum information community in observation of similar effects in solid state systems such as superconducting qubits [3]. Using our new setup for superconducting Circuit QED experiments, completed last year, and after the successful implementation of a number of key intermediate goals, we were able to carry out an experiment in which we observed geometric phase for the first time in a solid state qubit. Our results were reported in *Science* in December 2007 [4].

An illustrative example of how geometry induces transformation is the following. Raise your right arm above your head, with your thumb pointing left. Now bring your hand down so that it is in front of you, and then move your arm out to the right, without twisting it. Now raise your arm back above your head, and you will find that your thumb now points in a different direction (to the front). During the whole process, your arm did not twist, and yet it ends up rotated! Formally speaking this experiment deals with a vector living on the surface of a sphere (Fig. 1a) and changing its position without locally changing its direction. When the vector reaches its initial position again it has been rotated by a certain angle due to a global property of the surface, its curvature. For the case of a sphere, this angle turns out to be proportional to the area enclosed by the path on the surface. Corresponding effects are widespread in science with particularly important cases occurring in quantum physics, something that was first clearly pointed out by Berry in the 1980s [5]. The dependence of geometric phases only on global geometric properties, and their independence of path details may translate to good tolerance of errors in quantum computations [1].

In our experiment we manipulate the state of a superconducting charge qubit (a Cooper Pair Box) by radiating it with precisely controlled microwave fields. By tuning the amplitude and phase of the fields over time, the qubit state vector can be transported around a closed path in a certain parameter space, depicted in Fig. 1b. If the fields are changed slowly enough that the system evolution is adiabatic, the qubit state then acquires a geometric phase known as Berry's Phase, proportional to the solid angle enclosed by the path. The situation is analogous to having a spin-1/2 particle

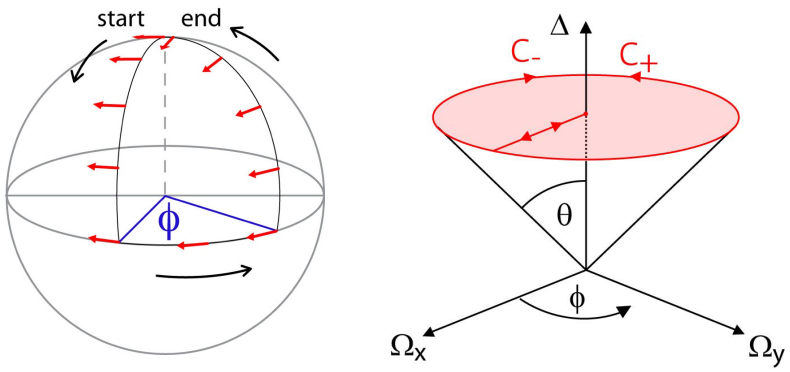

Figure 5.1: (a) Parallel transport of a vector around a closed loop on a curved surface causes it to rotate by a 'geometric angle'. This is the classical analogue of a geometric phase in quantum mechanics. (b) Parameter space paths traced in the experiment. Ω_x and Ω_y are the amplitudes of microwave fields applied to the qubit with x and y quadrature respectively, and Δ is the difference frequency between the microwave fields and the transition frequency of the qubit.

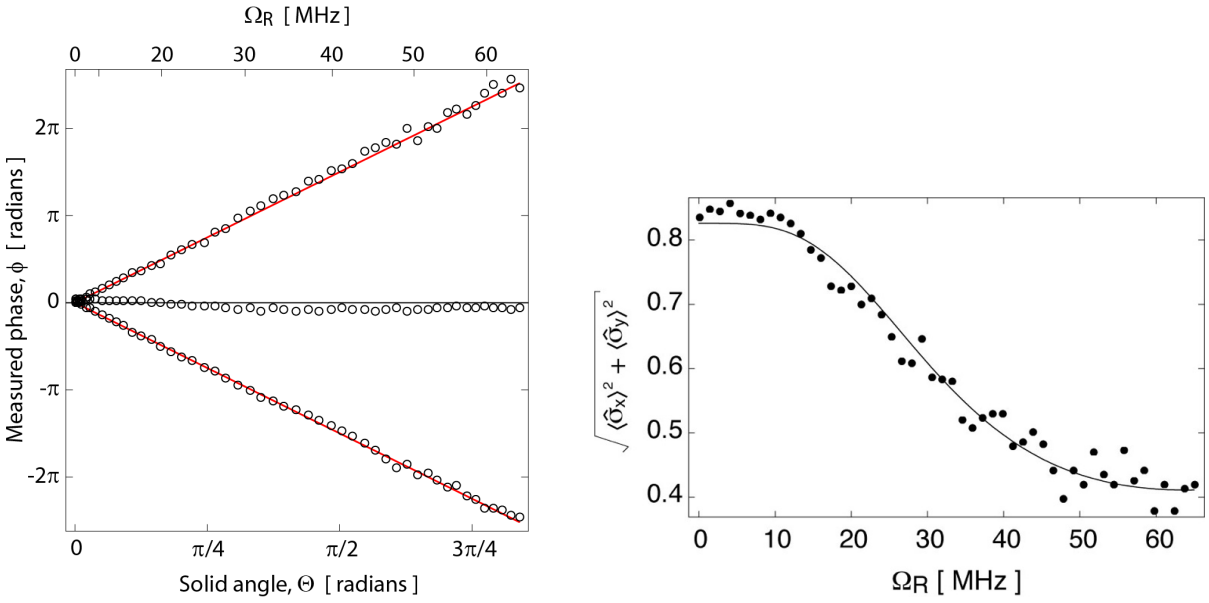

Figure 5.2: (a) Geometric phase measured as a function of parameter space solid angle. A positive or negative phase (upper and lower traces respectively) is seen depending which direction the geometric path is swept. (b) Equatorial Bloch vector component of the qubit as a function of the radius of the conical path, fitted to theory as explained in the text.

in a slowly changing magnetic field, with the magnetic field vector replaced instead by a vector of the radiation field parameters.

An important ingredient for the experiment is the fact that when a superconducting qubit is embedded in a transmission line resonator in the circuit QED architecture, it is isolated effectively from its electromagnetic environment, leading to a long energy relaxation time (in this case $T_1 \approx 10\ \mu$s). This is important for carrying out adiabatic evolutions within the qubit coherence time. In order to observe clearly the geometric phase, a 'spin echo' pulse sequence was used to accurately eliminate dynamic phases [6]. Qubit state tomography was also used, to measure all components of the qubit state vector and hence extract the phase [7].

The geometric phase measured in the experiment as a function of the solid angle of the parameter space path is shown in Fig. 2a. The dependence is seen to be linear, and in very good agreement with Berry's predictions. A number of different path symmetries were also used to further verify the geometric nature of the observed phase, and the effective elimination of dynamic phases (multiple lines in Fig. 2a).

In addition to measuring the geometric phase itself, it was also possible in our experiment to observe the effects of geometric dephasing (Fig. 2b). In superconducting charge qubits, dephasing is dominated by low frequency fluctuations in the qubit transition frequency induced by charge noise coupling to the qubit. The spin echo pulse sequence effectively cancels the dynamic dephasing due to the low frequency noise. However, the geometric phase is sensitive to slow fluctuations, since they cause the height of the conical path to change from one measurement to the next. The geometric dephasing that we observed (Fig. 2b) is in good agreement with theoretical predictions for this case of predominantly slow fluctuations [8].

The results are one of the clearest demonstrations of geometric phase in quantum systems. The experiments may be extendable in the future to look in more detail at the effects of adiabaticity and noise on geometric phases, topics that have been discussed extensively in theoretical literature, but not yet compared with experiment. In addition, two-qubit gates robust against errors may be constructed based on geometric phases. Such gates are extremely important as the building blocks of a future quantum computer.

[1] J. A. Jones, V. Vedral, A. Ekert, G. Castagnoli, *Nature* **403**, 869 (2000).

[2] D. Leibfried *et al.*, *Nature* **422**, 412 (2003).

[3] G. Falci *et al.*, *Nature* **407**, 355 (2000).

[4] P. J. Leek *et al.*, *Science* **318**, 1889 (2007).

[5] M. V. Berry, *Proc. R. Soc. London Ser. A* **392**, 45 (1984).

[6] L. Steffen, Semester Thesis, *Quantum Device Lab*, ETH Zürich (2007).

[7] P. Maurer, Semester Thesis, *Quantum Device Lab*, ETH Zürich (2007).

[8] G. De Chiara, G. M. Palma, *Phys. Rev. Lett.* **91**, 090404 (2003).

5.2 Charge noise insensitive superconducting qubits

M. Baur, R. Bianchetti, J. M. Fink, M. Göppl, P. J. Leek, A. Wallraff

One of the major challenges in current research towards the realization of a quantum computer is to reach long coherence times. For the Cooper pair box (CPB) qubit used in our previous measurements [9-12], the highest dephasing time $T_2 \approx 500$ ns reached so far is still several orders of magnitude too short for a scalable quantum information processor. Even by operating the CPB at its sweet spot (at which the qubit is to first order insensitive to charge noise), it is still mainly limited by 1/f charge noise and quasiparticle tunnelling through the Josephson junctions. A modified design of the CPB using higher Josephson energy to charging energy ratios, leads to a regime, where the qubit is completely insensitive to charge bias [10]. Those qubits, called transmons, show significantly enhanced dephasing times T_2 [11], while maintaining the ability to tune their transition frequencies over the whole spectrum with external flux bias. Another favorable characteristic of the transmon qubit is the high strength of electrical dipole coupling g to the resonator in a circuit QED system due to its large dimension, which enables fast qubit photon interactions that are advantageous for implementation of fast qubit-qubit gates and novel quantum optics experiments.

In December 2007 we have fabricated first transmon qubits coupled to a transmission line resonator in a circuit QED architecture. A colorized SEM picture of the geometry of such a transmon qubit is shown in Fig 5.3. In this system, ultra strong coupling between the qubit and the resonator field can be achieved. To probe the coupling, the qubit transition frequency ν_{ge} is tuned trough the resonator with external flux bias (see Fig 5.4a), while measuring the amplitude of a microwave signal transmitted through the resonator as a function of frequency. At half integers of a flux quantum, where the qubit transition frequency approaches zero, the resonator is completely unperturbed by the qubit and we see the transmission spectrum of the resonator at its bare resonator frequency ν_r with a linewidth of 0.45 MHz (see Fig. 5.4b). As the qubit and the resonator approach degeneracy, excitations become shared between them and the degeneracy is split into two qubit-atom superposition states, the Vacuum Rabi mode splitting (see Fig 5.4c). From the frequency separation of the two peaks $2g$ we find a large dipole coupling strength of $g/2\pi = 150$ MHz. The high ratio of the splitting to the individual peak line width of about 100 is a clear indication that we reached the ultra strong coupling in our system, where the coherent coupling rate g is much larger than the rate at which photons are lost by the resonator and the rate at which the qubit loses its coherence. This should enable us to do new interesting quantum

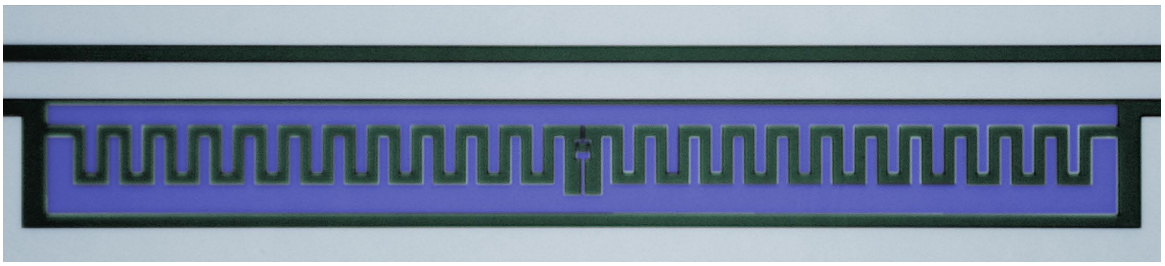

Figure 5.3: Colorized SEM picture of a transmon qubit (blue) with its big interdigitated shunt capacitor to lower the charging energy. The center conductor of the resonator and the ground planes are colored in grey whereas the substrate is green.

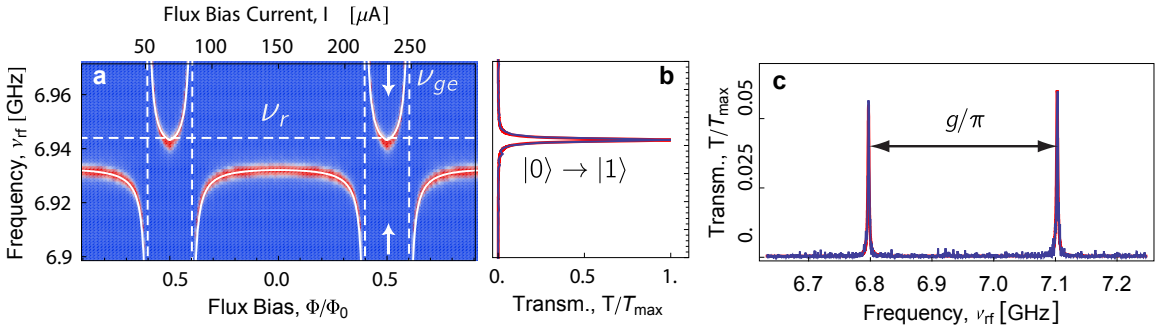

Figure 5.4: a) Measurement of the resonator transmission spectrum versus magnetic flux ϕ. The white dashed lines show the the bare resonator frequency ν_r and the qubit transition frequency ν_{ge} crossing the resonator. b) Resonator transmission T at the bare resonator frequency. c) Vacuum Rabi mode splitting at the degeneracy point with a Lorentzian fit in red.

optics experiments in the next years, such as the spectroscopic measurement of the square root of n nonlinearity of the Jaynes-Cummings energy ladder, where n is the intra cavity photon number.
The energy relaxation and dephasing times in this new transmon sample are $T_1 \leq 350$ ns resp. $T_2 \leq 100$ ns. We are confident to be able to increase these values into the microsecond range during the next year which will allow us to start to coherently couple several transmon qubits with a single resonator for multi-qubit Circuit QED and Quantum Information Processing and Communication (QIPC) experiments.

[9] P. J. Leek *et al.*, *Science* **318**, 1889 (2007).

[10] J. Koch *et al.*, *PRA* **76**, 42319 (2007).

[11] J. A. Schreier *et al.*, *arXiv:0712.3581* (2007).

[12] A. Wallraff *et al.*, *PRL* **99**, 50501 (2007).

5.3 Fabrication of Superconducting Resonators and Qubits

M. Göppl, M. Baur, R. Bianchetti, S. Fillip, J. Fink, P. Leek, L. Steffen, A. Wallraff

For the realization of a quantum computer the scalability of quantum electronic circuits is a crucial point. Superconducting qubits implemented into transmission lines have the advantage that standard microfabrication techniques can be used for their realization. The qubits contain sub-micron size Aluminum-Aluminumoxide-Aluminum tunnel junctions which are fabricated using electron beam lithography and shadow-evaporation. We have successfully implemented and improved these techniques in ETH's clean room facility FIRST. As key instrument for qubit fabrication, a

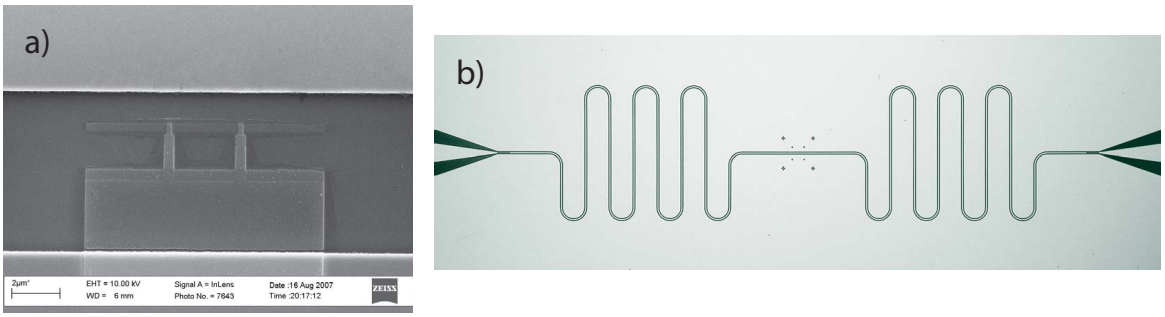

Figure 5.5: a) SEM image of a qubit structure, integrated into a coplanar waveguide resonator. The red circles indicate the Josephson junction positions. b) Optical image of an etched niobium resonator. The crosses in the central part are markers for the subsequent qubit implementation by e-beam lithography.

new electron-beam evaporator with advanced capabilities for making Josephson junction devices was installed, tested and calibrated in FIRST. A bi-layer electron-beam resist (PMMA/MAA) with controlled undercut and resist bridges was implemented. The upper layer (PMMA 950k) is about 60 nm thick and serves as mask for the subsequent evaporation of aluminum. The lower layer (PMMA/MAA) serves as spacer for the upper layer and is about 600 nm thick. A large undercut in the resist structure leads to free standing resist bridges. When evaporating aluminum under a certain angle the free standing resist bridge casts a shadow in the aluminum film on the substrate. Evaporating another aluminum film under a second angle leads to an overlap of two aluminum films. The two aluminum films form the two electrodes of a Josephson junction. A thin insulating layer of aluminum oxide is realized by oxidizing the bottom electrode after evaporation. Figure 5.5(a) shows a typical qubit structure after evaporation and lift-off. The junction size and the thickness of the oxide layer determine the Josephson and the charging energy, the two intrinsic energy scales of the structure, and therefore have to be well controlled. We have optimized these two parameters and have tested different qubit designs.
In parallel we have developed an etching process to fabricate Niobium thin film resonators on thermally oxidized silicon and sapphire substrates into which we integrate qubit structures in order to perform cavity QED experiments. Figure 5.5(b) shows an etched Niobium resonator. Resonators with quality factors up to several hundred thousand have been fabricated and tested at low temperatures. We have successfully integrated qubits into coplanar waveguide resonators and have successfully performed characterizations of several qubit structures. In the future, we will further improve the control of our process parameters and will continue doing experiments on single and multi qubit devices.

5.4 High Frequency Molecular Electronics

G. Puebla-Hellmann, P. Leek, A. Wallraff

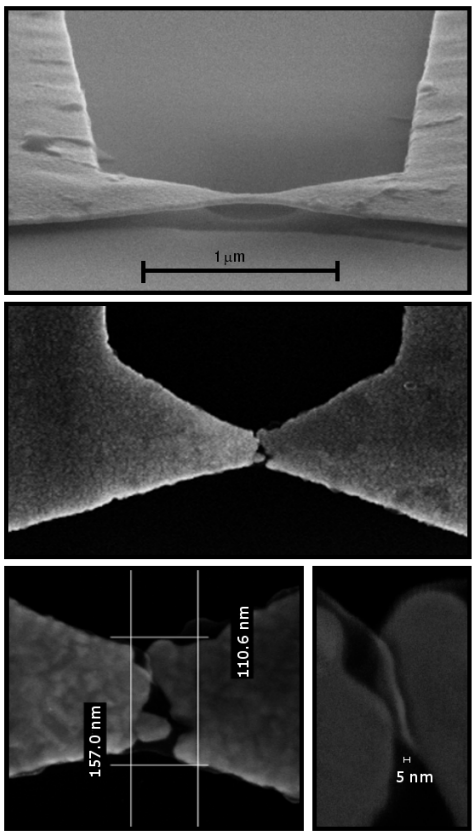

Figure 5.6: Sequential zoom in on a electromigrated break junction.

An essential ingredient for the progress in modern microelectronics and information technology is the miniaturization of the device components used in integrated circuit fabrication. The successive miniaturization of such device elements allows for a doubling of the number of components in an integrated circuit, e.g. a microprocessor, every 18 months. This increases the versatility of the device while at the same time reducing its cost. Currently, novel approaches for further reducing component size in integrated circuits are intensely investigated. These approaches are exploring the use of nano-scale objects such as nano wires, nano tubes and even individual molecules for integrated circuit technology. A number of important results have been obtained in this field already.
However, it still remains a difficult problem to manipulate and probe such electronic devices on short time scales. The band widths with which such operations can be performed are limited by the intrinsic high impedance of nano scale objects, the resistance of which are on the order of the quantum resistance or above. We intend to address this problem by embedding nano scale circuits into high-frequency impedance transformation circuits. This will allow us to address individual molecules on short time scales and explore their properties for integrated circuit fabrication in novel and efficient ways. Two important steps towards the reflectrometric measurement of single molecules were made in our lab in 2007: the fabrication of impedance transformers and of nm spaced contacts for the molecule.
In order to create nm spaced gold electrodes for embedding nm scale objects, gold nanowires with a cross section of 25×100 nm were broken in a controlled fashion by electromigration. This is a process in which the momentum transfer from electrons to the gold atoms leads to a mass flow, creating voids and hillocks. By ramping the voltage and monitoring the rate of change in resistance of the nanowire,

electromigration can be detected, allowing for a controlled thinning of the wire. Such an electromigrated wire is shown in Fig. 5.6, with a gap size of $\leq$7 nm. At cross sections of tens of atoms, the conductance through the wire becomes quantized, similar to a quantum point contact. As the wire is migrated, the conductance decreases in a stairway like fashion (Fig. 5.7 a.).
The second step has been the fabrication of superconducting high frequency impedance transformers and their characterization. The implemented transformers are single stub tuners in coplanar waveguide geometry. Here a changing load changes the reflection coefficient as the load moves in or out of match. Measurements of several unloaded devices have been made at temperatures down to 20 mK, allowing the extraction of characteristic parameters, such as microwave phase velocity and attenuation from the reflection spectrum. Temperature dependence measurements have been carried out confirming that the devices indeed work as impedance transformers. A stub tuner can match to its intrinsic losses in a temperature sweep as both phase velocity and loss are temperature dependent (Fig. 5.7 b.).
The next step toward probing single molecules will be the embedding of the nm spaced leads into a stub tuner. We will also be able to study the electromigration process in more detail using this setup. The first molecule of interest will be a carbon nanotube to verify the measurement technique. We are also investigating mechanically tunable break junctions as an alternative to the static electrodes currently used. In these junctions the electrode distance can be tuned by bending the substrate.

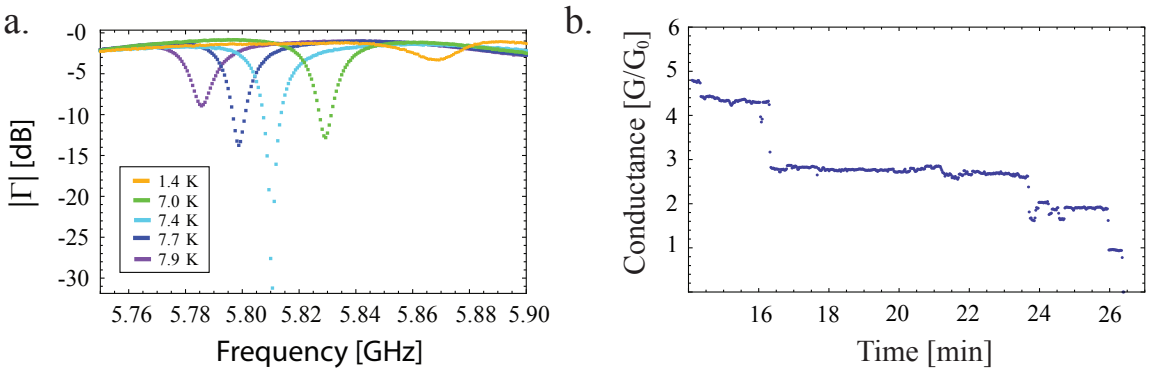

Figure 5.7: a. Quantized conductance observed while electromigrating a gold wire. b. Reflection spectrum of an open stub tuner for different temperatures.

Chapter 6

Publications

A. Akrap, E. Tutis, S. M. Zhigadlo, J. Karpinski, L. Forro,
Manifestations of fine features of the density of states in the transport properties of KOs_2O_6
Phys. Rev. B 75, 172501 (2007)

M. d'Astuto, M. Calandra, S. Reich, A. Shukla, M. Lazzeri, F. Mauri, J. Karpinski, N. D. Zhigadlo, A. Bossak, and M. Krisch,
Weak anharmonic effects in MgB_2 : A comparative inelastic x-ray scattering and Raman study,
Phys. Rev. B 75, 174508 (2007)

A. Baumgartner, T. Ihn, K. Ensslin, K. Maranowski and A. C. Gossard
Quantum Hall effect transition in scanning gate experiments
Phys. Rev. B 76, 085316 (2007)

B. Bilki, M. Erbudak, M. Mungan and Weisskopf Y.
Structure formation of a layer of adatoms on a quasicrystalline substrate: Molecular dynamics study
Phys. Rev. B 75, 045437 (2007)

A. Blais, J. Gambetta, A. Wallraff, D. I. Schuster, S. M. Girvin, M. H. Devoret, R. J. Schoelkopf
Quantum information processing with circuit quantum electrodynamics
Phys. Rev. A 75, 032329 (2007)

G. Blumberg, A. Mialitsin, B. S. Dennis, M. V. Klein, N. D. Zhigadlo, and J. Karpinski
Observation of Leggett's Collective Mode in a Multiband MgB_2 Superconductor
Phys. Rev. Lett. 99, 227002 (2007)

G. Blumberg, A. Mialitsin, B. S. Dennis, N. D. Zhigadlo, J. Karpinski,
Multi-gap superconductivity in MgB_2: Magneto-Raman spectroscopy
Physica C 456, 75-82 (2007)

D. Brémaud, D. Rudmann, M. Kaelin, K. Ernits, G. Bilger, M. Döbeli, H. Zogg, A. N. Tiwari
Flexible Cu(In,Ga)Se_2 on Al foils and the effects of Al during chemical bath deposition
Thin Solid Films 515 (15), 2007, p. 5857-5861

D. Brémaud, A. N. Tiwari
Flexible Cu(In,Ga)Se_2 solar cells and technologies
Proceedings 22nd European Photovoltaic Solar Energy Conference, Milano, 2007

M. Brühwiler, T. Schulze, S.M. Kazakov, Z. Bukowski, R. Puzniak, N.D. Zhigadlo, J. Karpinski and B. Batlogg,
Superconductivity in the Beta-pyrochlore osmates
Physica C 460-462, 62-65, (2007)

D. Daghero, A. Calzolari, M. Tortello, G. A. Ummarino, R. S. Gonnelli, V. A. Stepanov, N. D. Zhigadlo, K. Rogacki und J. Karpinski,
Point-Contact Spectroscopy in Mn-Doped MgB_2 Single Crystals: Effects of Magnetic Impurities in a Two-Band Superconductor,
J. Supercond. Nov. Magn. 20, 523-526 (2007).

D. Daghero, A. Calzolari, D. Delaude, R. S. Gonnelli, M. Tortello, G.A. Ummarino, V.A. Stepanov, N.D. Zhigadlo, J. Karpinski and M. Putti,
Point-contact study of the role of non-magnetic impurities and disorder in the superconductivity of MgB_2
Physica C 460-462, 975-976, (2007)

M. Eisterer, C. Krutzler, M. Zehetmayer, H.W. Weber, S.M. Kazakov and J. Karpinski
Influence of carbon doping on the reversible magnetization of MgB_2 single crystals
Physica C 460-462, 606-607 (2007)

M. Erbudak
Tek umudumuz nanoteknoloji / Nanotechnologie, letzte Hoffnung
http://www.gercekgundem.com/?p=97815

M. Erbudak
Nanoteknolojide ilk uygulama Nanobiyoloji
Bilim ve Ütopya 2, 18-19 (2007)

K. Ernits, D. Brémaud, S. Buecheler, C. J. Hibberd, M. Kaelin, G. Khrypunov, U. Müller, E. Mellikov, A. N. Tiwari
Characterisation of ultrasonically sprayed In_xS_y buffer-layers for Cu(In,Ga)Se_2 solar cells
Thin Solid Films 515 (15), 2007, p. 6051-6054

Y. Fasano, I. Maggio-Aprile, J. Karpinski and Ø. Fischer ,
Tunneling and pseudo point-contact spectroscopy on $YBa_2Cu_4O_8$,
Physica C 460-462, Part 2, 958-960, (2007)

F. Felder, M. Arnold, C. Ebneter, M. Rahim, H. Zogg
Wavelength tunable Resonant Cavity Enhanced Photodetectors based on lead-salts grown by MBE
Proc. 13th International Conference on Narrow Gap Semiconductors, Springer Proceedings in Physics Series, 2007, to be published

F. Felder, M. Arnold, M. Rahim, C. Ebneter, H. Zogg
Tunable lead-chalcogenide on Si resonant cavity enhanced mid-infrared detector
Appl. Phys. Lett. 91, 2007, 101102

J. Fujii, F. Borgatti, G. Panaccione, M. Hochstrasser, F. Maccherozzi and G. Rossi
Magnetic properties of epitaxial Fe films on MnPt/Fe(1 0 0)
Surface Science 601, 18, 4288-4291 (2007)

J. Gambetta, W. A. Braff, A. Wallraff, S. M. Girvin, R. J. Schoelkopf
Protocols for optimal readout of qubits using a continuous quantum nondemolition measurement
Phys. Rev. A 76, 012325 (2007)

A. E. Gildemeister, T. Ihn, C. Barengo, P. Studerus, and K. Ensslin
Construction of a dilution refrigerator cooled scanning force microscope
Rev. Sc. Instr. 78, 013704 (2007)

A. E. Gildemeister, T. Ihn, M. Sigrist, K. Ensslin, D. C. Driscoll, and A. C. Gossard
Measurement of the tip-induced potential in scanning gate experiments
Phys. Rev. B 75, 195338 (2007)

A. E. Gildemeister, T. Ihn, M. Sigrist, K. Ensslin, D. C. Driscoll, and A. C. Gossard
In Situ Treatment of a Scanning Gate Microscopy Tip
Appl. Phys. Lett. 90, 213113 (2007)

A. E. Gildemeister, T. Ihn, R. Schleser, K. Ensslin, D. C. Driscoll, and A. C. Gossard
Imaging a Coupled Quantum Dot - Quantum Point Contact System
J. Appl. Phys. 102, 083703 (2007)

F. Giubileo, F. Bobba, A. Scarfato, A. M. Cucolo, A. Kohen, D. Roditchev, N. D. Zhigadlo, and J. Karpinski,
Local tunneling study of three-dimensional order parameter in the π band of Al-doped MgB_2 single crystals,
Phys. Rev. B 76, 024507 (2007)

F. Giubileo, F. Bobba, A. Scarfato, D. Roditchev, N. Zhigadlo, J. Karpinski and A.M. Cucolo
Nanoscale Spatial non-Homogeneity of 3D Δ_π in $Mg_{0.9}Al_{0.1}B_2$ Single Crystals
Physica C 460-462, 585-586, (2007)

R. S. Gonnelli, A. Calzolari, D. Daghero, D. Delaude, M. Tortello, G. A. Ummarino, V. A. Stepanov, N. D. Zhigadlo, J. Karpinski und P. Manfrinetti,
Effect of Havy Al Doping on MgB_2: Point Contact Study of Crystals and Polycrystals,
J. Supercond. Nov. Magn. 20, 555-558 (2007).

R. S. Gonnelli, D. Daghero, G. A. Ummarino, M. Tortello, D. Delaude, V. A. Stepanov and J. Karpinski
Point-contact Andreev-reflection spectroscopy in MgB_2: The role of substitutions
Physica C 456, 134-143 (2007)

D. Graf, F. Molitor, K. Ensslin, C. Stampfer, A. Jungen, C. Hierold, and L. Wirtz
Spatially resolved Raman spectroscopy of single- and few-layer graphene
Nano Letters 7, 238 (2007)

D. Graf, F. Molitor, K. Ensslin, C. Stampfer, A. Jungen, C. Hierold, and L. Wirtz
Raman imaging of graphene
Solid State Comm. 143, 44 (2007)

D. Graf, F. Molitor, T. Ihn, and K. Ensslin
Phase-coherent transport measured in a side-gated mesoscopic graphite wire
Phys. Rev. B 75, 245429 (2007)

D. Graf, F. Molitor, K. Ensslin, C. Stampfer, A. Jungen, C. Hierold, and L. Wirtz
Raman imaging of a single-layer to double-layer graphene transition
Eur. Phys. J. 148, 177 (2007)

B. Grbic , R. Leturcq , T. Ihn , K. Ensslin , D. Reuter, and A. D. Wieck
Aharonov-Bohm oscillations in the presence of strong spin-orbit interaction
Phys. Rev. Lett. 99, 176803 (2007)

S. Gustavsson, R. Leturcq, T. Ihn, K. Ensslin, M. Reinwald, and W. Wegscheider
Measurements of higher-order noise correlations in a quantum dot with a finite bandwidth detector
Phys. Rev. B 75, 075314 (2007)

S. Gustavsson, R. Leturcq, T. Ihn, K. Ensslin, D.C. Driscoll, A.C. Gossard
Noise measurements in quantum dots using charge detection techniques
Physica E 40, 103 (2007)

S. Gustavsson, M. Studer, R. Leturcq, T. Ihn, K. Ensslin, D. C. Driscoll and A. C. Gossard
Frequency-selective single photon detection using a double quantum dot
Phys. Rev. Lett. 99, 206804 (2007)

S. Haas, A. F. Stassen, G. Schuck, K. P. Pernstich, D. J. Gundlach, B. Batlogg, U. Berens and H.-J. Kirner
High charge-carrier mobility and low trap density in a rubrene derivative
Phys. Rev. B 76, 115203(2007)

S. Haas, B. Batlogg, C. Besnard, M. Schiltz , C. Kloc, T. Siegrist
Large uniaxial negative thermal expansion in pentacene due to steric hindrance
Phys. Rev. B 76, 205203 (2007)

K. H. Hassdenteufel, A. R. Oganov, S. Katrych, and W. Steurer
Ab initio study of W-Al-Co-Ni, an approximant of the decagonal Al-Co-Ni quasicrystal
Phys. Rev. B, 17, 144114-1/144115-6 (2007)

T. Ihn, M. Sigrist, K. Ensslin, W. Wegscheider and M. Reinwald
Interference in a quantum dot molecule embedded in a ring interferometer
New Journal of Physics 9, 111 (2007)

W. L. Kalb, T. Mathis, S. Haas, A. F. Stassen, and B. Batlogg,
Organic small molecule field-effect transistors with Cytop(TM) gate dielectric: Eliminating gate bias stress effects
Appl. Phys. Lett. 90, 092104 (2007)

W. L. Kalb, T. Mathis, S. Haas, A. F. Stassen, and B. Batlogg,
High performance organic field-effect transistors with fluoropolymer gate dielectric
Proc. of SPIE Vol. 6658, 665807-7 (2007)

W. L. Kalb, F. Meier, K. Mattenberger, and B. Batlogg,
Defect healing at room temperature in pentacene thin films and improved transistor performance
Phys. Rev. B 76, 184112 (2007)

J. Karpinski, N.D. Zhigadlo, S. Katrych, R. Puzniak, K. Rogacki, R. Gonnelli
Single crystals of MgB_2: synthesis, substitutions and properties
Physica C, 456, 3-13, (2007)

J. Karpinski,
20 years High Pressure Materials Synthesis Group Activity After Discovery of High-T_c Superconductors
In: High Tc Superconductors and Related Transition Metal Oxides, Editors: A. Bussmann-Holder, H. Keller, Springer-Verlag, 167-175, (2007)

J. Karpinski, N. D. Zhigadlo, S. Katrych, R. Puzniak, K. Rogacki, R. Gonneli,
Review paper: Single crystals of MgB_2: Synthesis, substitutions and properties
Physica C 456, 3-13 (2007)

S. Katrych, Th. Weber, M. Kobas, L. Massüger, L. Palatinus, G. Chapuis,W.
Steurer: New stable decagonal quasicrystal in the system Al-Ir-Os,
Journal All. and Compounds, 428, 164-172 (2007)

S. Katrych, V.M. Petyukh, A.A. Bondar, W. Steurer
Phase relations in the Al-Ir-Os system in the range up to 70 at.% Al
Powder Metallurgy and Metal Ceramics, 46, 357-364 (2007)

R. Khasanov, N. D. Zhigadlo, J. Karpinski, and H. Keller,
In-plane magnetic penetration depth in $Ca_{2-x}Na_xCuO_2Cl_2$: Role of the apical sites ,
Phys. Rev. B 76, 094505 (2007)

R. Khasanov, A. Shengelaya, A. Bussmann-Holder, J. Karpinski, H. Keller, K. A. Müller,
S-wave Symetry Along the c-axis and s+d In plane Superconductivity in Bulk $YBa_2Cu_4O_8$,
J.Supercond. Nov. Magn., DOI 10.1007/s10948-007-0302-z. (2007)

R. Khasanov, A. Shengelaya, D. Di Castro, D. G. Eshchenko, I. M. Savic, K. Conder, E. Pomjakushina, J. Karpinski, S. Kazakov, H. Keller,
Magnetic field dependence of the oxygen isotope effect on the magnetic penetration depth in hole-doped cuprate superconductors
Phys. Rev. B 75, 060505 (2007)

T. Kondo, R. Khasanov, J. Karpinski, S. M. Kazakov, N. D. Zhigadlo, T. Ohta, H. M. Fretwell, A. D. Palczewski, J. D. Koll, J. Mesot, E. Rotenberg, H. Keller, and A. Kaminski,
Dual Character of the Electronic Structure of $YBa_2Cu_4O_8$: The Conduction Bands of CuO_2 Planes and CuO Chains,
Phys. Rev. Lett. 98, 157002 (2007)

G. Krauss, Q.F. Gu, S. Katrych, S. Deloudi, W. Steurer
A high-pressure study of Co-rich decagonal Al-Co-Ni and its approximant, the W phase
Phil. Mag. 87, 2921-2927, (2007)

G. Krauss, Q. Gu, S. Katrych, and W. Steurer
In-situ study of icosahedral Zn-Mg-Dy and Co-rich decagonal Al-Co-Ni at high pressures and high temperatures
Journal of physics-condensed matter, 19 (11) (2007)

C. Krellner, S. Haas, C. Goldmann, K. P. Pernstich, D. J. Gundlach, and B. Batlogg
Density of bulk trap states in organic semiconductor crystals: Discrete levels induced by oxygen in rubrene
Phys. Rev. B 75, 245115 (2007)

C. Krutzler, M. Zehetmayer, M. Eisterer, H.W. Weber, N.D. Zhigadlo, J. Karpinski
Comparative study of neutron irradiation and carbon doping in MgB_2 single crystals
Phys. Rev. B 75, 224510 (2007)

C. Krutzler, M. Zehetmayer, M. Eisterer, H.W. Weber, N.D. Zhigadlo and J. Karpinski,
Modification of the defect structure in MgB_2 single crystals by carbon doping and neutron irradiation
Physica C 460-462, 555-556, (2007)

M. Lavagnini, A. Sacchetti, L. Degiorgi, K.Y. Shin, and I.R. Fisher
Optical properties of the Ce and La ditelluride charge density wave compounds
Phys. Rev. B 75, 205133 (2007)

L. Lecren, W. Wernsdorfer, Y.-G. Li, A. Vindigni, H. Miyasaka and R. Clerac
One-Dimensional Supramolecular Organization of Single-Molecule Magnets
J. Am. Chem. Soc. 129, 5045 (2007)

P. J. Leek, J. M. Fink, A. Blais, R. Bianchetti, M. Goppl, J. M. Gambetta, D. I. Schuster, L. Frunzio, R. J. Schoelkopf, and A. Wallraff
Observation of Berry's Phase in a Solid State Qubit
Science, 318, 1889 (2007)

J.-N. Longchamp
Thin films on icosahedral AlPdMn quasicrystal
Logos Verlag, Berlin, 2006; ISBN 978-3-8325-1781-6

J.-N. Longchamp, S. Burkardt, M. Erbudak and Y. Weisskopf
CdTe and PbTe nanostructures on the oxidized pentagonal surface of an icosahedral AlPdMn quasicrystal
Surface Science 601, 5441-5444 (2007)

J.-N. Longchamp, S. Burkardt, M. Erbudak and Y. Weisskopf
Formation of a well-ordered ultra-thin aluminum-oxide film on icosahedral AlPdMn quasicrystal
Phys. Rev. B 76, 094203 (2007)

J.-N. Longchamp, Y. Weisskopf and M. Erbudak
Stabilization of the pentagonal surface of the icosahedral AlPdMn quasicrystal by controlled Si adsorption
Appl. Surf. Sci. 253, 5947-50 (2007)

F. Maccherozzi, G. Panaccione, G. Rossi, M. Hochstrasser, M. Sperl, M. Reinwald, G. Woltersdorf, W. Wegscheider and C.H. Back
Surface treatments and magnetic properties of $Ga_{1-x}Mn_xAs$ thin films
Surface Science 601, 18, 4283-4287 (2007)

J. Majer, J. M. Chow, J. M. Gambetta, J. Koch, B. R. Johnson, J. A. Schreier, L. Frunzio, D. I. Schuster, A. A. Houck, A. Wallraff, A. Blais, M. H. Devoret, S. M. Girvin, R. J. Schoelkopf
Coupling Superconducting Qubits via a Cavity Bus
Nature, 449, 443 (2007)

C. May, K. Ensslin, and M. Troyer
Self-consistent potential calculation for locally oxidized Ga[Al]As heterostructures
J. Computer-Aided Mater. Des. 10.1007/s10820-006-9023 (2007)

C. May and M. Troyer and K. Ensslin
Self-consistent simulation of quantum wires defined by local oxidation of Ga(Al)As Heterostructures
Phys. Rev. B 76, 235321 (2007)

L. Meier, G. Salis, I. Shorubalko, E. Gini, S. Schon, and K. Ensslin
Measurement of Rashba and Dresselhaus spin-orbit magnetic fields
Nature Physics 3, 650 (2007)

L. Meier, G. Salis, N. Moll, C. Ellenberger, I. Shorubalko, U. Wahlen, K. Ensslin, and E. Gini
Optimized stray-field-induced enhancement of the electron spin precession by buried Fe gates
Appl. Phys. Lett. 91, 162507 (2007)

A. Mialitsin, B. S. Dennis, N. D. Zhigadlo, J. Karpinski, G. Blumberg,
Anharmonicity and self-energy effects of the E_{2g} phonon in MgB_2,
Phys. Rev. B 75, 020509 (2007)

T. Michlmayr
Local Magnetic Field Generation
Logos Verlag, Berlin, ISBN 978-3-8325-1544-7

F. Molitor, J. Güttinger, C. Stampfer, D. Graf, T. Ihn, and K. Ensslin
Local gating of a graphene Hall bar by graphene side gates
Phys. Rev. B 76, 245426 (2007)

M. Mungan, Y. Weisskopf and M. Erbudak
Deposition of atoms on a quasicrystalline substrate: Molecular dynamics study in three dimensions
Phys. Rev. B 76, 195443 (2007)

D. Oberhoff, K, P. Pernstich, D. J. Gundlach, and B, Batlogg
Arbitrary Density of States in an Organic Thin-Film Field-Effect Transistor Model and Application to Pentacene Devices
IEEE Transactions on electron devices, Vol. 54, No. 1, 17-25, (2007)

D. Pacile', M. Papagno, M. Lavagnini, H. Berger, L. Degiorgi, and M. Grioni
Photoemission and optical studies of $ZrSe_3$, $HfSe_3$, and ZrS_3
Phys. Rev. B 76, 155406 (2007)

B. Pedrini, S. Wessel, J.L. Gavilano, H.R. Ott, S.M. Kazakov, J. Karpinski
Quenching of the Haldane gap in $LiVSi_2O_6$ and related compounds
Eur. Phys. J. B 55, 219-228 (2007)

A. Pfund, I. Shorubalko, K. Ensslin, and R. Leturcq
Suppression of spin relaxation in an InAs nanowire double quantum dot
Phys. Rev. Lett. 99, 036801 (2007)

A. Pfund, I. Shorubalko, K. Ensslin and R. Leturcq
Spin state mixing in InAs double quantum dots
Phys. Rev. B 76, 161308(R) (2007)

A. Pioda, S. Kicin, D. Brunner, T. Ihn, M. Sigrist, K. Ensslin, M. Reinwald and W. Wegscheider
Single electron charging of impurity sites visualized by scanning gate experiments on a quantum point contact
Phys. Rev. B 75, 045433 (2007)

M. Pissas, D. Stamopoulos, N. Zhigadlo, and J. Karpinski,
Influence of aluminum substitution on the vortex matter properties of MgB_2,
Phys. Rev. B 75, 184533 (2007)

M. Powalla, F. Kessler, D. Hariskos, G. Voorwinden, A.N. Tiwari, D. Brémaud, M. Edoff, S. Schleussner, L. Stolt, B. Dimmler et al.
Highly productive manufacturing of CIS-based large-area modules
Proceedings 22nd European Photovoltaic Solar Energy Conference, Milano, 2007

R. Puzniak, A. Wisniewski, A. Szewczyk, K. Kapcia, J. Jun, N.D. Zhigadlo, S.M. Kazakov and J. Karpinski ,
Anisotropic upper critical field of chemically substituted MgB_2 single crystals studied by torque magnetometry
Physica C 460-462, 616-617, (2007)

N. Quack, I. Züst, S. Blunier, J. Dual, M. Arnold, F. Felder, M. Rahim, H. Zogg
Electrostatically actuated Micromirror for Resonant Cavity Enhanced Detectors
MEMS 2007, Proc. 20th IEEE International Conference on MEMS, Kobe, Japan, Jan. 21-25, 2007

N. Quack, S. Blunier, J. Dual, M. Arnold, F. Felder, C. Ebneter, M. Rahim, H. Zogg
Tunable Resonant Cavity Enhanced Detectors using Vertical MEMS Mirrors
Proc. IEEE/LEOS Optical MEMS and Nanophotonics 2007, Hualien, Taiwan, 2007, pp. 165-166

M. Rahim, M. Arnold, F. Felder, I. Zasavitskiy, H. Zogg
Mid-Infrared lead-salt VECSEL (Vertical External Cavity Surface Emitting Laser) for Spectroscopy
Proc. 13th International Conference on Narrow Gap Semiconductors, Springer Proceedings in Physics Series, 2007, to be published

M. Rahim, M. Arnold, F. Felder, K. Behfar, H. Zogg
Mid-infrared lead-chalcogenide vertical external cavity surface emitting laser with $5\ \mu\mathrm{m}$ wavelength
Appl. Phys. Lett. 91, 2007, 151102

B. Rössner, H. von Känel, D. Chrastina, G. Isella, and B. Batlogg
Effective mass measurement: Influence of hole band nonparabolicity in SiGe/Ge quantum wells
Semicond. Sci. Technol. 22, 191-194 (2007)

A. Sacchetti, E. Arcangeletti, A. Perucchi, P. Postorino, S. Lupi, N. Ru, I.R. Fisher, and L. Degiorgi
Pressure dependence of the charge-density-wave gap in rare-earth tritellurides
Phys. Rev. Lett. 98, 026401 (2007)

N. Saratz, T. Michlmayr, O. Portmann, U. Ramsperger, A. Vaterlaus and D. Pescia
Stripe-domain nucleation and creep in ultrathin Fe films on Cu(100) imaged at the micrometre scale
Journal of Physics D: Applied Physics 40, 1268-1272 (2007)

S. Scheinert, K. P. Pernstich, B, Batlogg, G. Paasch
Determination of trap distributions from current characteristics of pentacene field-effect transistors with surface modified gate oxide
J. Appl. Phys. 102, 104503 (2007)

R. Schleser, S. Kicin, C. Roth, C. Ebneter, R. Leturcq, K. Ensslin , D. C. Driscoll and A. C. Gossard
Influence of HCl etching on the electronic properties of AFM-defined nanostructures
Semicond. Sci. Technol. 22, 337 (2007)

G. Schuck, S. Haas, A. F. Stassen, H.J. Kirner and B. Batlogg
5,12-Bis(4-tert-butylphenyl)-6,11-diphenylnaphthacene
Acta Cryst. E63, 02893 (2007)

G. Schuck, S. Haas, A. F. Stassen, U. Berens and B. Batlogg
5,11-Bis(4-tert-butylphenyl)-6,12-diphenylnaphthacene (formA)
Acta Cryst. E63, 02894 (2007)

D. I. Schuster, A. A. Houck, J. A. Schreier, A. Wallraff, J. M. Gambetta, A. Blais, L. Frunzio, B. Johnson, M. H. Devoret, S. M. Girvin, R. J. Schoelkopf
Resolving photon number states in a superconducting circuit
Nature 445, 515-518 (2007)

T. Siegrist, C. Besnard, S. Haas, M. Schiltz, P. Pattison, D. Chernyshov, B. Batlogg, and C. Kloc
A Polymorph Lost and Found: The High-Temperature Crystal Structure of Pentacene
Advanced Materials 19, 2079 (2007)

M. Sigrist, T. Ihn, K. Ensslin, M. Reinwald, and W. Wegscheider
Coherent Probing of Excited Quantum Dot States in an Interferometer
Phys. Rev. Lett. 98, 036805 (2007)

M. Sigrist, T. Ihn, K. Ensslin, M. Reinwald and W. Wegscheider
Is inelastic cotunneling phase coherent?
J. Appl. Phys. 101, 081701 (2007)

B. Sipos, N. Barisic, R. Gaal, L. Forró, J. Karpinski, and F. Rullier-Albenque,
Matthiessen's rule in MgB_2 : Resistivity and T_c as a function of point defect concentration,
Phys. Rev. B 76, 132504 (2007)

A.V. Sologubenko, T. Lorenz, H.R. Ott, A. Freimuth
Thermal Conductivity via Magnetic Excitations in Spin-Chain Materials
Journal of Low Temperature Physics 147, 387-402 (2007)

C. Stampfer, L. Wirtz, A. Jungen, D. Graf, F. Molitor, C. Hierold, and K. Ensslin
Raman imaging of doping domains in graphene on SiO_2
Appl. Phys. Lett. 91, 241907 (2007)

S. Strässle, J. Roos, M. Mali, H. Keller and J. Karpinski,
^{1}B NMR study of single-crystal MgB_2 in the normal conducting phase,
Physica C 466, Issues 1-2, 168-173, (2007)

E. V. Sukhorukov, A. N. Jordan, S. Gustavsson, R. Leturcq, T. Ihn, and K. Ensslin
Conditional statistics of electron transport in interacting nanoscale conductors
Nature Physics 3, 243 (2007)

D. Vengust, F. Pfuner, L. Degiorgi, I. Vilfan, V. Nicolosi, J.N. Coleman, and D. Mihailovic
Optical properties of $Mo_6S_3I_6$ nanowires
Phys. Rev. B 76, 075106 (2007)

R. Verma, D. Brémaud, S. Bücheler, S. Seyrling, H. Zogg and A. N. Tiwari
Physical vapor deposition of In2S3 buffer on Cu(In,Ga)Se_2 absorbers: optimization of processing steps for improved cell performance
Proceedings 22nd European Photovoltaic Solar Energy Conference, Milano, 2007

I. Vobornik, J. Fujii, M. Hochstrasser, D. Krizmancic, M. Mulazzi, C. E. Viol, G. Panaccione and G. Rossi
k-Space tomography of the Fermi surface by spatially resolved photoemission spectroscopy with variable photon energy
Surface Science 601, 18, 4246-4249 (2007)

I. Vobornik, J. Fujii, M. Hochstrasser, D. Krizmancic, C. E. Viol, G. Panaccione, S. Fabris, S. Baroni and Rossi G. and
Three-Dimensional Tomography of the Beryllium Fermi Surface: Surface Charge Redistribution
Phys. Rev. Lett. 99, 166403 (2007)

P. Wachter
Similarities between Copper and Plutonium containing "high T_c" superconductors
J. Alloys and Compounds 442, 42-48 (2007)

P. Wachter
Similarities between Cu and Pu containing "high T_c" superconductors
Physica C 453, 1-11 (2007)

A. Wallraff, D. I. Schuster, A. Blais, J. M. Gambetta, J. Schreier, L. Frunzio, M. H. Devoret, S. M. Girvin, R.J. Schoelkopf
Sideband Transitions and Two-Tone Spectroscopy of a Superconducting Qubit Strongly Coupled to an On-Chip Cavity
Phys. Rev. Lett., 99, 050501 (2007)

Y. Weisskopf, S. Burkardt, M. Erbudak and J.-N. Longchamp
The quasicrystal-crystal interface between icosahedral Al-Pd-Mn and deposited Co: evidence for the affinity of the quasicrystal structure to the CsCl structure
Surf. Sci. 601, 544-551 (2007)

A. Wisniewski, R. Puzniak, A. Bienias, M. Baran, J. Jun, N.D. Zhigadlo and J. Karpinski,
Anisotropy of the lower and of the upper critical fields in $Mg_{1-x}Al_xB_2$ single crystals
Physica C 460-462, 614-615, (2007)

A. Wisniewski, R. Puzniak, J. Judek, C. Krutzler, M. Eisterer, H. W. Weber, J. Jun, S. M. Kazakov, J. Karpinski,
Comparison of the influence of carbon substitution and neutron induced defects on the upper critical field and flux pinning in MgB_2 single crystals,
Supercond. Sci. Technol., 256-260 (2007)

S. Wu, J.Zhang, A.Belousov, J. Karpinski, and Roman Sobolewski,
Ultra long-lived coherent acoustic phonons in GaN single crystals,
Phonons 2007, Journal of Physics, Conference Series 92, 012021 (2007)

S. Wu, P. Geiser, J. Jun, J. Karpinski, and R. Sobolewski,
Femtosecond optical generation and detection of coherent acoustic phonons in GaN single crystals,
Phys. Rev. B 76, 085210 (2007)

S. Wu, D. Wang, P. Geiser, J. Jun, J. Karpinski, R. Sobolewski,
Intervalley transitions in single crystals GaN
J. Appl. Phys. 101, 043701 (2007)

M. Zehetmayer, M. Eisterer, C. Krutzler, J. Jun, S. M. Kazakov, J. Karpinski, H.W. Weber
Order-disorder transition in theflux line lattice of superconducting MgB_2 single crystals with artificially introduced defects: comparison with theory
Supercond. Sci. Technol. 20, 247-256 (2007)

N. D. Zhigadlo and J. Karpinski,
High-pressure synthesis and superconductivity of $Ca_{2-x}Na_xCuO_2Cl_2$,
Physica C 460-462, 372-373, (2007)

S. P. Zimin, E. S. Gorlachev, I. I. Amirov, M. N. Gerke, H. Zogg, D. Zimin
Role of threading dislocations during treatment of PbTe films in argon plasma
Semicond. Sci. Technol. 22 929-932 (2007)

Chapter 7

Presentations

(* = invited talk)

Arnold, M.
Wavelength tunable resonant cavity enhanced detectors
MIOMD-8, Bad Ischl, Austria, 14-16.5.2007

Arnold, M.
Bleisalz-VECSEL mit $5\ \mu\mathrm{m}$ Emissionswellenlänge
DMBE WS07, Deutscher MBE-Workshop, Hamburg, Germany, 1-2.10.2007

Batlogg B.
Low temperature magnetism and high temperature Na ordering in Na_xCoO_2
Mobile Fermions and Bosons on Frustrated Lattice, Dresden, 11-13.1.2007

Batlogg B.
Organische Halbleiter - Plastik Elektronik
ETH Zürich, Switzerland, 08.02.2007

* Batlogg B.
Fermi surface instabilities in Na_xCoO_2
Novel materials and superconductors, Donnersbach, Austria, 10.02.2007

Batlogg B.
Intrinsic transport anisotropy in single-crystal-FETs on new rubrene derivatives
APS March Meeting, Denver, USA, 04.03.2007

Batlogg B.
Weak coupling SDW and strong Fermi surface gapping in $Na_{0.8}CoO_2$
APS March Meeting, Denver, USA, 04.03.2007

Batlogg B.
Technik im Alltag
Festansprache am Bundesgymnasium Bludenz, Austria, 22.06.2007

* Batlogg B.
Correlated electrons: materials
PSI Summer School, Zuoz, Switzerland, 18.08.2007

Batlogg B.
Wieviel Technik brauchen wir?
Techday, Kantonsschule Limmattal, Urdorf, Switzerland, 30.10.2007

Belousov A.
Nitride bulk crystals growth under high pressure,
2nd Graduate Symposium, Zurich, Switzerland, 27.06.2007

Belousov A.
$Al_xGa_{1-x}N$ crystals grown under high N_2 pressure,
Swiss Workshop on Materials with Novel Electronic Properties, Les Diablerets, Switzerland, 29.09.2007

Bianchetti R.
Circuit Quantum Electrodynamics: Superconducting Qubits and Cavities
QUROPE Winter School on Quantum Information Obergurgl, Austria, 18.02.2007

Brémaud, D.
Alternative back contacts for Cu(In,Ga)Se_2 solar cells
MRS 2007 Spring Meeting, San Francisco, CA, USA, 9-13.4.2007

Brémaud, D.
Flexible Cu(In,Ga)Se_2 solar cells and technologies
22nd European Photovoltaic Solar Energy Conference, Milano, Italy, 3-7.9.2007

* Brémaud, D.
High efficiency flexible solar cells: challenges and prospects of manufacturing and applications
Pro Flex 2007, Dresden, 11-12.9.2007

Brémaud, D.
Development of nanocrystalline dye-sensitised / Cu(In,Ga)Se_2 tandem solar cells
EMPA Thin Film PV Workshop, Dübendorf, Switzerland, 5.10.2007

Brémaud, D.
Development of high efficiency and stable thin film solar cells
EMPA Thin Film PV Workshop, Dübendorf, Switzerland, 5.10.2007

Buecheler, S.
Ultrasonically Sprayed Indium Sulfide Buffer Layer for Cu(In,Ga)$(S,Se)_2$ Thin-Film Solar Cells
EMPA Thin Film PV Workshop, Dübendorf, Switzerland, 5.10.2007

Bukowski Z.
Single crystal growth and properties of superconducting Beta-pyrochlore KOs_2O_6, $RbOs_2O_6$ and related compounds
Swiss Physical Society Meeting, Zurich, Switzerland, 20.02.2007

Bukowski Z.
Single crystalline studies of superconducting Beta-pyrochlore osmates AOs_2O_6 (A=K,Rb),
Swiss Workshop on Materials with Novel Electronic Properties, Les Diablerets, Switzerland, 28.09.2007

Bukowski Z.
Low temperature ion exchange in the pyrochlore osmates,
Swiss Workshop on Materials with Novel Electronic Properties, Les Diablerets, Switzerland, 29.09.2007

Burkardt S.
Growth mode of ferromagnetic nanostructures on icosahedral Al-Pd-Mn quasicrystal
Schweizerische Arbeitsgemeinschaft Oberflächen und Grenzflächen (SAOG), Fribourg, Switzerland, 26.1.2007

Burkardt S.
Self-assembly of crystalline Co nanostructures on icosahedral Al-Pd-Mn quasicrystal
Quasicrystals, The Silver Jubilee, Tel Aviv, Israel, 18.10.2007

Csontos, M.
Interference effects in p-type GaAs quantum rings
3rd EuropeanC onference on the Fundamental Problems of Mesoscopic Physics and Nanoelectronics, Spain, Mojacar, 09.09.2007

Csontos, M.
Interference effects in p-type GaAs quantum rings
Joint EUROCORES FoNE, Spi-Co-SPINCURRENT-Spintra Workshop, Pozzuoli, Italy, 10.12.2007

* Degiorgi L.
Wo Experimente entstehen
Treffpunkt Science City, Wissenschaft erleben, ETH Zürich, Zürich, Switzerland, 25.02.2007

Degiorgi L.
Chemical pressure and hidden one-dimensional behaviour in rare-earth tri-telluride charge-density-wave compounds
March Meeting of the American Physical Society, Denver, U.S.A., 05.03.2007

* Degiorgi L.
Magneto-optical properties of EuB_6
March Meeting of the American Physical Society, Denver, U.S.A., 05.03.2007

* Degiorgi L.
Electrodynamic response of low-dimensional correlated systems
Seminar at the Physics Department of the Akron University, Akron, U.S.A., 13.03.2007

* Degiorgi L.
Electrodynamic response of correlated systems
Symposium in Honor of Prof. H.R. Ott on Highly Correlated Electron Systems, Magnetism and Superconductivity, ETH Zurich, Zurich, Switzerland, 11.05.2007

* Degiorgi L.
Electrodynamic response of low dimensional correlated systems
Solid State Physics Seminar, Department of Physics, Freie Universität Berlin, Berlin, Germany, 29.06.2007

* Degiorgi L.
Optical spectroscopic studies of correlated materials
6th Summer School on Condensed Matter Research, Zuoz, Switzerland, 18.08.2007

* Degiorgi L.
Infrared study of the pressure dependence of the charge-density-wave gap in rare-earth tri-tellurides
4th International Workshop on Infrared Microscopy and Spectroscopy with Accelerator Based Sources, Awaji Island, Hyogo, Japan, 25.09.2007

* Degiorgi L.
Electrodynamic response of low dimensional correlated systems
Solid State Physics Seminar, Department of Physics, University of Geneva, Geneva, Switzerland, 26.10.2007

* Ensslin, K.
Coherent probing of excited quantum dot states
Nonequilibrium Transport of Strongly Correlated Systems Towards Simulation of Novel Devices, Bad Honnef, Germany, 30.01.2007

* Ensslin, K.
Elektronische Eigenschaften von Halbleiter-Nanostrukturen
DFG/FHI Rundgespräch Neue Entwicklungen am Rande der Festkörperphysik, Bad Honnef, Germany, 21.02.2007

* Ensslin, K.
Raman Imaging of Graphene
Springmeeting of the German Physical Society, Regensburg, Germany, 26.03.2007

* Ensslin, K.
Raman Imaging of Graphene
Conference on Quantum Phenomena in Confined Dimensions, Trieste, Italy, 04.06.2007

* Ensslin, K.
Electrons in nanostructures - one-by-one
Wiener Physikalisches Kolloquium, Vienna, Austria, 11.06.2007

* Ensslin, K.
Electron counting, single photon detection and time-resolved Aharonov Bohm oscillations
Seminar, Harvard University, Cambridge, USA, 18.06.2007

* Ensslin, K.
Scanning gate microscopy - how local does it get?
Low-Temperature Scanning Probe Microscopy (LTSPM) Symposium, International conference on Nanoscience and Nanotechnology, Stockholm, Sweden, 02.07.2007

* Ensslin, K.
Graphene
Seminar at Teledyne Scientific & Imaging, Thousand Oaks, USA, 10.07.2007

* Ensslin, K.
Electron counting, single photon detection and time-resolved Aharonov Bohm oscillations
CNSI seminar, University of California, Santa Barbara, USA, 13.07.2007

* Ensslin, K.
Kondo effect, coherence and electron counting in mesoscopic rings
Workshop on New Frontiers in Quantum Impurity Physics: from Nano-Structures to Molecular Devices, Dresden,

Germany, 13.08.2007

* Ensslin, K.
Quantum physics in quantum dots
School on Magnetic Fields for Science, Cargèse, Corsica, France, 27.08.2007

Ensslin, K.
Phase-coherent effects in p-type GaAs with strong spin orbit interaction
Workshop on Quantum Transport, Magnetic Nanodevices and Spintronics, Naples, Italy, 09.12.2007

Erbudak, M.
Ordnung in der Struktur natürlicher Objekte
Vortrag an der Senioren-Universität, Zürich, Switzerland, 9.1.2007

* Erbudak, M.
Structural and electronic observations at crystal-quasicrystal interfaces
Chemistry Seminar Bilkent University, TR-Ankara, 8.3.2007

* Erbudak, M.
Structural and electronic observations at crystal-quasicrystal interfaces
Physics Seminar, Bogazici University, TR-Istanbul, 12.3.2007

Erbudak, M.
Eigenschaften und Formation unserer Planete
ENKA Schulen, Adapazari, Turkey, 14.6.2007

Erbudak, M.
Quantum-well formation at quasicrystal surfaces
14th Conf. Stat. Phys., Istanbul, Turkey, 21.6.2007

Erbudak, M.
Geometrische Anordnung natürlicher Objekte
Kiwanis Club Uster, Uster, Switzerland, 18.7.2007

Felder, F.
Narrowband Resonant Cavity Enhanced mid-IR Photodetectors tuneable within a broad wavelength region
EUROMBE 14, 14th European Molecular Beam Epitaxy Workshop, Granada, Spain, 5-7.3.2007

Felder, F.
Resonant Cavity Photodetektoren mit durchstimmbarer Wellenlänge im mittleren Infrarot
37. IR-Kolloquium, Freiburg, Germany, 27-28.3.2007

Felder, F.
Wavelength tunable Resonant Cavity Enhanced Photodetectors based on lead-salts grown by MBE
NGS-13, 13th International Conference on narrow Gap Semiconductors, Guilford, UK, 8-12.7.2007

Felder, F.
Durchstimmbare resonanzverstärkte Photodetektoren für das mittlere Infrarot
DMBE WS07, Deutscher MBE-Workshop, Hamburg, Germany, 1-2.10.2007

Fink J.M.
Observation of Berry's Phase in a Solid State Qubit
DPG - Physics School 2007: Quantum Information and Quantum Simulation Physics Center Bad Honnef, Germany, 16.09. 2007

Gildemeister, A.
Scanning Gate Microscopy - How local does it get?
17th International Conferences on Electronic Properties of Two-dimensional Systems (EP2DS), Genova, Italy, 18.07.2007

Grbic, B.
Spin interference in hole quantum rings
17th International Conferences on Electronic Properties of Two-dimensional Systems (EP2DS), Genova, Italy, 18.07.2007

* Gustavsson, S.
Time-resolved detection of single-electron interference
Seminar, Institut fuer Nanotechnologie, Forschungszentrum Karlsruhe, Germany, 17.4.2007

Gustavsson, S.
Time-resolved interference experiments in a solid state environment
17th International Conferences on Electronic Properties of Two-dimensional Systems (EP2DS), Genova, Italy, 18.07.2007

* Gustavsson, S.
Time-resolved detection of single-electron interference
TU Delft, Delft, Netherlands, 21.8.2007

* Gustavsson, S.
Time-resolved detection of single-electron interference
Seminar, Division of Solid State Physics, Lund University, Lund, Sweden, 26.10.2007

* Gustavsson, S.
Time-resolved detection of single-electron interference
Seminar, Microtechnology and Nanoscience, Chalmers University of Technology, Gothenburg, Sweden, 27.10.2007

* Gustavsson, S.
Time-resolved detection of single-electron interference
Seminar, Institute for Chemical Research, Kyoto University, Kyoto, Japan, 26.11.2007

Güttinger, J.
Mesoscopictransport in graphene
2nd MRC Graduate Symposium at the ETH Zurich, Zürich, Switzerland, 27.06.2007

Hochstrasser M.
Relationship between degree of oxidation and magnetic anisotropy in $Pt/Co/AlO_x$ trilayers
3rd CHIRALTEM workshop, Trieste, Italy, 31.05-01.06.2007

Hüfner, M.
Low Temperature Scanning Probe Microscopy on Low Dimensional Structures
3rd European Conference on the Fundamental Problems of Mesoscopic Physics and Nanoelectronics, Spain, Mojacar, 09.09.2007

* Ihn, T.
Measuring the full counting statistics of the current through quantum dots
13th Brazilian Workshop on Semiconductor Physics, Sao Paulo, Brazil, 05.04.2007

* Ihn, T.
Quantum circuits based on electronic materials
Universität Ulm, Germany, 05.06.2007

* Ihn, T.
Transport and Noise in AFM-defined Nanostructures
UK Compound Semiconductors, Sheffield, UK, 05.07.2007

Ihn, T.
Phase-coherent transport in a mesoscopic few-layer graphite wire
International Conference on Modulated Semiconductor Structures (MSS13), Genova, Italy, 15.07.2007

* Ihn, T.
Scanning Probe Measurements on Semiconductor Nanostructures
Int. Conf. on Solid State Devices and Materials, Tsukuba, Japan, 05.09.2007

* Ihn, T.
Single-electron detection in quantum dot circuits
Virtual Conference on Nanoscience and Nanotechnology, Fayetteville, USA, 05.10.2007

* Ihn, T.
Electronic Transport in Quantum Dots and Quantum Dot Circuits
Universität Regensburg, Regensburg, Germany, 01.12.2007

Kalb W.
Eliminating gate bias stress effects in organic field-effect transistors,
APS March Meeting 2007, Denver, USA 05.03.2007

Kalb W.
SCLC trap spectroscopy in organic semiconducting crystals: bulk in gap states modified by structural and chemical defects,
APS March Meeting 2007, Denver, USA 06.03.2007

Kalb W.
High performance field-effect transistors with a cyclic fluoropolymer gate dielectric
ECOER'07, Varenna, Italy, 30.09.2007

Karpinski J.
Li hole doping and Li-C hole and electron co-doping in MgB_2 single crystals
Swiss Physical Society Meeting, Zurich, Switzerland, 20.02.2007

Karpinski J.
Single crystals of MgB_2: synthesis, substitutions and properties
The Fifth International Conference on Solid State Crystals, Zakopane Poland, 20.05.2007

* Karpinski J.
Single crystals of MgB_2: high-pressure growth, substitutions and properties
XV International Conference of Crystal Growth, Salt Lake City, USA, 12.08.2007

Karpinski J.
Li hole doping and Li/C hole/electron co-doping in MgB_2 single crystals,
Eucas 2007, Brussels, Belgium, 16.09.2007

Karpinski J.
Li hole doping and Li/C hole/electron co-doping in MgB_2 single crystals
Swiss Workshop on Materials with Novel Electronic Properties, Les Diablerets, Switzerland, 28.09.2007

* Karpinski J.
Hole doping in MgB_2 and oxychloride $Ca_{2-x}Na_xCuO_2Cl_2$ superconductors
High Temperature Superconductivity in Cuprates, Original Concept and New Developments, Tbilisi, Georgia, 07.10.2007

* Karpinski J.
Single crystals of MgB_2: synthesis, substitutions and properties
13th National Superconductivity School, Ladek, Poland, 06.11.2007

Küng, B.
Frequency-tunable single photon detection with a double quantum dot
3rd European Conference on Fundamental Problems of Mesoscopic Physics and Nanoelectronics, Mojacar, Spain, 11.09.2007

Lavagnini M.
Pressure-induced deconfinement of the charge transport in the quasi-one-dimensional Mott insulator $(TMTTF)_2AsF_6$
Journal Club, Laboratorium für Festkörperphysik, ETH Zurich, Zurich, Switzerland, 12.01.2007

Lavagnini M.
Optical study of the Ce and La di-telluride charge density wave compounds under pressure
6th Summer School on Condensed Matter Research, Zuoz, Switzerland, 18-25.8.2007

Lavagnini M.
Optical study of the Ce and La di-telluride charge density wave compounds under pressure
MaNEP Workshop on Materials with Novel Electronic Properties, Les Diablerets, Switzerland, 28-30.9.2007

Leek P.J.
Observation of Berry's Phase in an Electronic Circuit
Gordon Research Conference on Quantum Information Science, Il Ciocco Lucca (Barga), Italy, 15.04.2007

* Leturcq, R.
Spin-dependent transport in double quantum dots realized in InAs nanowires
International Conference on Nanoelectronics, Nanostructures and Carrier Interactions, Atsugi, Japan, 20.02.2007

* Leturcq, R.
Shot noise measured by counting electrons in a quantum dot
Workshop on Mesoscopic Quantum Physics, Aussois, France, 19.03.2007

* Leturcq, R.
Spindependent transport in quantum dots realized in InAs nanowires
European Workshop on Multifunctional Materials, Averoy, Norway, 17.06.2007

Leturcq, R.
Strong spin-orbit interaction in carbon doped p-type GaAs heterostructures
International Conference on Modulated Semiconductor Structures (MSS13), Genova, Italy, 15.07.2007

Leturcq, R.
Frequency selective single-photon detection with a double quantum dot
International Conference on Modulated Semiconductor Structures (MSS13), Genova, Italy, 15.07.2007

Leturcq, R.
Single electron transport in quantum dots realized in InAs nanowires
International Conference on Modulated Semiconductor Structures (MSS13), Genova, Italy, 15.07.2007

Leturcq, R.
Spin transport in InAs nanowire double quantum dots
The Second International Conference on One-dimensional Nanomaterials, ICON 2007, Malmö, Sweden, 26.09.2007

Leturcq, R.
Single electron and spin transport in InAs nanowire quantum dots
Heraeus Seminar on Semiconducting Nanowires: Physics, Materials and Devices, Bad Honnef, Germany, 14.10.2007

Longchamp J. N.
Formation of a well-ordered ultra-thin aluminum-oxide film by oxidation of the pentagonal surface of i-AlPdMn quasicrystal
Int. Conf. on Surf. Sci., ICSS-13, Stockholm, 12.-16.7.2007

Meier, L.
Measurementof Rashba and Dresselhaus magnetic fields,
17th International Conferences on Electronic Properties of Two-dimensional Systems (EP2DS), Genova, Italy, 18.07.2007

Molitor, F.
Disorder and mesoscopic transport in few-layer graphene
International Winterschool on Electronic Properties of Novel Materials: Molecular Nanostructures, Kirchberg/Tirol, Austria, 10.03.2007

Molitor, F.
Mesoscopic transport in graphene
Conference on Quantum Phenomena in Confined Dimensions, Trieste, Italy, 04.06.2007

* Monnier, R.
Fondements dela théorie de la fonctionnelle de densité (lecture series)
1ère écoled'été en physique, Université Mouloud Mammeri, Tizi-Ouzou, Azeffoun, Algeria, 22.08.2007

Monnier, R.
Theory of the thermoelectricity in intermetallic compounds with Ce or Yb ions
Graduate colloquium, University of Zurich, Zurich, Switzerland, 12.11.2007

Mungan M.
Adatoms on a Quasicrystalline Substrate: A Molecular Dynamics Study
Statphys 23, Genoa, Italy, 10.7.2007.

Müller, T.
Charge Sensing with a Radio-Frequency Quantum Point Contact
3rd European Conference on the Fundamental Problems of Mesoscopic Physics and Nanoelectronics, Spain, Mojacar, 09.09.07

* Ott H.R.
Transport and Magnetism in Low Dimensional Spin Systems
Colloquium University College London, United Kingdom, 25-26.4.2007

* Ott H.R.
Electronic and magnetic Properties of Na_xCoO_2
International Conference on coherence and incoherence in strongly correlated systems, Rome, Italy, 3-8.7.2007

* Ott H.R.
3 Lectures on BCS Theory vis à vis Experiment
Summer School from BCS to Exotic Superconductivity, Ajaccio Korsika, France, 16-22.7.2007

* Ott H.R.
5f electrons and the Kondo effect
International Conference on The Heavy Fermion Frontier, Santa Fe, USA, 10-16.11.2007

* Ott H.R.
Magnetism and electronic transport in Na_xCoO_2
International Conference on Magnetic Materials (ICMM-2007), Kolkata, India, 7-12.12.2007

Pernstich K.
The Seebeck Effect in pentacene and rubrene field-effect transistors
4th European Conference on Organic electronic and Related Phenomena ECOER 2007, Varenna, Italy, 01.04.2007

Pernstich K.
Seebeck effect in rubrene and pentacene field-effect transistors
EMRS spring meeting, Strasbourg, France, 31.05.2007

Pernstich K.
Gate voltage modulated Seebeck coefficient in organic FET structures
Alpine workshop on Organic FET, Braunwald, Switzerland, 16.12.2007

* Pescia D.
Ultrathin magnetic films: a playground for statistical physics
Pokrovsky Fest on Statistical Physics and Quantum Field theory, College Station, Texas, 12-14.1.2007

* Pescia D.
Topological Phase Transitions
Colloqium CNR-Istituto dei sistemi complessi, CNR, Firenze, 3.5.2007

* Pescia D.
New Ideas in Magnetism
Symposium in honor of W. Baltensperger, Herrenhaus Grafenort, Grafenort, Switzerland, 8.6.2007

* Pescia D.
Subpanel Magnetization and spin dynamics
Workshop ”Science for a New Class of Soft X-rays light sources”, Berkeley, Lawrence Berkeley Laboratory, 8-10.10.2007

* Pescia D.
Perpectives for experiments with highest temporal and spatial resolution
Workshop ”Science for a New Class of Soft X-rays light sources”, Berkeley Lawrence Berkeley Laboratory, 8-10.10.2007

Pfund, A.
Single electrons and spins in quantum dots realized in InAs nanowires
2nd MRC Graduate Symposium, Zurich, Switzerland, 27.06.2007

Pfund, A.
Mixing and relaxation of spin states in InAs double quantum dots
17th International Conferences on Electronic Properties of Two-dimensional Systems (EP2DS), Genova, Italy, 18.07.2007

Pfuner F.
Charge localization due to RKKY interaction in the Spin Glass AuFe
Journal Club, Laboratorium für Festkörperphysik, ETH Zurich, Zurich, Switzerland, 05.01.2007

Pfuner F.
Magneto-optical investigation of the Zintl compound $EuIn_2P_2$
6th Summer School on Condensed Matter Research, Zuoz, Switzerland, 18-25.8.2007

Pfuner F.
Magneto-optical investigation of the Zintl compound $EuIn_2P_2$
MaNEP Workshop on Materials with Novel Electronic Properties, Les Diablerets, Switzerland, 28-30.9.2007

Powalla, M.
Highly productive manufacturing of CIS-based large-area modules
22nd European Photovoltaic Solar Energy Conference, Milano, Italy, 3-7.9.2007

Quack, N.
Electrostatically actuated Micromirror for Resonant Cavity Enhanced Detectors
MEMS 2007, 20th IEEE International Conference on MEMS, Kobe, Japan, 21-25.1.2007

Quack, N.
MEMS Mirrors for the use in Resonant Cavity Enhanced Detectors
MNE 2007, 33rd International Conference on Micro- and Nano-Engineering, Copenhagen, Denmark, 23-26.9.2007

Rahim, M.
Mid-Infrared Vertical External Cavity Surface Emitting Lasers grown by MBE
EUROMBE 14, 14th European Molecular Beam Epitaxy Workshop, Granada, Spain, 5-7.3.2007

Rahim, M.
Mid-Infrared Vertical External Cavity Surface Emitting Lasers grown by MBE
37. IR-Kolloquium, Freiburg, Germany, 27-28.3.2007

Rahim, M.
Mid-Infrared vertical external cavity surface emitting lasers grown by MBE
MIOMD-8, Bad Ischl, Austria, 14-16.5.2007

Rahim, M.
Mid-Infrared Vertical External Cavity Surface Emitting Lasers for Spectroscopy
NGS-13, 13th International Conference on narrow Gap Semiconductors, Guilford, UK, 8-12.7.2007

* Ramperger U.
Spintronics and Micromagnetism
14th Istanbul Statistical Physics Days, Bogazici University Istanbul, 21.-23.7.2007

Rogacki K.
Studying transport properties of MgB_2 single crystals doped with holes and electrons,
The 8th International Conference on Spectroscopies in Novel Superconductors (SNS 2007), Sendai, Japan, 20.08.2007

Ruh, E.
Investigation of the local Ge concentration in Si/ SiGe multi quantum well structure by CBED analysis and FEM calculations
Microscopy of Semiconducting Materials XV, Cambridge, UK, 02.04.2007

Sacchetti A.
Optical properties of rare-earth tri-tellurides
MANEP internal meeting 2007, Neuchâtel, Switzerland, January 2007

* Sacchetti A.
Optical properties of rare-earth tri-tellurides
Solid State Physics Department of ETH Zurich, Switzerland, February 2007

* Sacchetti A.
Optical properties of rare-earth tri-tellurides,
Laboratory for Neutron Scattering at Paul Scherrer Institute, Switzerland, May 2007

Sacchetti A.
Optical properties of rare-earth tri-telluride charge density wave compounds
MaNEP 2007 workshop Les Diablerets, Switzerland, September 2007

Sacchetti A.
Control of the effective phase of a manganite by mode-selective vibrational excitation
Journal Club at the Solid State Physics Department of ETH Zurich Switzerland, November 2007

Saratz N.
Magnetization Profile in Magnetic Stripe Domains in ultrathin Fe films on Cu(001))
ICNM (Intl. Conference on Nanscale Magnetism) 27.06.2007

Saratz N.
Magnetization Profile in Magnetic Stripe Domains in ultrathin Fe films on Cu(001))
PSI Summer School on Condensed Matter Research, Zuoz, Switzerland, 22.08.2007

Saratz N.
Magnetization Profile in Magnetic Stripe Domains in ultrathin Fe films on Cu(001))
Intl. Conference on Magnetism and Magnetic Materials), Tampa, USA, 09.11.2007

Schnez, S.
Scanning Gate Microscopy on Low Dimensional Structures
The 4th Windsor Summer School on Condensed Matter Theory: Quantum Transport and Dynamics in Nanostructures, Windsor, UK, 16.08.2007

Shorubalko, I.
Quantum dots in InAs nanowires for single charge and spin studies
International Baltic Sea Region conference and Functional materials and nanotechnologies, Riga, Latvia, 02.04.2007

Shorubalko, I.
Spin-dependent transport in double quantum dots realized in InAs nanowires
International Conference on Nano Science and Technology, Stockholm, Sweden, 02.07.2007

* Shorubalko, I.
Post CMOS devices based on semiconductor nanowires
The 9th International Conference-School, Advanced Materials and Technologies, Palanga, Lithuania, 27.08.2007

Stampfer, C.
Raman imaging of individual carbon nanotubes and graphene flakes
International Winterschool on Electronic Properties of Novel Materials: Molecular Nanostructures, Kirchberg/Tirol, Austria, 15.03.2007

Stampfer, C.
Spatially resolved Raman spectroscopy of Single- and Few-Layer Graphene
Conference on Quantum Phenomena in Confined Dimensions, Trieste, Italy, 04.06.2007

* Stampfer, C.
Electromechanical Transducers based on Single-Walled Carbon Nanotubes
Institute for Electronic, Microelectronic and Nanotechnology (IEMN), Lille, France, 19.06.2007

Stampfer, C.
Raman imaging of graphene and carbon nanotubes
2nd MRC Graduate Symposium at the ETH Zurich, Zürich, Switzerland, 27.06.2007

* Stampfer, C.
Ultra Miniaturized Pressure Sensors
Sensors and Nanotech, the 20th anniversary of the Swiss Society for Sensor Technology(SSST), Fribourg, Switzerland, 03.07.2007

* Stampfer, C.
Ultra miniature Pressure Sensors based on Nanotubes on ultra thin alumina membranes
INFICON Limited, Balzers, Liechtenstein, 20.09.2007

Stampfer, C.
Tunable Coulomb blockade in nanostructured graphene
Workshop on Electrons in Graphene, Orsay, France, 03.12.2007

Stampfer, C.
Piezoresistance of Single-Walled Carbon Nanotubes
The 14th International Conference on Solid State Sensors, Actuators, Microsystems, Transducers, Lyon, France, 12.06. 2007

* Vaterlaus A.
The training of physics teachers at the physics department of the ETH Zurich
PSME 07 Konferenz in St. Petersburg, Russland, 7.06.07

* Vaterlaus A.
Teaching of physics at High School level
Workshop SPbSPU-ETHZ, Frauenfeld, CH, 11.10.07

Verma, R.
Physical vapor deposition of In_2S_3 buffer on Cu(In,Ga)Se_2 absorbers: optimization of processing steps for improved cell performance
22nd European Photovoltaic Solar Energy Conference, Milano, Italy, 3-7.9.2007

Vindigni A.
Temperature-induced domain shrinking in Dipolar Frustrated Ising Ferromagnet
APS March Meeting 2007, Denver, 5-9.3.2007

* Vindigni A.
Low Dimensional Magnetism: model systems for the Ising model
Universidad Nacional de Cordoba, Cordoba, Argentina, 28.3.2007,

Vindigni A.
Temperature-induced domain shrinking in Dipolar Frustrated Ising Ferromagnet
XII Convegno Nazionale di Fisica Statistica, Parma, 20-21.6.2007

Vindigni A.
Temperature-induced domain shrinking in Dipolar Frustrated Ising Ferromagnet
StatPhys 23, Genoa, Italy, 9-13.7.2007

* Wachter P.
Similarities between Cu and Pu containing ”high T_c” superconductors
37iémes Journées des Actinides, Sesimbra Portugal, 25.03.2007

* Wachter P.
Specific Heat Measurements under Pressure (0-15 kbar) and low temperature (4-300 K) on Condensed Excitons in TmSeTe: Strong Phonon Softening
Phonons 2007, Paris, France, 18.07.2007

Wallraff A.
Photons, Qubits and Computers - A Quantum Mechanic‘s Lab on a Chip
Gordon Research Conference on Quantum Information Science, Il Ciocco Lucca (Barga), Italy, 15.04.2007

* Wallraff A.
Photons, Qubits and Computers - A Quantum Mechanic‘s Lab on a Chip
ETH Zurich Public Introductory, ETH Zurich, Zurich, Switzerland, 26.04.2007

* Wallraff A.
Quantum Information Processing with Superconducting Qubits and Cavities
European Conference on Lasers and Electro-Optics and the International Quantum Electronics Conference (CLEO®/Europe-IQEC) Munich, Germany; 17.06.2007

Wallraff A.
Quantum Systems for Information Technology
ETH Homecoming Day Alumni Lecture, Departement Physik, ETH Zurich, Zurich, Switzerland, 22.06.2007

* Wallraff A.
Quantum Optics and Quantum Information Processing with Superconducting Circuits
Solid State Physics Seminar, Institut für Festkörperphysik, Forschungszentrum Karlsruhe, Karlsruhe, Germany, 28.06.2007

* Wallraff A.
Cavity Quantum Electrodynamics with an Electronic Circuit
SFB on Control and Measurement of Coherent Quantum Systems (annual meeting), Atominstitut österreichischer Universitäten, TU Wien, Vienna, Austria, 05.07.2007

* Wallraff A.
Photons, Qubits and Computers - A Quantum Mechanics Lab on a Chip
Colloquium of LMU and TU Departement fuer Physik, Ludwig-Maximilians-Universitaet Muenchen, Muenchen, Germany, 16.07.2007

* Wallraff A.
Geometric Phases in Superconducting Qubits
Seminar Department of Physics, University of Erlangen-Nuremberg, Germany, 18.07.2007

* Wallraff A.
Geometric Phases in Superconducting Qubits
Seminar SPEC, CEA-Saclay, Gif-sur-Yvette Cedex, France, 31.07.2007

* Wallraff A.
Photons, Qubits and Computers - A Quantum Mechanics Lab on a Chip
DPG - Physics School 2007: Quantum Information and Quantum Simulation Physics Center Bad Honnef, Germany; 16.09.2007

* Wallraff A.
Circuit Quantum Electrodynamics - Quantum Information Processing with Superconductors
QIPC 2007 International Conference on Quantum Information Processing and Communication Barcelona, Spain; 15.10.2007

* Wallraff A.
Photons, Qubits and Computers - A Quantum Mechanics Lab on a Chip
Symposium - ”FIRST Anniversary- The FIRST five years” (FIRST - Frontiers In Research: Space & Time), ETH Zurich, Zurich, Switzerland, 26.10.2007

* Wallraff A.
Berry's Phase in a Cooper Pair Box Qubit
Seminar Departments of Applied Physics and Physics, Yale University, New Haven, CT, USA, 15.11.2007

* Wallraff A.
Observation of Berry's Phase in a Solid State Qubit
Seminar Département de Physique, Université de Sherbrooke, Sherbrooke, QC, Canada, 20.11.2007

* Wallraff A.
Photons, Qubits and Computers - A Quantum Mechanics Lab on a Chip
Micro and Nano Science Platform (MNSP) Advisory Board Meeting, Presentation "Research Highlights", ETH Zurich, Zurich, Switzerland, 28.11.2007

Weller M.
Low temperature NMR study of $CeAl_3$ under hydrostatic pressure
SCES, Houston, USA, 13-19.5.2007

Weller M.
Low temperature NMR study of $CeAl_3$ under hydrostatic pressure
Swiss Workshop on MaNEP, Les Diablerets, Switzerland, 29.9.2007

Weller M.
Low temperature magnetic properties of $PrCu_2$
Swiss Workshop on MaNEP, Les Diablerets, Switzerland, 29.9.2007

* Weller M.
NMR Experiments in Solid State Physics
AMP-Kolloquium ETH Zürich, Switzerland, 4.12.2007

Zhigadlo N.
Superconductivity in a single-layer oxychloride $(Ca,Na)_2CuO_2Cl_2$: high pressure synthesis, structural and physical properties
Swiss Physical Society Meeting, Zurich, Switzerland, 20.02.2007

Zhigadlo N.
High pressure synthesis of cuprate superconductors with apical halogen,
2nd Graduate Symposium, Zurich, Switzerland, 27.06.2007

Zhigadlo N.
High pressure synthesis and superconductivity of $Ca_{2-x}Na_xCuO_2Cl_2$: role of the apical sites
Gordon Research Conference "Superconductivity", Les Diablerets, Switzerland, 10.09.2007

Zhigadlo N.
Synthesis and bulk properties of oxychloride superconductor $Ca_{2-x}Na_xCuO_2Cl_2$
Eucas 2007, Brussels, Belgium, 16.09.2007

Zhigadlo N.
High pressure synthesis and superconducting properties of cuprate superconductor $Ca_{2-x}Na_xCuO_2Cl_2$ with apical halogen atom,
Swiss Workshop on Materials with Novel Electronic Properties, Les Diablerets, Switzerland, 29.09.2007

* Zogg, H.
Epitaxial lead-chalcogenides on Si for mid-IR detectors and emitters including cavities
AITA, Advanced Infrared Technology and Applications International Workshop, Leon, Mexico, 8-12.10.2007

* Zogg, H.
Heteroepitaxial narrow gap lead-chalcogenide structures for IR-optoelectronic applications
AITA, Advanced Infrared Technology and Applications International Workshop, Leon, Mexico, 8-12.10.2007

* Zogg, H.
Lead Chalcogenide (IV-VI) IR-Materials and Devices
- Infrared Detector Arrays for Thermal Imaging
- Narrow gap IV-VI materials & Epitaxial Layers
- Lead Chalcogenide on Silicon Infrared Focal Plane Arrays for Thermal Imaging
Microphysics Laboratory (Prof. S. Sivananthan), Department of Physics, University of Illinois at Chicago, IL, USA, 15-17.10.2007

* Zogg, H.
Seminar, Epitaxial leadchalcogenides on Si for mid-IR detectors and emitters including cavities
Center for Quantum Devices (Prof. Manijeh Razeghi), Dept. Electrical Engineering & Computer Science, Northwestern University, Evanston, IL, USA, 18.10.2007

* Zogg, H.
Epitaxial lead-chalcogenides on Si for mid-IR detectors and emitters including cavities
U.S. Workshop on the physics and chemistry of II-VI materials, Baltimore, MD, USA, 30.10 - 1.11.2007